

An Experimental Study of Disc Brake Squeal

Thesis submitted in accordance with the
requirements of the University of Liverpool
for the degree of Doctor in Philosophy by
Simon James

May 2003

Summary

Disc brake vibrations are a cause of concern for automobile users and manufacturers. The user can find the noise of brake squeal annoying and sometimes worrying. The manufacturer suffers the immediate costs involved in vehicle warranty claims and may lose sales if a particular vehicle model develops a reputation for noise problems.

The measurement of disc brake squeal and its relationship to audible and structure-borne vibration measurement is difficult to determine without influencing the vibration by the measurement technique. Ideally, measurements would be taken under 'real' conditions. The complexity and cost of 'in-car' testing was prohibitive. Instead, the approach taken was to use a real car brake system, but mounted in such a way that the support structure carrying the knuckle was as rigid as practically possible. This allowed an array of non-contact displacement transducers to measure the vibration at the disc surface.

This experimental approach was used to investigate how the displacement signals produced by a squealing disc could be processed to determine the mode shapes of the disc and the behaviour of the waves that generate the audible squeal noise.

The two methods used in the analysis of the squeal data were the fast Fourier transform of each data channel and the least-squares analysis of the time domain data. The least-squares approach was the more difficult to achieve, but successfully produced detailed analysis of the behaviour of the wave motion in the disc from the available data.

A finite element analysis of the brake structure compared favourably with the frequencies and mode shapes obtained by both modal hammer tests and squeal tests.

The use of this type of dynamometer, measurement system and analysis method has proved successful in providing a deeper understanding of the mechanisms involved in disc brake squeal.

Acknowledgements

I would like to thank all those in the Department of Engineering who have encouraged me during this research. In particular, I appreciate the guidance I have received from Professor Mottershead, Dr. Brookfield, Dr. Ouyang and Dr. Cao.

The experimental brakes research conducted at Liverpool in the last few years could not have started without the initial support from BBA Friction at Cleckheaton who financed the dynamometer construction and provided the Rover brake parts. Later collaboration with Lucas Varsity (later to become TRW) allowed the broadening of the test base to include two types of Mercedes disc brakes.

My special thanks goes to my wife, Pat, for her unceasing encouragement and patience and for proof reading this thesis.

Contents

Chapter		Page
	Acknowledgements	
	Summary	
	Contents	i
	List of Figures	v
	List of Tables	ix
1	Introduction	1-1
	1.1 Problem description	1-1
	1.2 Scope and description of contents	1-2
	1.3 Author's contribution	1-3
2	Literature survey	2-1
	2.1 Early work	2-1
	2.2 Theoretical studies	2-4
	2.2.1 Sprag-slip	2-4
	2.2.2 Cantilever-disc model	2-5
	2.2.3 Kinematic constraint instability – Pin-on-disc models	2-5
	2.2.4 Binary flutter	2-6
	2.2.5 Friction follower force	2-8

Chapter		Page
2.3	Experimental investigations	2-10
	2.3.1 Pad design and friction	2-12
2.4	Squeal visualisation	2-12
	2.4.1 Laser holography	2-12
	2.4.2 Laser Doppler vibrometry	2-14
	2.4.3 Laser speckle interferometry	2-14
2.5	Research reviews	2-15
3	Experimental dynamometer – design and use	3-1
3.1	Initial design parameters	3-1
3.2	Dynamometer layout	3-3
3.3	Choice of displacement transducers	3-9
	3.3.1 Laser methods	3-9
	3.3.2 Non-contact displacement transducer array	3-10
3.4	Dynamometer use	3-11
3.5	Brake tests	3-12
	3.5.1 Method 1 – Standard recording	3-13
	3.5.2 Method 2 – Throughput recording	3-15
	3.5.3 Method 3 – High speed recording	3-16
3.6	Hammer tests	3-18
4	Theory	4-1
4.1	Nomenclature	4-1
4.2	Squeal waves in disc brakes	4-2
4.3	The wave equation	4-3
5	Data analysis method	5-1
5.1	Data preparation	5-2

Chapter		Page
	5.2	Time domain data 5-2
	5.3	Squeal frequency estimate 5-5
	5.4	Travelling and standing waves 5-6
	5.5	Nodal diameter evaluation 5-12
	5.6	Squeal parameter determination 5-15
	5.6.1	Travelling wave analysis 5-15
	5.6.2	Standing wave analysis 5-21
6	Hammer test results	6-1
	6.1	Introduction 6-1
	6.2	Hammer test on the full disc 6-2
	6.3	Hammer test on the disc with the brake applied 6-8
	6.4	Hammer test results 6-9
	6.5	Full brake hammer tests 6-17
7	Squeal test results	7-1
	7.1	Recording squeal events 7-1
	7.2	Squeal test results 7-2
	7.2.1	Rover brake with solid disc 7-3
	7.2.2	Mercedes brake with solid disc 7-11
	7.2.3	Mercedes brake with vented disc 7-17
8	Finite element results	8-1
	8.1	Finite element analysis of brakes at Liverpool 8-1
	8.1.1	The combined FE and analytical model 8-3
	8.1.2	The full FE model 8-7
	8.2	Comparison of FE results with hammer tests 8-7
	8.3	Comparison of FE results with squeal tests 8-11

Chapter		Page
9	Conclusions and future work	9-1
9.1	Conclusions	9-1
9.2	Future work	9-2
9.2.1	Drive parameter variation	9-2
9.2.2	Mounting stiffness	9-3
9.2.3	High speed recording	9-4
9.2.4	Analysis development	9-5
9.2.5	Squeal test development	9-5
9.2.6	Finite element development	9-6
	References	R-1
	Appendix A : Measurement method	A-1
A.1	Data logging instrumentation	A-1
A.2	Monitoring instrumentation	A-2
	Appendix B : Calibration procedures	B-1
B.1	Temperature calibration	B-1
B.2	Speed calibration	B-2
B.3	Torque calibration	B-2
B.4	Pressure calibration	B-3
B.5	Displacement calibration	B-3
B.6	Trigger calibration	B-4
	Appendix C : Disc details	C-1

List of Figures

Figure	Page
Chapter 3	
3-1	Dynamometer drive train – schematic 3-3
3-2	Rover knuckle support 3-4
3-3	Mercedes knuckle support 3-5
3-4	Flexible drive shaft arrangement 3-6
3-5	Hydraulics layout – schematic 3-7
3-6	Transducer layout viewed from driven side 3-8
3-7	Transducer adjustment mechanism 3-9
3-8	Instrumentation schematic 3-12
3-9	Comparison of power spectra from a displacement transducer and a microphone 3-15
Chapter 4	
4-1	Disc geometry 4-2
Chapter 5	
5-1	Typical time history of a squeal event 5-4
5-2	Typical power spectrum plot for the full frequency range 5-5
5-3	Power spectrum plot of the 7507.5 Hz squeal signal 5-6
5-4	Typical time trace of filtered squeal data 5-7

Figure		Page
5-5	Determination of a forward travelling wave from simulation data	5-8
5-6	Determination of a forward travelling wave from recorded data	5-9
5-7	Determination of a backward travelling wave from recorded data	5-10
5-8	Determination of a standing wave from simulation data	5-11
5-9	Determination of a standing wave from recorded data	5-11
5-10	Range of antinode pitch angles for 60% to 90% antinode compression for each disc mode order	5-13
5-11	Plot of free mode frequency / node pitch angle for the three discs	5-14
5-12	Least squares error for a simulated backward travelling wave (equation 5.2)	5-17
5-13	Least squares error for a simulated backward travelling wave (equation 5.1)	5-18
5-14	Least squares error for a simulated backward travelling wave (equation 5.1)	5-19
5-15	Least squares error for a simulated standing wave (equation 5.1)	5-19
5-16	Least squares errors from a recorded forward travelling wave squeal event	5-20
5-17	Least squares errors for all channels from a recorded squeal event	5-20
 Chapter 6		
6-1	Mercedes vented disc – full disc mode shapes	6-3 to 6-8
6-2	Mercedes vented disc – mode alignment for $[j = 2, n = 0]$	6-14

Figure	Page	
6-3	Mercedes vented disc – mode alignment for [$j = 1, n = 1$]	6-15
6-4	Mercedes vented disc – mode alignment for [$j = 3, n = 1$]	6-16
6-5	Mercedes vented disc mode shapes from the full brake hammer test	6-18 to 6-21

Chapter 7

7-1	Amplitude / frequency plot for the Rover disc brake	7-6
7-2	Temperature / frequency plot for the Rover disc brake	7-6
7-3	Disc speed / frequency plot for the Rover disc brake	7-7
7-4	Torque / frequency plot for the Rover disc brake	7-7
7-5	Pressure / frequency plot for the Rover disc brake	7-8
7-6	Torque / pressure plot for the Rover disc brake	7-8
7-7	Amplitude / frequency plot for the Mercedes solid disc brake	7-13
7-8	Temperature / frequency plot for the Mercedes solid disc brake	7-13
7-9	Disc speed / frequency plot for the Mercedes solid disc brake	7-14
7-10	Torque / frequency plot for the Mercedes solid disc brake	7-14
7-11	Pressure / frequency plot for the Mercedes solid disc brake	7-15
7-12	Torque / pressure plot for the Mercedes solid disc brake	7-15
7-13	Amplitude / frequency plot for the Mercedes vented disc brake	7-19
7-14	Temperature / frequency plot for the Mercedes vented disc brake	7-19
7-15	Disc speed / frequency plot for the Mercedes vented disc brake	7-20
7-16	Torque / frequency plot for the Mercedes vented disc brake	7-20

Figure		Page
7-17	Pressure / frequency plot for the Mercedes vented disc brake	7-21
7-18	Torque / pressure plot for the Mercedes vented disc brake	7-21
Chapter 8		
8-1	Schematic brake assembly for a vented disc	8-2
8-2	Photographs of the Mercedes vented disc brake assembly	8-2
8-3	Smooth rendered FE model of the Mercedes vented disc brake assembly	8-3
Chapter 9		
9-1	Proposed flexible knuckle mounting	9-3
Appendix C		
C-1	Detail of Rover disc	C-1
C-2	Detail of Mercedes solid disc	C-2
C-3	Detail of Mercedes vented disc	C-3

List of Tables

Table	Page
 Chapter 6	
6-1 Rover disc – comparison of mode shapes and frequencies from hammer tests	6-10
6-2 Mercedes solid disc – comparison of mode shapes and frequencies from hammer tests	6-11
6-3 Mercedes vented disc – comparison of mode shapes and frequencies from hammer tests	6-12
6-4 Mercedes vented disc – Z direction [n = 0] disc modes compared with other brake component modes	6-22
6-5 Mercedes vented disc – comparison of squeal modes with disc modes from the full brake assembly hammer test	6-23
 Chapter 7	
7-1 Symbols used in the graphic results	7-3
7-2 Rover brake – test results with standing waves	7-4
7-3 Rover brake – test results with backward travelling waves	7-5
7-4 Mercedes solid disc brake – test results with standing waves	7-11
7-5 Mercedes solid disc brake – test results with forward travelling waves	7-12
7-6 Mercedes solid disc brake – test results with backward travelling waves	7-12

Table	Page	
7-7	Mercedes vented disc brake – test results with standing waves	7-17
7-8	Mercedes vented disc brake – test results with backward travelling waves	7-18
 Chapter 8		
8-1	Mercedes vented disc – comparison of mode shapes and frequencies between the hammer test on the full disc and the equivalent finite element analysis	8-9
8-2	Mercedes vented disc – comparison of mode shapes and frequencies between the hammer test with the brake and the equivalent finite element analysis	8-10
8-3	Mercedes vented disc – comparison of mode shapes and frequencies between the mean squeal frequency and the equivalent finite element analysis	8-12
 Appendix C		
C-1	Brake disc run-out and thickness variation	C-4
C-2	Brake pad effective radius and angular length	C-4

Chapter 1 : Introduction

1.1 Problem Description

Engineers have encountered vibration problems with spinning discs for many years. Circular saws, turbine discs, computer discs, railway wheels, and disc brakes are but a few. The scale of the problems are various – from the catastrophic destruction of a large turbine disc, to an efficiency loss when a saw blade resonates, to a pedestrian's mild annoyance from a passing bus with a squealing brake.

To a pedestrian, a squealing disc brake may be an annoyance, but to the owner of a new car, the occurrence of a squealing brake can be more than annoying and result in a warranty claim to the manufacturer. The cost to the manufacturers of these warranty claims is one of the driving forces behind research into squealing disc brakes. The more that is understood about the mechanisms which cause squeal, the better chance engineers have to design braking systems that are less prone to squeal.

For the past eighty years at least, engineers have been interested in the problems associated with the vibration of discs. Analysis of plate dynamics has led to knowledge of the modal behaviour of discs with various boundary conditions. Analysis of non-linearity and friction follower loads has led to a greater understanding of some of the mechanisms that are believed to cause disc brake squeal. Large finite-element models are now used to attempt to predict the behaviour of new designs. Sophisticated model updating techniques are being developed to allow the finite element models to include a more realistic representation of the contact surfaces in a disc brake.

Much has also been achieved in developing experimental techniques for measuring squeal. Some have been concerned with providing experimental evidence to corroborate theoretical models. Consequently, the experimental conditions were simplified to suit the analytical model. The 'single-pin-on-disc', 'double-pin-on-disc' and 'static disc with rotating mass' types are typical of this approach. Experimental methods used on rotating discs with calliper brake pads have used a variety of measurement methods, notably laser speckle interferometry, laser Doppler vibrometry, laser holography and inductive and capacitive non-contact transducers.

A combination of analysis with an ability to experimentally verify the efficacy of the analytical techniques will eventually allow design engineers to predict the vibration behaviour of a new design. For example, this will allow vehicle brake manufacturers to produce a quieter brake design from the drawing board without having to manufacture so many prototype systems which are both expensive and time consuming to produce and test.

1.2 Scope and description of contents

The scope of this thesis is to provide detailed information about the design and implementation of a disc brake test rig for measuring friction induced disc squeal. It also shows a method of using the measured data to extract information about the disc mode shapes and the characteristics of the forward and backward travelling waves and stationary waves inherent at squeal frequencies.

A brief introduction to previous work in the field of brake squeal is given in Chapter 2. It includes references to early classical plate dynamics, simple model analysis and the more recent analytical work with finite-element methods, non-linear behaviour and model updating. Some experimental methods are mentioned, in particular those using laser speckle interferometry, laser Doppler vibrometry, laser holography and various non-contact transducers.

The design, construction and use of the experimental brake dynamometer is explained in Chapter 3. The design parameters and limitations are shown and the operating procedures are described. Details of the test procedures for the three brake systems on the dynamometer are given. These include modal hammer tests on the discs and modal tests on the brake assembly in its squeal test configuration.

The theory of travelling and stationary waves in a disc brake is described in Chapter 4. How this theory is used to analyse the test data is shown in Chapter 5, with the analysis process and outcomes explained using simulation data.

The results of the hammer tests on the three brake discs and the hammer test on the complete Mercedes vented disc brake are given in Chapter 6. Chapter 7 gives the results of the squeal tests from the three brake systems. Details from a few example tests are given as comparison to the previous simulation analysis. A summary of the finite element work on the Mercedes vented disc brake carried out by others at Liverpool follows in Chapter 8, with a comparison of results from Chapters 6 and 7.

A summary of the discussion with conclusions is given in Chapter 9. Proposals are also given for future work which would further the aims and goals of the brake design engineer.

1.3 Author's contribution

As a piece of experimental research, the dynamometer was probably the most significant part of the project. The general layout was agreed in conjunction with BBA Friction. Apart from the bought-in components and the initial fabrication and machining, the dynamometer was designed, built and commissioned by the author. BBA Friction provided the Rover knuckle, several brake discs and a brake unit with several pairs of brake pads. When Lucas Varity (later to become TRW) became interested in a parallel research contract in association with BBA Friction, they contributed a Mercedes knuckle with brake units for a solid and vented disc. As the

dynamometer was initially designed for the Rover knuckle, modifications were made to accommodate the Mercedes knuckle.

Software for the Mentor motor controller was written so that the dynamometer could be controlled in different ways. It could act as a standard flywheel dynamometer or run at controlled constant speed against the brake torque.

A program was written using LabView software to allow constant monitoring of disc temperature, disc speed, braking torque and hydraulic pressure on the dynamometer during squeal tests.

A method was found for balancing the calibration values of the twelve displacement transducers so that they would give a unified picture of the squeal modes.

Many squeal tests were recorded from each of the three brake systems using a high speed data logging system. Specific Matlab (1995) programs were written to convert the recorded data to matrix form, produce power spectra, generate filtered data sets, show time-stepped disc shapes and make comparative parameter evaluations of these results.

Modal hammer tests were performed on the three brake systems using the LMS modal analysis system. The mode shapes and frequencies from these hammer tests were compared with the squeal test results.

The squeal test results and the hammer test results for the Mercedes vented disc system were compared with finite element results obtained by others at Liverpool University.

Chapter 2 : Literature Survey

Extensive research has been carried out on the vibrational behaviour of brake discs over the last eighty years. The methods used have varied from the purely theoretical to the descriptive experimental with almost every combination in between. This chapter has been divided into several sections in an attempt to group specific types of research. It starts with a synopsis of early work to show the way in which research in this field developed. As the research became more specialised, it has been grouped into three main sections; theoretical studies, experimental investigations and squeal visualisation. Finally there is a section on research reviews.

2.1 Early work

After seeing some 'pretty experiments' on rotating india-rubber membranes, Lamb and Southwell (1921) carried out fundamental analytical research on the transverse vibration of an unconstrained spinning disc. Their interest lay in the problems associated with the failure of turbine discs caused by resonance between the periodic forces from the steam jets and the natural frequencies of the spinning disc. In this paper they assumed that the mode shapes were fixed in disc co-ordinate space. In the same year Southwell (1921) extended this to include a disc clamped at some radius. He found that this form of clamping radically changed the circumferential modes and the first few radial modes of the disc, but did not change the higher radial modes very much. This formed the basis of further analysis of spinning disc vibration theory, particularly with regard to problems of thin spinning discs, such as computer discs and circular saw blades, in which the stiffening effect of the centrifugal forces was

more important than the static flexural rigidity. Although the problems associated with centrifugal forces in the spinning disc are not important with regard to the slow rotation speed of the disc in an automotive disc brake, these papers form an extremely important basis from which further analysis of disc vibration problems was developed.

Changes in the way the disc brake parts interacted were investigated by Fosberry and Holubecki (1959) who experimented on disc brake squeal by varying the way in which the pad was mounted in the calliper and by using a circumferentially split brake disc to increase disc damping. They found that squeal was reduced by offsetting the pad from the piston in the direction of rotation, supporting the pad friction material directly against the calliper instead of the backing plate, using a split disc and using an auxiliary pair of pads at a disc antinode. They continued their experimentation (Fosberry and Holubecki, 1961), making changes to the calliper design and using various pad backing plates to find an appropriate mechanism for reducing brake squeal. They found that the most effective method was the use of a slightly dished steel disc inserted between the piston and the pad backing plate.

The problems were not confined to the automotive industry. In research for the rail industry, Spurr (1961) developed theories about the development of squeal in railway disc brakes. This work compared experimental results from a dynamometer with those recorded from London Underground trains. He concluded that disc brake squeal was dependent on three main factors – high friction coefficient, specific brake pressures and the arrangement of the elastic support for the brake pad.

To consolidate the theory of friction induced vibration in a spinning disc, Jarvis and Mills (1963) used cantilever-disc experiments to verify the friction model and investigate the coupling effects between the natural frequencies of the cantilever pin and those of the disc.

Iwan and Stahl (1973) investigated the problem of the instability of computer discs by first analysing the behaviour of a stationary disc excited by a moving mass-spring-damper system. They used a truncated eigenfunction expansion from which a

large number of modes could be extracted. Iwan and Moeller (1976) extended the analysis for the rotating disc excited by a static mass-spring-damper system. Both of these papers were concerned with rapidly rotating discs or loads where an important factor was the first critical speed, when the disc rotation speed equals the lowest natural frequency. The behaviour of computer discs above this critical speed is important as increased load damping can cause increased instability in the disc. For the study of automotive disc brakes this critical speed is never achieved. However, these papers provide an important contribution to the body of analysis related to spinning discs with stationary loads.

Also in 1976, North (1976) was examining the four theories given since 1960 to explain disc brake squeal. These theories were:-

1. Two degree-of-freedom with kinematic constraint (sprag-slip model).
2. Non-linear self-excited oscillation (cantilever-disc model).
3. Three degree-of-freedom with kinematic constraint (pin-on-disc model).
4. Eight degree-of-freedom binary flutter model.

North compared these models of squeal generation to the observable facts that were known about the phenomenon, namely:

1. Generation of harmonics.
2. Generation of squeal over a limited pressure range.
3. Generation of simultaneous disc modes.
4. Generation of vibrations over a wide frequency range.

North concluded that binary flutter of two disc modes was the more realistic model for the analysis of disc brake squeal. Some of these models are discussed in more detail in the following sections.

A descriptive paper by Lang and Smales (1983) defined the various types of vibration problems that were encountered by the disc brake industry. In it they describe squeal as “the lowest frequency geometrically induced instability which

involves transverse disc vibration”. They described this low frequency squeal in terms of the relationship between the pad length and the disc mode wavelength and considered it to be low frequency squeal up to four nodal diameters and high frequency squeak for modes with greater than four nodal diameters. It not only described squeal, but also categorised judder, groan and hum which were at lower frequencies than squeal and high frequency squeak, squelch and wire-brush.

The generic term ‘squeal’ has been used in this thesis for all the geometrically induced instabilities measured on the discs, with modes from 2 nodal diameters to 8 nodal diameters, a frequency range between 1 kHz and 8 kHz.

2.2 Theoretical studies

Several theoretical models for disc squeal have been investigated. The following studies were for disc noise from diametral disc modes from 2-diameters to 8 diameters. For a car disc brake, the noise frequencies would be between 1 kHz and about 10 kHz.

2.2.1 Sprag-Slip

Prior to 1960, the generally accepted squeal theory assumed the squeal generation mechanism was the variation in the dynamic friction coefficient. The first development away from this assumption was by Spurr (1961) who investigated the geometric relationship between the disc and calliper and developed a model that was independent of the dynamic friction coefficient. He concluded that the geometry of the system determined the cycle of sprag and slip that took place. However, this theory assumed that the disc was rigid and so could not be used to predict squeal in the disc.

2.2.2 Cantilever-disc model

Jarvis and Mills (1963) used a cantilever-disc experimental arrangement to verify their theoretical friction model. They concluded that, for the cantilever-disc model, the cause of the vibration was the coupling effect between the natural frequencies of the cantilever pin and those of the disc. Variation in the coefficient of friction with relative velocity was not sufficient to cause this instability. This led to the important conclusion that unwanted vibration in a disc-friction situation could be controlled by the design of the components.

2.2.3 Kinematic constraint instability – Pin-on-disc models

A mathematical simulation of an experimental cantilever-disc model was first given by Jarvis and Mills (1963) and was discussed earlier. However, it was twenty years later that this model was extended by Earles and Badi (1984), who added a second pin to form the analysis of a double-pin-on-disc system. In their analysis, supported with experimental evidence, they reinforced the earlier conclusions that the disc vibration was a kinematic constraint instability in which the instability can be induced and possibly controlled by the geometry of the system. They also concluded that at least one of the pins must have a negative (digging-in) angle of orientation to the disc for instability to occur. This angle must be in the range $0^\circ < \theta < \tan^{-1} \mu$ where for 0° the pin is normal to the disc and μ is the friction coefficient. This paper is an important step in the theoretical understanding of the effect that pin orientation angle, friction coefficient, disc stiffness and pin support torsional stiffness have on squeal behaviour.

The theoretical basis of a double pin-on-disc system was given by Earles and Chambers (1987) which showed how changes of model parameters affected the predicted squeal generation in the disc. A year later they (Earles and Chambers, 1988) produced a paper that described some of the contributing factors for the instability of an experimental single-sided disc brake. In this they used an

experimental brake with a large pad contact area. Although this was not a true representation of a commercial disc brake, they were able to change many of the operating parameters over wide ranges to compare with their theoretical predictions. Generally, they found that an increase in stiffness of any part of the brake increased the tendency to squeal and an increase in damping reduced the tendency to squeal. However, these parameters are not easily changed in an independent fashion. For example an increase in disc damping would be difficult to achieve without decreasing the disc stiffness.

A general theory for many aspects of friction induced noise was given by Akay (2002) in which he used an experimental pin-on-disc for verification. In this he explains the development of mode lock-in between the pin and the disc in which the mode shape in the disc is stationary in space co-ordinates. The term 'mode lock-in' used by Akay referred to the interaction between different components of a structure in which the vibration behaviour of one component influenced that of another. It is interesting to note here that the mode-locked frequency is at the higher of the split frequencies that represents a cosine mode in the disc. That is, the antinode of the disc mode shape is aligned with the pin position. Inspection of the experimental results in Chapter 5 shows that for the diametral modes the brake pad is aligned with the antinode for the lower frequency and the node for the higher frequency.

2.2.4 Binary flutter

North (1976) concluded that binary flutter was the most promising of the analyses that were available as it allowed for two degrees of freedom in the disc. The pin-on-disc model was limited to one degree of freedom. North's model represented the disc sandwiched between two flexible pads that had both translational and rotational stiffness. In this binary flutter model, it was assumed that the pad backing plate was stationary (i.e. did not vibrate) which meant that any axial displacement of the disc would cause an increase in pressure on one pad and a decrease on the other pad.

This variation in pad pressure would cause equivalent changes to the local frictional forces that would induce a moment in the disc. If this fluctuating friction-induced moment resonated with a natural frequency of the disc then it was possible for squeal to occur. North's model was extended by Millner (1978) to include two degree of freedom models of the pad and calliper, coupled by a kinematic constraint. This fixed calliper analytical model included mass and stiffness parameters and allowed for pad and piston contact variations.

An attempt to clarify the mechanisms that produced disc brake squeal was given by Murakami et al. (1984) using both finite element analysis of the various brake components and comparing the frequencies obtained with holographic images from a squealing disc brake. However, the combination of findings to both support and refute the idea that coupled modes can induce squeal, show that brake squeal is a complex subject.

This methodology was continued by Brooks et al. (1993) who used a twelve degree of freedom lumped parameter model of a disc brake to carry out an eigenvalue sensitivity analysis of brake squeal. In this they used a complex brake arrangement with two independently pressurised pairs of pistons, one pair near the leading edge of the pads, the other pair near the trailing edge of the pads.

A four degree of freedom model was produced by Nishiwaki (1993) which compared the mechanisms of drum brake squeal, disc brake squeal and disc brake groan. He concluded that drum brake squeal, disc brake squeal and disc brake groan (lower frequency than squeal) all had the same causal mechanism and could be approached with the same analytical procedures.

2.2.5 Frictional follower force

Several authors have studied the influence of the frictional follower forces on the dynamics of a rotating disc. In this analysis, the reaction of the mass (force, stiffness and damping) remains normal to the deformed disc surface.

Shen and Mote (1991) examined the instabilities of a stationary disk, moving load system to explain the mechanisms involved. Following this, still with computer discs in mind, Chen and Bogy (1992) investigated the parameters that affect the analysis of a flexible spinning disc with a stationary load system. This work was of particular interest with regard to the dissemination of the disc vibration into forward and backward circumferentially travelling waves. They also reported (Chen and Bogy, 1993) that when the in-plane membrane stress field was included in the analysis, the first order stability of the disc was not affected. Plate damping was included in the analysis by Shen (1993). All this work was important for two reasons: (1) it confirmed that friction follower forces were a potential candidate for generating disc vibrations when the disc was rotating at speeds less than the critical speed and (2) it developed analytical techniques for studying the effect of follower forces in disc vibrations.

The PhD thesis by Chan (1993) produced a comprehensive study of disc brake vibration with specific emphasis on the analysis of follower force induced squeal. He used state-space and multiple scales analysis on a static annular plate with a rotating concentrated mass-spring-damper load that remained normal to the disc surface. With this analysis he concluded that (1) the plate was unstable with a small force when a nodal diameter mode was present, (2) for the nodal diameter mode, backward travelling waves were destabilised and forward travelling waves were more stable and (3) this form of instability can occur at disc speeds less than the critical speed and are not related to disc speed.

The analysis by Chan et al. (1994) was for a stationary disc with a rotating mass-spring-damper system. A frictional follower force was assumed. Two analysis

methods were compared for sub-critical disc speeds, the method of multiple time scales and the state-space eigenvalue analysis. They both showed a strong correlation indicating discrete conditions of instability at low brake pressures merging to an almost constant instability at high brake pressures. The effects of varying the mass, stiffness and damping were also investigated. This showed that an increase in stiffness slightly increased instability, an increase in mass-produced a large increase in instability and an increase in damping tended to reduce the instability.

Again, looking at a stationary disc with a rotating follower force type mass-spring-damper, Mottershead and Chan (1995) used a finite element approach to investigate flutter instability. Amplitude and phase plots that were anticipated from the flutter of doublet (split) nodal diameter modes of the disc were illustrated.

Research on the stability of 'floppy' computer discs by Huang and Mote (1996) produced a theoretical analysis for a spinning disc with rotating damping forces. The main interest here lies in the instability caused by increased damping when disc speeds are above the critical speed. The paper is important in that it tackles the inclusion of large damping values in an analysis of follower forces on a rotating disc and includes the centrifugal stiffening forces in the disc.

The stability of a rotating disc with a stationary frictional follower force was studied by Lee and Waas (1997) who looked at the interaction of forward and backward travelling waves in a laminated isotropic disc and a polar orthotropic disc.

Meanwhile, Mottershead et.al. (1997) continued the finite element approach and concluded that for sub-critical speeds of the disc, parametric resonances were caused by friction follower forces. The effect of disc damping was stronger than that of pad damping in stabilising these resonances.

Research on the full disc brake system was continuing. Ouyang et al. (1999, 2000) suggested a procedure for determining disc brake instabilities using a state-space method. An analytical structure (the disc) combined with a finite element structure

(the brake calliper and pads) was used to find the instabilities of the brake system. The friction model used was simple Coulomb friction and the squeal generation mechanism was assumed to be binary flutter. The finite element model of the brake structure and the analytical model of the disc were the equivalent of the Mercedes vented disc brake, for which experimental results have been recorded in Chapter 7.

2.3 Experimental Investigations

Harding and Wintle (1978) combined theory with experimental tests on disc brake pads to determine the critical length of the brake pad. The critical length here is the pad length that remains in contact with the disc when pressure is applied to the brake and is related to the stiffness of the back plate and friction material, the pad / piston contact geometry and the pad / calliper contact geometry.

Squeal parameter measurements were made by Bracken and Sakioka (1982) using brake dynamometers to measure noise with a microphone. An FFT analyser was used to measure squeal frequency and amplitude.

Other dynamometer tests were conducted by Tarter (1983) who compared the noise produced by production brakes to those where the component material or geometry had been modified. Several pad materials were tested. The pad geometry was modified by milling parts of the pad material away, and the disc was modified by cutting radial slots into the surface. Measurements of squeal were recorded using a microphone and an accelerometer placed on the calliper. Although changes to the noise behaviour were noticed, very little systematic analysis of the results was given. Schwartz et al. (1985) conducted both dynamometer tests and in-vehicle tests (primarily for creep-groan) with a view to systematically modifying the pad material and the geometry of the pad and calliper to reduce brake noise. The noise measurements were recorded with a microphone and fast Fourier transform methods were used to determine the squeal frequencies and amplitudes.

Yu and Mote (1987) were working on both the analysis and experimentation of circular saw blades. A simplification of a circular saw blade was given as a thin steel disc with either three, four or six equally spaced short radial slots cut into the perimeter that introduce cyclic symmetry. This serves to split the appropriate repeated modes. For, say, a disc with four slits, the two diameter repeated mode splits into two distinct frequencies. The mode shape of the lower frequency (referred to as a sine mode) has the slits aligned with the node and the higher frequency has the slits aligned with the antinode (referred to as a cosine mode). This paper is important in that it developed a method of analysing the vibration behaviour of asymmetric discs. The brake squeal problem is asymmetric due to the brake pad contact.

Samie and Sheridan (1990) investigated the brake pad contact pressure using both finite element analysis and experimental validation. However, no account of the effect of torque or friction could be included as pressure sensitive paper was used to measure the pad contact pressure.

Ghesquiere (1992) performed both in-car and dynamometer tests on disc brakes with an analysis that included calliper and pad effects. However, the work lacked a comparison between the theory and experiment.

A method was developed by Butcher and Ewins (1997) for multidimensional decomposition of time varying response signals from rotating shafts and discs. Short-time Fourier transforms were used to build the time-frequency distribution of the instability from measured data.

Lee and Kim (1996) carried out experiments on a stationary disc excited axially by a non-contact shaker near its rim. They produced a method of determining directional frequency response functions to separate and identify the forward and backward travelling waves in the disc.

Dunlap et al. (1999) investigated various types of brake noise including low and high frequency squeal. In this overview, low frequency squeal was explained as disc

vibration modes normal to the disc surface between about 1000 Hz and 5000 Hz. High frequency squeal was classified as that above 5000 Hz, predominantly from circumferential modes of the disc usually coupling with another mode of the brake structure. These tests were apparently carried out in-vehicle, but the paper does not detail the test set-up.

2.3.1 Pad design and friction

Road and traffic conditions changed dramatically in the 1980s. New legislation preventing the use of asbestos, a primary ingredient in brake linings, meant that fundamental changes had to be made to brake lining materials. Longley and Gardner (1988) and McLellan (1988) outlined some of the problems encountered in the design of new materials to conform to the new legislation.

Bergman et al. (2000) investigated the affect of changing the pad area on the generation of disc brake squeal. He found that reducing the pad circumferential length reduced the propensity to squeal but recognised that the method was impractical as a cure for squeal on the grounds of increased thermal loading.

2.4 Squeal visualisation

2.4.1 Laser holography

Holographic interferometry was used by Felske et al. (1978) to measure squeal vibration in the disc brake of a car running on jacks in a laboratory environment. With it, they were able to view disc and calliper vibration patterns during squeal tests. The process involved taking two holographic images that were triggered from the peak amplitudes measured by a proximity probe at an antinode of the required squeal mode.

In Huddersfield, Fieldhouse and Newcomb (1991, 1992) used interferometry methods to visualise both drum and disc brake squeal. Their method used a pulsed ruby laser to illuminate the disc. An interferogram is produced by superimposing two reflected holographic images of the vibrating disc, separated in time by a half squeal cycle to give the maximum fringe density. The interferogram fringe pattern shows the instantaneous shape of the disc from which the mode shape can be deduced. The system can also be used to visualise vibration on the brake pads and callipers.

Laser holography was used by Fieldhouse and Newcomb (1991) on a disc brake that was driven with its drive shaft in a laboratory rig that simulated the mounting arrangement in the vehicle. With no wheel present, holographic images of the disc were produced which showed stationary disc squeal modes (with respect to the pads) and that a trailing edge pad abutment was more stable than a leading edge pad abutment. They also showed that brake noise was coupled to the natural frequencies of the individual parts of the brake mechanism and that noise inhibition may be achieved by making the parts more asymmetric. In a later paper (Fieldhouse and Newcomb, 1992) they made similar conclusions with the exception that the squeal mode was a forward travelling wave rotating in the disc rotation direction at a speed equal to the squeal frequency divided by the disc mode order.

At about the same time, Nishiwaki (1993) was using the results from tests using double-pulsed laser holography to compare with theoretical work.

Further work by Talbot et al. (2000) and Fieldhouse and Talbot (2003) used the same process with time-stepped imagery to show modal animations of the disc, pad and calliper vibrations. With this method, several holographic reconstructions per squeal cycle can be produced. These are digitised, converted to three-dimensional images and animated to enable the mode to be viewed without the need for the subjective hologram interpretation previously required. The information can also be used to estimate the coefficients and phase angles for the forward and backward travelling wave equation for the disc.

2.4.2 Laser Doppler vibrometry

Laser Doppler vibrometry was developed by Stanbridge and Ewins (1996) to look at modal patterns on vibrating discs. The laser Doppler technique uses an interferometer to measure the Doppler shift of a reflected laser light beam from a point on the disc. The Doppler shift is a measure of the velocity of the surface of the disc in the direction of the beam. By building up a pattern of point measurements over the surface of the disc, the mode shape of the disc is found. Richmond et al. (1996) also used laser vibrometry to view the modes of a complete brake system to compare with finite element theory. Their experiments used a stationary disc clamped by the brake pads. A shaker at the pad position excited the 3-diameter mode of the disc.

2.4.3 Laser speckle interferometry

Laser speckle interferometry was being used by Dixon (1998) to record disc vibration mode shapes. A specklegram is produced by mixing a coherent reference beam with a speckle pattern in the image plane. When two specklegrams are superimposed, dark fringe patterns are produced which indicate the magnitude of out of plane displacement. The fringe patterns are the result of the summation of amplitudes from the specklegrams and so can be resolved 'non-optically' (sic, Dixon).

Reeves et al. (2000) used high speed speckle pattern interferometry and near-field sound pressure measurements to verify some of the tests by Fieldhouse. He used the term 'complex mode' for a travelling wave, consisting of a forward and backward wave in the disc.

All these visualisation techniques use information collected over a very short time span to analyse the behaviour of the brake disc and associated components. They are very good at measuring transient behaviour but are not able to view the longer term

development of vibration modes. For example, does a disc squeal mode have a consistent shape or does it switch between travelling and stationary modes? For this type of information, continuous measurement over many squeal cycles is necessary and requires the type of measurement outlined in this thesis.

2.5 Research reviews

Many papers contain reviews of the relevant research. However, because of the plethora of research that has been done on this subject over the last few decades, review papers form an invaluable source of information. Three noteworthy reviews are a discussion paper that outlined the theoretical approaches to disc vibrations (Mottershead, 1998), a short review (Abendroth, 1999) that outlined the experimental and visual techniques that have been used and a comprehensive review of both theoretical and experimental work (Kinkaid et al., 2002). Kinkaid concluded that research into disc brake squeal has come a long way in the seventy years that it has been seriously studied, but that to get much further, non-linear modelling of instability is necessary. This type of finite element analysis of brake structures is now being addressed in Liverpool. It is hoped that the combination of this analysis with the experimental verification capability that is available with the dynamometer will help the industry to design quieter brakes.

Chapter 3 : Experimental dynamometer – design and use

Measurement of disc brake squeal directly from a vehicle would be the ideal method for analysing the phenomenon. However, the irregular and often transitory nature of squeal in disc brakes invites the adoption of more rigorous laboratory investigation techniques. 'In-car' testing is both complex and expensive and the physical application of the detailed measurements needed to analyse the behaviour of the disc would probably affect the squeal event being measured. It was for these reasons that laboratory testing was chosen as the most appropriate means of obtaining meaningful results from a car brake.

Tests on a high volume production car brake system were considered necessary to provide data from squeal events that were relevant to the design of this type of brake. Consequently the complete brake assembly consisting of the hub, steering knuckle, carrier, calliper, brake pads and disc needed to be tested. A dynamometer was designed to provide the necessary disc rotation speed and reaction torque to the brake application.

3.1 Initial design parameters

The design of the dynamometer was achieved through a compromising process, with the desire to be able to cover as large a testing envelope as possible given the constraints of laboratory capability and finance. The most powerful drive motor that could be readily accommodated in the laboratory from the 440 V 3-phase a.c. supply

was 42 kW. The motor chosen was a d.c. motor with a variable speed controller and had a maximum speed of 180 rad s^{-1} (1130 rpm).

The hydraulic pressure in a disc brake system given by the manufacturer was 80 bar, but the problem of brake squeal rarely occurs at such high pressures. The majority of squeal problems occur at pressures of less than 20 bar and because of this, the dynamometer was designed with the maximum power obtainable from the motor matching the power absorbed by the brake with a hydraulic pressure of 20 bar.

If a maximum hydraulic pressure of 20 bar is assumed, then a piston area of 0.00229 m^2 gives a maximum normal force at the pad of 4580 N. For a friction coefficient of 0.4, the effective in-plane reaction force per pad is 1832 N, which, for both pads, gives the maximum in-plane reaction force for the brake as 3664 N. The mean pad radius is 0.11 m, hence the maximum torque at the disc is 403 Nm. The maximum disc speed for which the 42 kW motor is able to give 403 Nm of torque is 104 rad s^{-1} (equivalent to a road speed of about 30 m s^{-1} or 108 km h^{-1}). Thus a speed reduction of 7:4 was necessary to fully utilise the available power from the drive motor.

The need for a speed reduction was fortuitous in that it could be achieved using a toothed belt drive and allowed the drive motor to be positioned above the test rig and thus shorten its overall length, as shown in figure 3-1. This allowed the test rig to be mounted on an existing cast iron test table.

The brake disc was driven from the wheel flange, not from the drive shaft, so that the source of the braking torque appeared to emanate from the torsional resistance of a tyre and not from the transmission. Flexible couplings were used in the drive train between the motor and the torque transducer and between the torque transducer and the brake disc. These flexible couplings allowed lateral misalignment but were rigid in torsion.

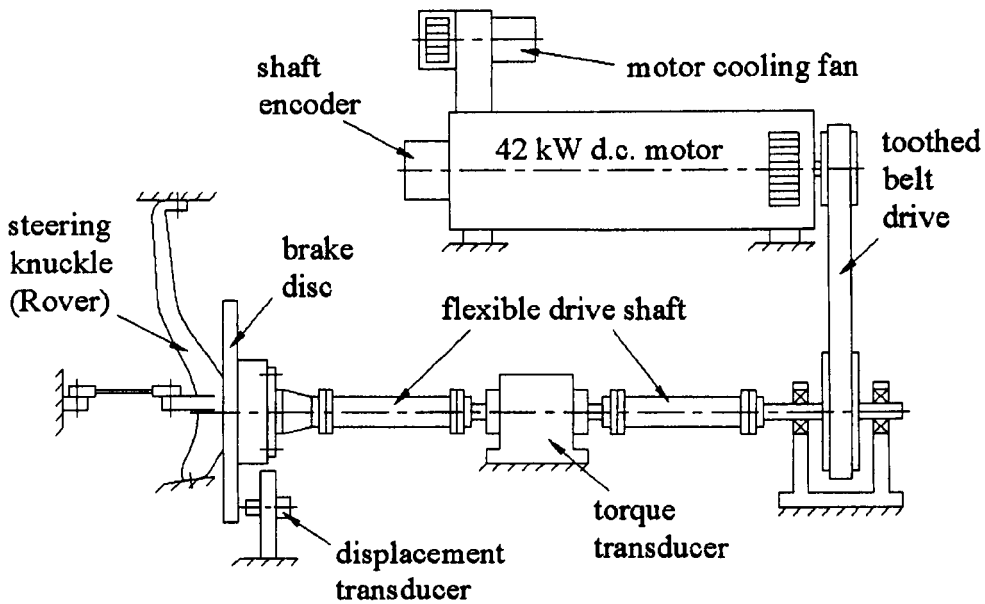


Figure 3-1 : Dynamometer drive train – schematic

3.2 Dynamometer layout

The bed of the dynamometer was an existing cast iron table 1.8 m long and 1.2 m wide with five longitudinal slots on which various supports for the dynamometer components were mounted. The following is a description of the drive train working from the brake disc back to the drive motor.

The brake disc and knuckle were mounted on one end of the table in such a way that either the Rover knuckle (figure 3-2) or the Mercedes knuckle (figure 3-3) could be mounted and have the same drive centre line and brake disk/flange connection position. The Rover knuckle was rigidly attached to the support bracket at the top bolted joint, the bottom ball joint and the steering arm bolted joint. The steering arm was attached to the support with a turnbuckle fitted with a rose bearing at each end to allow the disc to be aligned with the drive shaft. The Mercedes knuckle was rigidly bolted to the support with the two upper bolts and the lower ball joint. The steering

joint was not attached, so alignment was achieved by moving the support on the table.

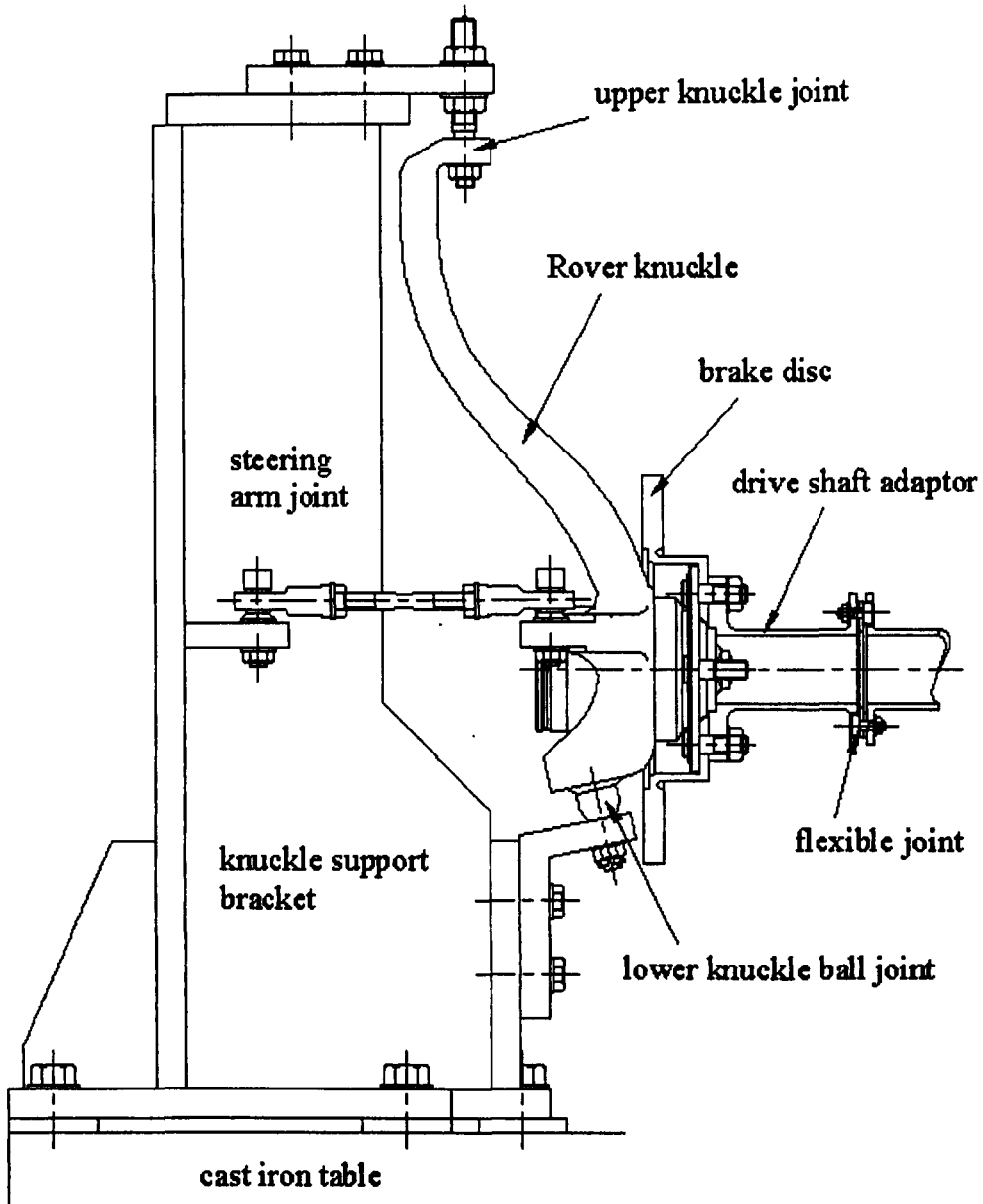


Figure 3-2 : Rover knuckle support

The brake disc was mounted on the knuckle and, using the standard wheel studs and nuts, bolted to a flexible drive shaft connected to the torque transducer. The drive shaft allowed for a small lateral misalignment without imposing large bending forces on the brake disc, but was rigid in the circumferential direction and so would directly

transmit the torque. A section of the drive shaft and couplings is shown in figure 3-4. The coupling at each end of the shaft consisted of a flexible laminated steel disc between two rigid flanges. The laminated disc had 6 bolt positions on its circumference, 3 being bolted to one rigid flange and the alternating 3 being attached to the other rigid flange.

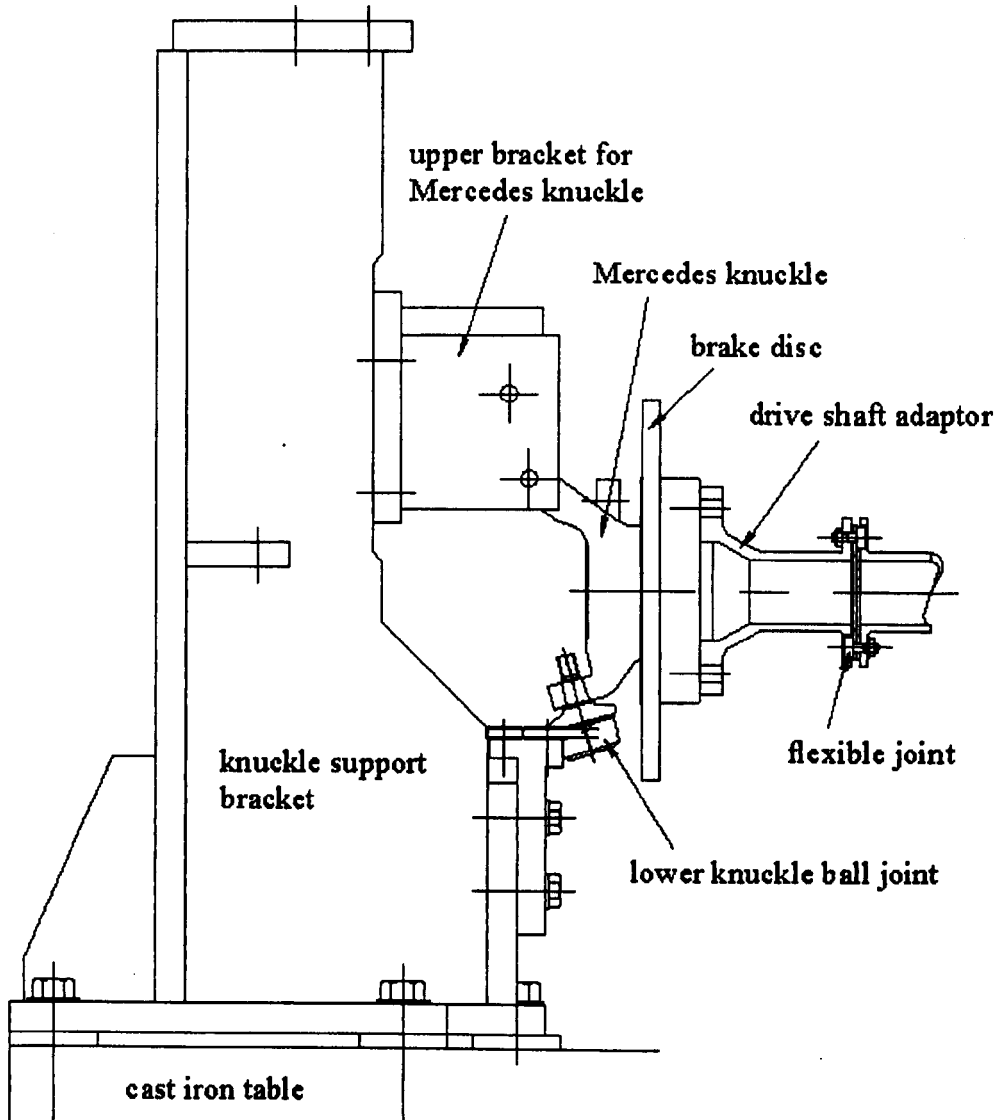


Figure 3-3 : Mercedes knuckle support

The torque transducer was mounted on its own support. The torque transducer chosen was an in-line shaft transducer, which uses the fringe pattern from a pair of

concentric cylinders to produce a voltage which was proportional to shaft torque. Another flexible drive shaft connected the torque transducer to the driven pulley from the motor.

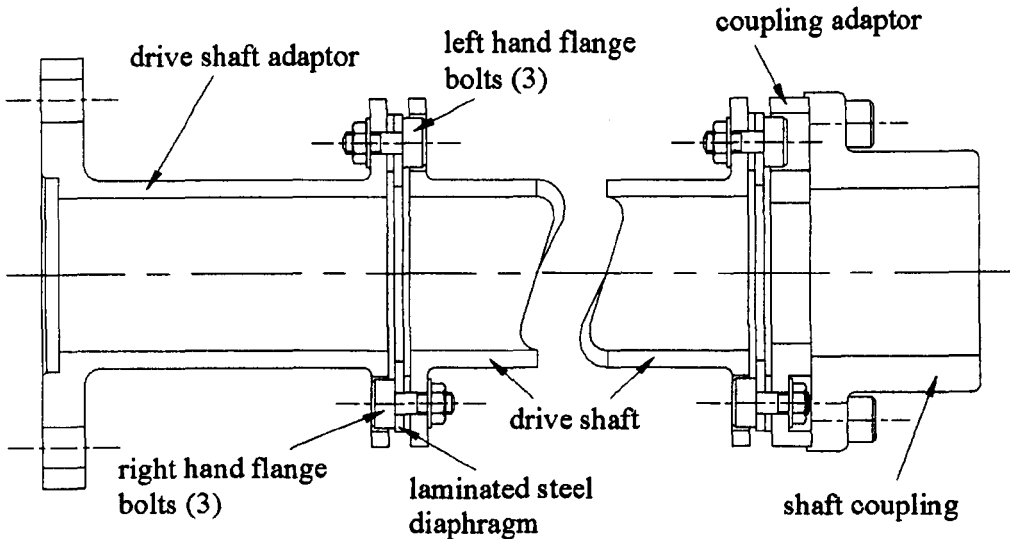


Figure 3-4 : Flexible drive shaft arrangement

The driven pulley on the main shaft was mounted on its own support. This consisted of a solid steel shaft running through two plummer block bearings between which was a Fenner toothed belt pulley. The plummer blocks were fitted with self-aligning bearings. The Fenner pulley was attached to the shaft with a Fenner Taperlock bush. One end of the shaft was connected to the flexible drive shaft, whilst the other end was free. It was expected that the free end would be needed to accommodate an angular measurement or trigger mechanism, but that was not found to be necessary. Instead, an optical switch aligned with a mark on one of the drive shaft flanges was able to provide trigger information to indicate each revolution of the shaft.

A frame above the drive shaft supported the drive motor such that the drive pulley was vertically aligned with the driven pulley on the main shaft. The Fenner drive pulley was fitted to the motor shaft with a Fenner Taperlock bush and connected to the driven pulley with a Fenner toothed belt. The drive motor was mounted on an adjustable frame to allow the drive belt to be tensioned. The motor was fitted with

an external cooling fan. The non-drive end of the motor was fitted with a shaft encoder that allowed accurate values of shaft speed to be recorded.

The motor support frame was attached to the table through rubber blocks so that any high frequency vibrations produced by the motor were isolated from the brake mechanism.

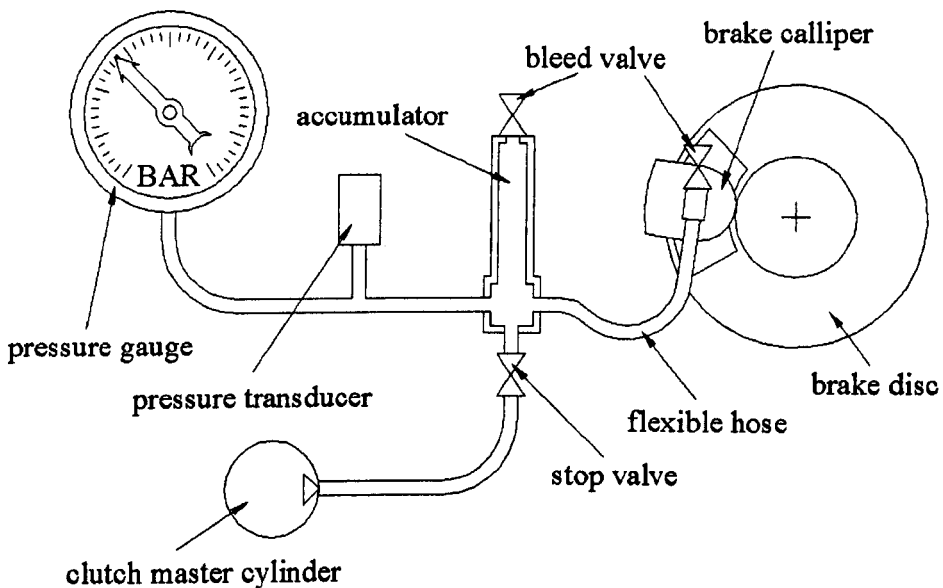


Figure 3-5 : Hydraulics layout – schematic

The brake calliper was attached to the knuckle in the normal way. Hydraulic pressure was applied to the brake piston manually by using an automotive clutch master cylinder. The line pressure was measured with a Bell & Howell pressure transducer for the purposes of data logging and a Bourdon gauge for visual inspection. A small line chamber was used to allow a quantity of air to remain in the hydraulic system to act as an accumulator. This was situated as close to the piston as possible so that a more constant brake pressure could be maintained during a squeal test. A schematic of the hydraulic layout is shown in figure 3-5.

The temperature of the brake disc was measured with a copper-faced thermocouple that provided an analogue voltage for data logging and a digital readout for visual

inspection. The thermocouple location was always on the disc at a point immediately after the disc had passed under the brake pad and near to the outer radius of the disc.

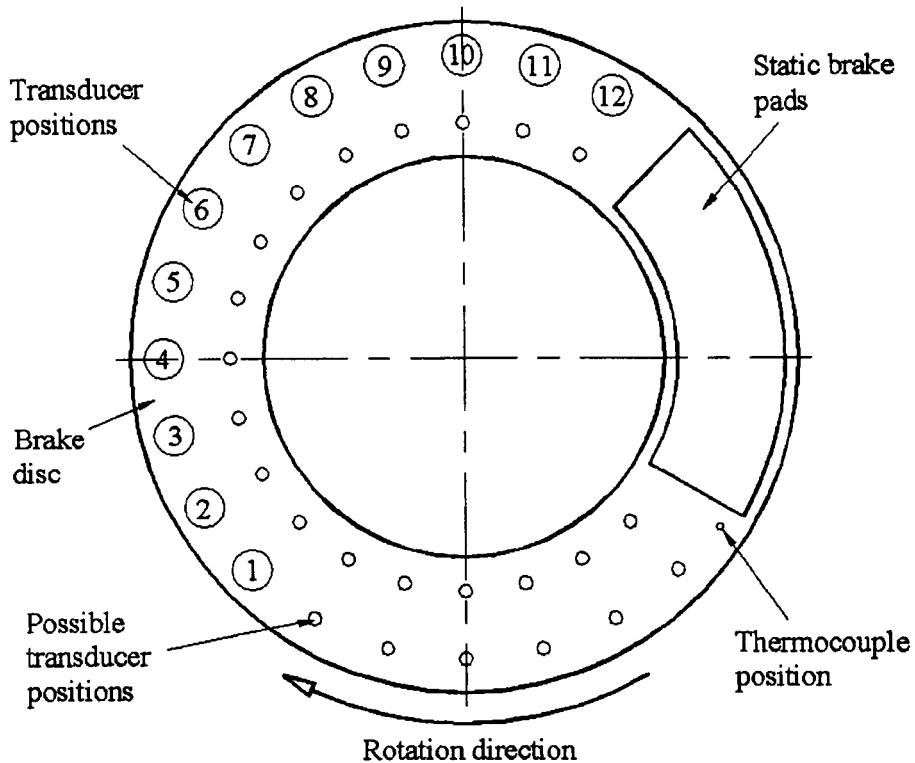


Figure 3-6 : Transducer layout viewed from driven side

A support on the drive side of the disc held the carrier plate for the axial displacement transducers that measure the disc vibration in the axial direction. The support is extremely stiff and can be positioned so that the transducer array is concentric to the disc. The carrier plate has an array of tapped holes at two radii and spaced at intervals of 15 degrees to cover the exposed area of the disc. The arrangement of the transducer array is shown in figure 3-6. Four bolts support the carrier plate to allow the accurate alignment of the transducer faces with the brake disc. The alignment mechanism is shown in figure 3-7.

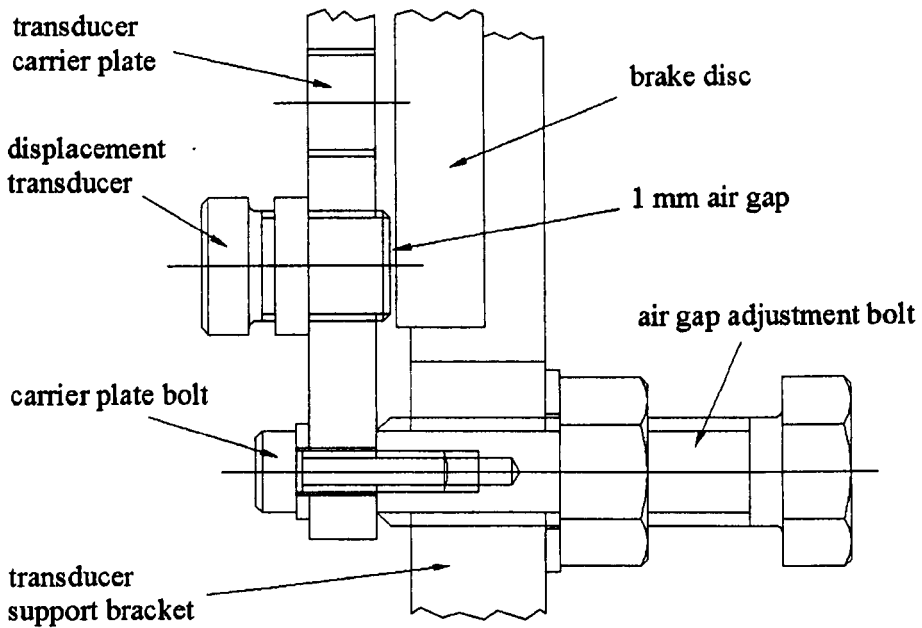


Figure 3-7 : Transducer adjustment mechanism

3.3 Choice of displacement transducers

It was necessary to measure the transverse displacement of the disc face during a squeal event to measure the vibration mode shape of a squealing disc. Ideally, a time history of the complete disc surface should be measured, but, for practical reasons, a compromise was reached. It was evident that, as the measurement process must not interfere with the squeal event, it must be a non-contact method. Two main methods of measurement were investigated, namely laser methods and fixed non-contact transducer arrays.

3.3.1 Laser Methods

There have been many investigations using laser methods of displacement measurement. Of particular relevance are those of Fieldhouse et al. (1991, 1992,

2003) and Talbot et al. (2000) as these investigations have been on disc brake applications.

Of the various types of laser measurement, perhaps the most relevant is holographic interferometry. This method uses a ruby laser to capture a full field image of the disc mode shape at a particular point within a squeal cycle. A fringe pattern showing the displacement of the disc, pad and attached structure is produced by superimposing two holograms, time-stepped by half a squeal cycle. Work on this method of analysing disc brake squeal is continuing at Huddersfield whereby several of these time-stepped images taken at different squeal wave phase positions can be digitised and converted to a 3-dimensional animation of the squealing brake system.

As a visualisation technique, laser holography is undoubtedly successful. However, it is a method that takes a 'snapshot' of a single squeal frequency cycle and does not address the longer time span needed either to view the development of squeal or to investigate the continuity behaviour of the squeal wave. It was for this reason that a different method of measurement was investigated.

3.3.2 Non-contact Displacement Transducer Array

Two types of non-contact transducers were investigated; the inductive type that measured velocity and the capacitive type that measured displacement. The inductive type of transducer was limited to about 5 kHz frequency range due to its use of a carrier frequency and its output would have to be integrated to give displacement measurements. Of the two types of capacitive transducers found, one was limited to a 5 kHz frequency range due to the carrier frequency inherent in its signal conditioning system. The second type did not use a carrier frequency, but relied on a high bias voltage in the conditioning system. Consequently this type of transducer did not suffer from a high frequency limit but did have a low frequency threshold of about 20 Hz. For the squeal tests, this limitation would not pose a problem, consequently this type of transducer was selected.

The chosen transducer was a Bruël & Kjær type MM0004 which has a footprint of about 10 mm diameter and a threaded barrel with locking rings so that it can be inserted into a mounting plate. The exposed surface of the disc allowed a transducer mounting plate to be made with two arcs of transducer positions at different radii and eighteen positions on each arc spaced at 15-degree intervals. Financial constraints limited the number of transducers to 12, which was thought sufficient to allow an analysis of the transverse disc motion during a squeal event.

3.4 Dynamometer Use

The motor controller was supplied with an RS232 serial link for computer control. Programs were written in Microsoft QuickBasic to drive the dynamometer for any tests other than constant speed. For example, it could be driven as a standard flywheel dynamometer using a programmed inertia value.

Both the motor speed and the hydraulic pressure were controlled manually during disc squeal tests. A computer using LabView software was used to monitor the drive parameters and provide a permanent analogue display of disc temperature, disc rotation speed, shaft torque and brake hydraulic line pressure. The disc speed and the hydraulic pressure remained constant during data collection from a squeal test. A schematic diagram of the instrumentation layout is shown in figure 3-8.

A squeal event was recorded in one of three ways. Early tests were recorded as described in method 1 (details of methods 1, 2 and 3 are given later in this chapter) using standard recording methods with the LMS system. Later tests were recorded as in method 2 using the throughput system and finally the high speed recording of method 3 was used which gave the most successful results for analysis.

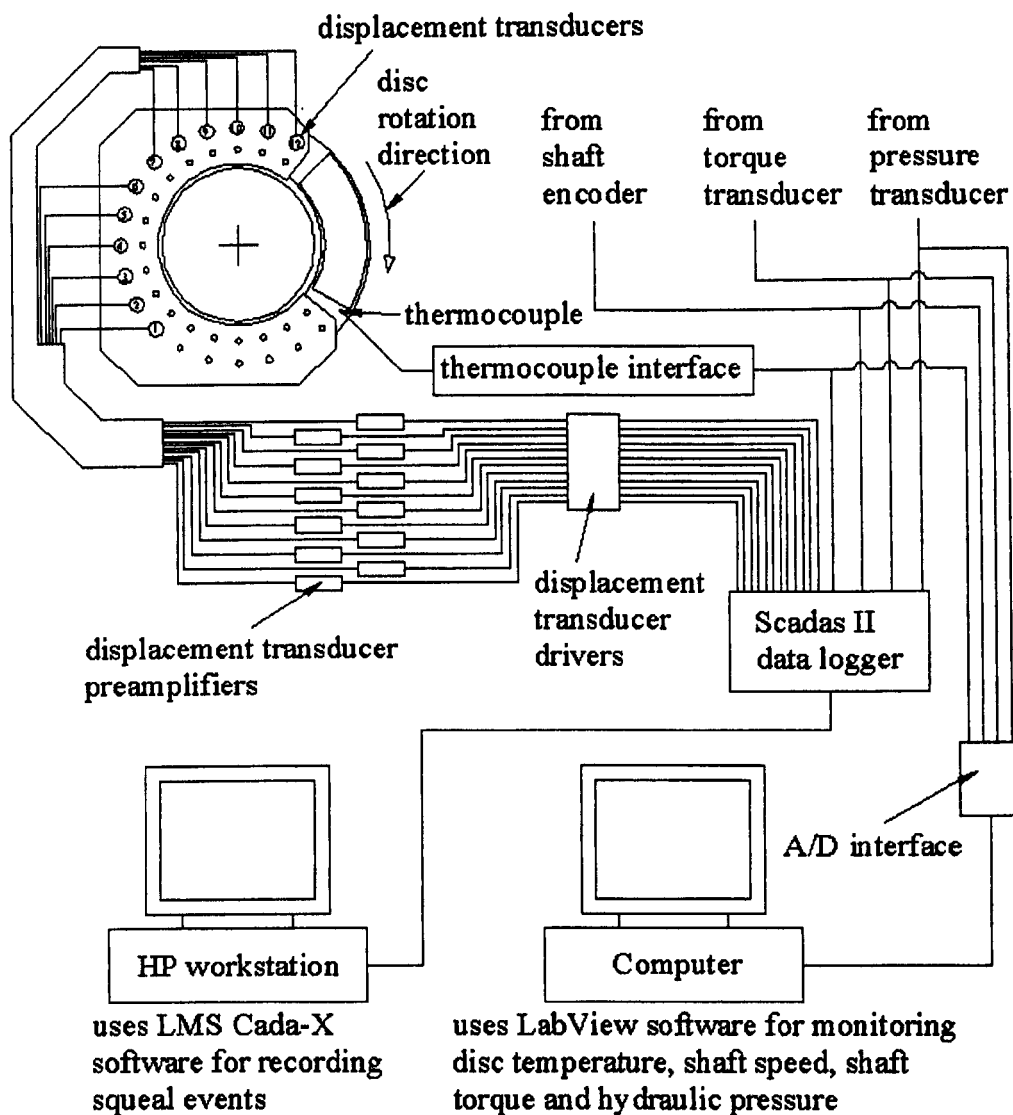


Figure 3-8 : Instrumentation schematic

3.5 Brake tests

The early tests from method 1 (below) were limited by the size of the data collection buffer that allowed for 0.5 seconds of continuous data to be recorded for the number of channels and the logging frequency required. The tests from method 2 were recorded using special throughput monitoring software provided by LMS which logged data directly to the hard disk. For these tests, 8 seconds of data were

collected. Method 3 used a recording speed which allowed the forward and backward travelling waves to be seen without the problems of aliasing. These methods are described below. The detailed procedure of the analysis from method 3 is explained in Chapter 5 using simulation data. The results from recorded squeal tests are given in Chapter 7.

3.5.1 Method 1 – Standard recording

During a squeal event, data from the dynamometer was collected using the LMS Cada-X Fourier Monitor set for logging time domain data. A description of the LMS system is given in Appendix A. An optical switch was set to give one pulse per drive shaft revolution. This was used to begin the data logging process after the system was manually activated. The logging system recorded data simultaneously from 18 channels as follows :

Channel 1	Trigger voltage – triggers at 25% of 10 V rising.
Channels 2 to 13	Displacement transducers 1 to 12 – individually calibrated
Channel 14	Microphone – gain set to 1
Channel 15	Temperature – set at $101.01\text{ }^{\circ}\text{CV}^{-1}$
Channel 16	Speed – set at $10.2326\text{ rad s}^{-1}\text{V}^{-1}$
Channel 17	Torque – set at 40 NmV^{-1}
Channel 18	Pressure – set at 3 barV^{-1}

A full description of the transducer calibration procedures and values is given in Appendix B.

For the tests recorded here the displacement transducers were set as a continuous sequence on the outer arc of the carrier plate with transducer 12 near to the leading edge of the brake pad. Transducer number 1 was considered to be at 0° and transducer 12 was at 165° with a constant 15° spacing between the transducers. For

the disc rotating in the forward direction, viewed from the knuckle side, rotation was positive (anticlockwise). Viewed from the driven side, as in figure 3-6, positive rotation was clockwise.

The expected maximum frequency for squeal events was 8 kHz. The 18 data channels were logged at 16384 Hz to give a Nyquist frequency of 8192 Hz. The maximum number of points the system was able to record at this frequency was 8192 points per channel giving a 0.5 s sample time and 2 Hz frequency resolution.

Although with the recording frequency at approximately 16 kHz, analysis of the squeal event was able to show squeal frequencies up to about 8 kHz, noise in the data made it difficult to extract phase shift information to determine the nature of the squeal waves in the disc. However, the power spectra from these squeal events gave clear indication of squeal frequencies. Some squeal events, particularly those at lower frequencies, gave a good indication of the disc mode, but confident recognition of travelling wave events was not possible. Power spectra from the microphone data confirmed that the information from the transducers was related to audible squeal noise. Figure 3-9 shows the comparison between the power spectra from one of the displacement transducers and the microphone, both recorded during test Sq02t1 on the Mercedes solid disc brake. Both data sets have been smoothed using a 5-point moving average. The power values from the microphone have been normalised to the peak power value from the displacement transducer at the 1666 Hz squeal frequency.

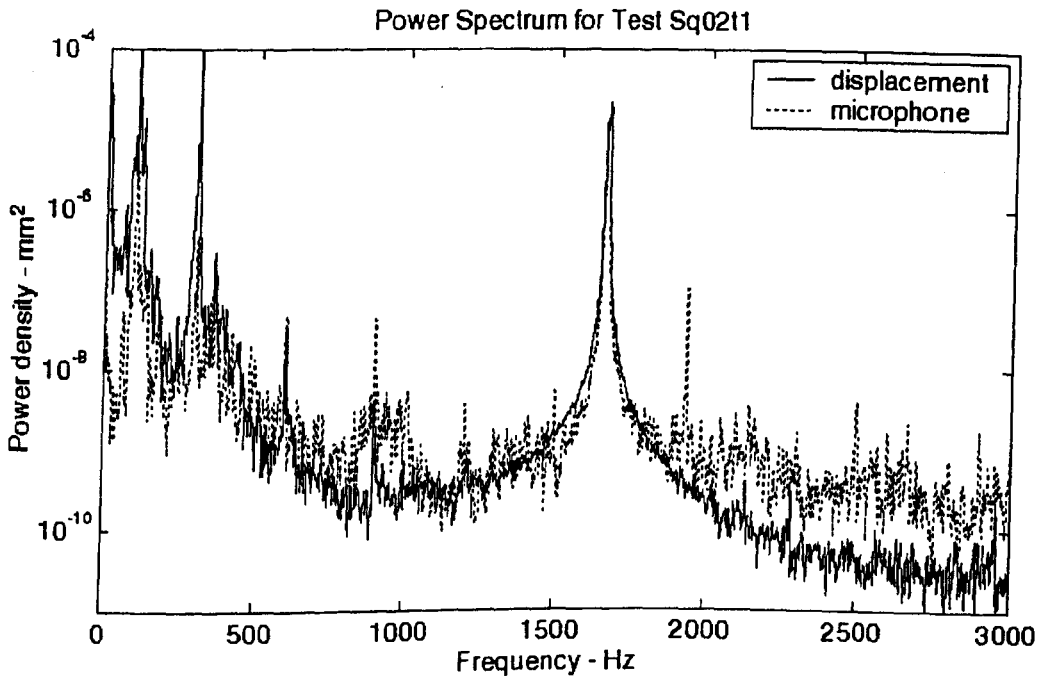


Figure 3-9 : Comparison of power spectra from a displacement transducer and a microphone

3.5.2 Method 2 – Throughput recording

From preliminary work, it was expected that some of the squeal modes were combinations of forward and backward travelling waves (see Chapter 4). Simulation of these waves gave two adjacent peaks in the power spectrum plot that were displaced in frequency by twice the disc rotation speed. It was hoped that by increasing the recording time of the squeal event to 8 seconds with a frequency resolution of 0.125 Hz these two adjacent peaks in the power spectrum would be visible, but this was not the case.

In method 2, data from the dynamometer was collected using the LMS Cada-X Fourier Monitor set for throughput logging of time domain data. Using this method, the size of the recorded data set is not restricted by the Scadas II data logger memory, but is transferred directly to the hard disc of the computer. The system was manually

activated, so the optical trigger was not used. The logging system recorded data simultaneously from the 17 channels as follows :

Channels 1 to 12	Displacement transducers 1 to 12 – individually calibrated
Channel 13	Temperature – set at $101.01\text{ }^{\circ}\text{C}\text{V}^{-1}$
Channel 14	Speed – set at $10.2326\text{ rad s}^{-1}\text{V}^{-1}$
Channel 15	Torque – set at $40\text{ Nm}\text{V}^{-1}$
Channel 16	Pressure – set at $3\text{ bar}\text{V}^{-1}$
Channel 17	Microphone – gain set to 1 (occasionally used)

For the tests recorded here, the displacement transducers were set up as described in method 1.

The expected maximum frequency for squeal events was 8 kHz. The 17 data channels were logged at 16366 Hz to give a Nyquist frequency of 8183 Hz. About 10 seconds of continuous squeal data was recorded. The LMS throughput analysis program was able to transfer the data in 2 second time slices, so for each channel, 4 contiguous 2 second data sets were concatenated to make a continuous 8 second data sample. Thus the frequency resolution from the data was 0.125 Hz.

This method was not successful, partly from data noise, but also from variation of both frequency and amplitude in the squeal event during such a long time period.

3.5.3 Method 3 – High speed recording

The analysis of the squeal event with this method required a different approach. In addition to the use of the fast Fourier transform to produce a power spectrum, a method of analysis was required to allow travelling waves to be recognised as they passed each transducer position. For this, a similar style of data recording to that of method 1 was used in which the data was held in the data logger memory, allowing data to be recorded as quickly as possible.

The displacement transducers were arranged in the same way as in method 2 above, with the exception that there were 11 displacement transducers, with transducer 11 near to the leading edge of the brake pad and the microphone was not utilised.

Previous use of the microphone had confirmed that the spectra from the displacement transducers matched the audible squeal noise and that with fewer channels being logged, a faster logging rate could be achieved. With the minimum number of channels now being recorded, the logging frequency was set to its maximum of 56180 Hz. The maximum number of points that could be recorded was now 16384 points per channel. Manual triggering was used. For the tests at disc speeds of less than 20 rad s^{-1} , the logged squeal event was not able to cover a complete revolution of the disc. The channels were set as follows:

Channels 2 to 12	Displacement transducers 1 to 11 – individually calibrated
Channel 13	Temperature – set at $101.01 \text{ }^{\circ}\text{CV}^{-1}$
Channel 14	Speed – set at $10.2326 \text{ rad s}^{-1}\text{V}^{-1}$
Channel 15	Torque – set at 40 NmV^{-1}
Channel 16	Pressure – set at 3 barV^{-1}

With this data recording speed, travelling waves passing sequential transducer positions at a frequency up to 28090 Hz could be recognised without aliasing. Typically, a 2400 Hz squeal would be of a 3-diameter mode in the disc. If this were a travelling wave, its circumferential travelling speed would be 800 Hz and the rate at which it would pass sequential transducers would be 19200 Hz. Consequently, the analysis of individual time steps would show the wave travelling direction without aliasing.

The power spectrum of the squeal event was used to give an approximation of squeal frequency, but wave directions were found by digitally filtering the squeal data across a narrow frequency passband that straddled the approximate squeal frequency found from the power spectrum. The time stepped amplitudes from the filtered transducer data were compared using a contour plot to show the wave travelling

direction. Details of frequency and amplitude were calculated using least squares analysis of the filtered data.

This method is fully detailed in Chapter 5.

3.6 Hammer tests

For each of the brake discs used in the squeal experiments, a series of roving hammer tests were conducted using the LMS system. The tests were carried out with the disc bolted to the hub and the hub / knuckle installed in the squeal test rig. Three tests were performed:- (1) with no brake installed, (2) with the brake and pads installed but with no hydraulic pressure, (3) with 10 bar hydraulic pressure on the brake.

For the Mercedes vented disc brake, a fixed hammer test was also performed to measure the modes of the disc, hub (knuckle), cage (carrier) and calliper to compare with those found by finite element analysis.

Chapter 6 gives details of the hammer test results with comparisons between hammer test frequencies and squeal frequencies. Chapter 8 gives details of the finite element model results with comparisons between frequencies produced by finite elements, hammer tests and experimental squeal events.

Chapter 4 : Theory

4.1 Nomenclature

A_s	-	standing wave amplitude – m
A	-	forward wave amplitude – m
a, b	-	inner and outer radii of the disc – m
B	-	backward wave amplitude – m
D	-	disc flexural rigidity – N
E	-	Modulus of elasticity – N m^{-2}
f	-	frequency – Hz
h	-	disc half-thickness – m
j	-	mode number (number of modal diameters)
$R(r)$	-	radial space function
r	-	radial parameter where $r \in [a, b]$ – m
$T(t)$	-	time function
t	-	time – s
w	-	transverse displacement – m
w_f	-	forward wave transverse displacement – m
w_b	-	backward wave transverse displacement – m
α	-	forward wave phase angle – rad
β	-	backward wave phase angle – rad
$\Theta(\theta)$	-	circumferential space function
θ	-	disc circumferential position where $\theta \in [0, 2\pi]$ – rad
κ	-	constant used in the separation of variables
ν	-	Poisson's ratio

- ρ - disc density – kg m^{-3}
 $\Psi(r, \theta)$ - space function
 Ω - disc rotation speed – rad s^{-1}
 ω - frequency – rad s^{-1} ($= 2\pi f$)
 ω_p - a natural frequency of the disc – rad s^{-1}

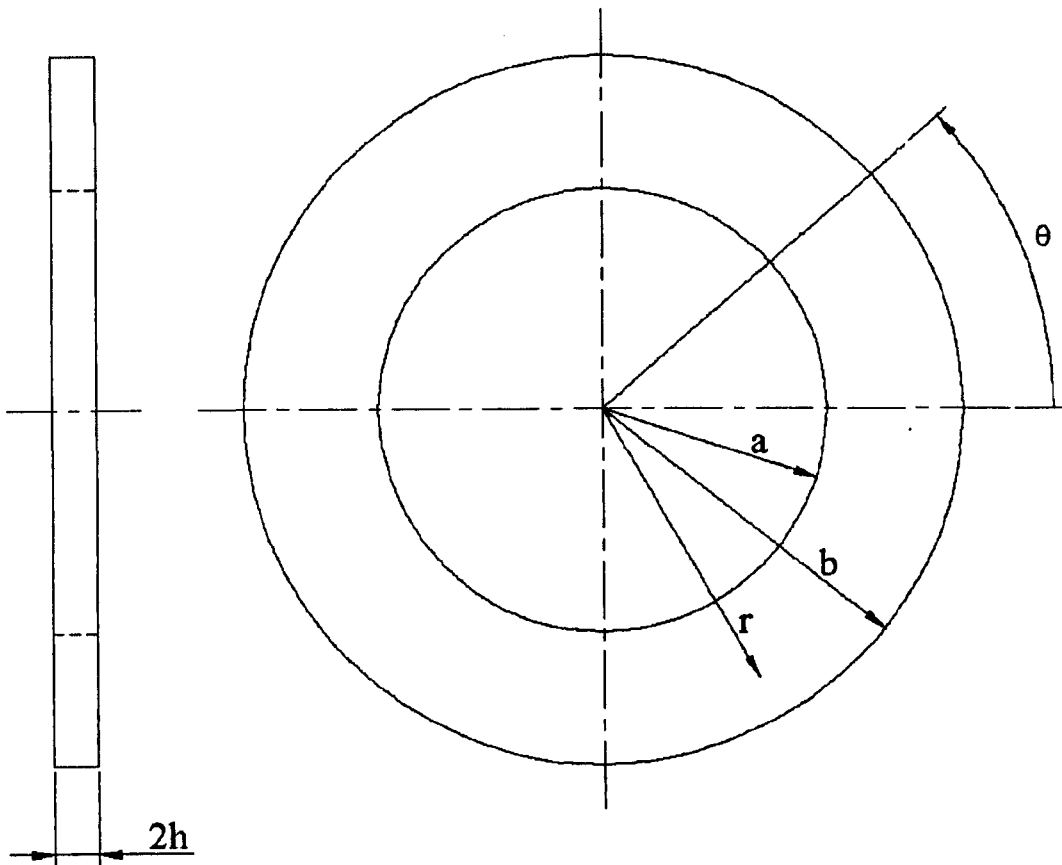


Figure 4-1 : Disc geometry

4.2 Squeal waves in disc brakes

A squeal wave in a brake disc can take one of several forms and can exist at several simultaneous frequencies. The most common form is that of a standing wave in the disc that is stationary with respect to the global coordinate system. Less common

forms are of a progressive wave in the disc, either travelling forward in the direction of disc rotation, or backward, or some combination of forward and backward waves. The following sections outline the equations used to fit to the recorded squeal data and indicate the assumptions made in the analysis.

4.3 The Wave Equation

The behaviour of squeal vibrations in disc brakes needs an understanding of how the wave equation can be applied to the brake disc. Southwell (1921), quoting from earlier work by Kirchhoff and Rayleigh, gives the differential equation that governs the free transverse vibration of the mid surface of a non-rotating thin circular disc clamped at its centre as follows :-

$$\rho \frac{\partial^2 w}{\partial t^2} + \frac{Eh^2}{3(1-\nu^2)} \left[\frac{\partial^2}{\partial r^2} + \frac{1}{r} \frac{\partial}{\partial r} + \frac{1}{r^2} \frac{\partial^2}{\partial \theta^2} \right] w = 0 \quad (4.1)$$

By using the method of separation of variables in equation (4.1), the transverse displacement can be expressed as a combination of functions of time and space such that

$$w = T(t)\Psi(r, \theta) \quad (4.2)$$

Substitution of equation (4.2) into equation (4.1) yields an ordinary differential equation,

$$\frac{d^2 T}{dt^2} + \omega_p^2 T^2 = 0 \quad (4.3)$$

and a partial differential equation,

$$\left(\frac{\partial^2}{\partial r^2} + \frac{1}{r} \frac{\partial}{\partial r} + \frac{1}{r^2} \frac{\partial^2}{\partial \theta^2} \right) \Psi - \kappa^4 \Psi = 0 \quad (4.4)$$

where

$$\omega_p^2 = \frac{D\kappa^4}{\rho h} \quad (4.5)$$

In equation (4.5), ω_p represents a natural frequency of the disc and D is the flexural rigidity of the disc expressed as

$$D = \frac{Eh^2}{3(1-\nu^2)} \quad (4.6)$$

The solution to equation (4.4) is the combined solution of two differential equations

$$\left(\frac{\partial^2}{\partial r^2} + \frac{1}{r} \frac{\partial}{\partial r} + \frac{1}{r^2} \frac{\partial^2}{\partial \theta^2} \right) \Psi \pm \kappa^2 \Psi = 0 \quad (4.7a, b)$$

The method of separation of variables, this time applied to Ψ gives the expression

$$\Psi(r, \theta) = R(r)\Theta(\theta) \quad (4.8)$$

Substitution of equation (4.8) into equations (4.7a) and (4.7b) gives the ordinary differential equations

$$\frac{d^2\Theta}{d\theta^2} + j^2\Theta = 0 \quad (4.9)$$

and

$$\left(\frac{d}{dr^2} + \frac{1}{r} \frac{d}{dr} - \frac{j^2}{r^2} \pm \kappa^2 \right) R = 0 \quad (4.10a, b)$$

Due to the geometry of the disc (figure 4-1), the function $\Theta(\theta)$ has to be continuous and cyclic over the period $(0, 2\pi)$, so that j must be an integer such that $j = 0, 1, 2, \dots$. The equations (4.10a) and (4.10b) are in the form of an ordinary Bessel equation and a modified Bessel equation. The solutions to these equations are in the form of Bessel functions, so that the function $R(r)$ can be expressed as

$$R(r) = \alpha J_j(\kappa r) + \beta Y_j(\kappa r) + \gamma I_j(\kappa r) + \delta K_j(\kappa r) \quad (4.11)$$

where $J_j(\kappa r)$ and $Y_j(\kappa r)$ are the Bessel functions of the first and second kind of order j and $I_j(\kappa r)$ and $K_j(\kappa r)$ are the modified Bessel functions of the first and second kind of order j . Ratios of the constants α , β , γ , δ and the parameter κ can be found from the boundary conditions of the disc.

From this analysis, an eigenfunction expansion solution from the classical plate equation can be expressed as

$$w = \sum_{j=0}^{\infty} \sum_{n=0}^{\infty} R_{jn}(r) \sin(\omega_{p_{jn}} t - \chi_{jn}) \sin(j\theta - \Psi_{jn}) \quad (4.12)$$

where $\omega_{p_{jn}}$ is the natural frequency of the disc with a mode shape of j nodal diameters and n nodal circles. The constants χ_{jn} and Ψ_{jn} can be found from the initial conditions.

A simplification of equation (4.12) for a stationary disc vibrating in a mode with j nodal diameters and n nodal circles can be written in the form

$$w = R_{jn}(r) \sin j\tilde{\theta} \cos \omega_{jn} t \quad (4.13)$$

where the constants χ_{jn} and Ψ_{jn} have been set to zero without loss of generality.

Equation (4.13) can be rearranged using a trigonometric identity to give

$$w = \frac{R_{jn}(r)}{2} \sin(j\tilde{\theta} - \omega_{jn} t) + \frac{R_{jn}(r)}{2} \sin(j\tilde{\theta} + \omega_{jn} t) \quad (4.14)$$

which can be interpreted as two waves travelling in opposite directions around the disc at a speed of $\pm \frac{\omega_{jn}}{j}$ and with a wave shape of $\frac{R_{jn}(r)}{2} \sin j\tilde{\theta}$. The co-ordinate $\tilde{\theta}$ is fixed to the disc and the forward travelling wave is in the direction of increasing $\tilde{\theta}$.

If the case of a rotating disc is now considered, where a stationary harmonic load with frequency ω is applied as the disc rotates at an angular velocity of Ω , then the mode shape in the disc will be locked to the stationary load. In this case the space-fixed circumferential co-ordinate is given by

$$\theta = \tilde{\theta} + \Omega t \quad (4.15)$$

The combination of equations (4.14) and (4.15) gives the response of the rotating disc as

$$w = \frac{R_{jn}(r)}{2} \sin\{j\theta - (\omega_{jn} + j\Omega)t\} + \frac{R_{jn}(r)}{2} \sin\{j\theta + (\omega_{jn} - j\Omega)t\} \quad (4.16)$$

in which there are two resonance conditions given by $\omega_{jn} - j\Omega$ and $\omega_{jn} + j\Omega$.

The primary source of the above development of equation (4.16) given here is Mottershead (1998).

An interesting aside to this analysis is the phenomenon of critical speed, where

$\Omega = \frac{\omega_{jn}}{j}$. Although it is of interest in general when considering disc rotation

phenomena, it is of little interest to research in automotive brake squeal. For a typical squeal frequency of 2400 Hz, the disc would have a three diameter mode shape. The critical speed would be 800 Hz which, for a wheel diameter of 0.6 m, represents a vehicle speed of about 45 times the legal limit. Similarly, because of the slow rotation speeds of squealing discs, the effects of centrifugal forces on disc rigidity have been ignored.

Further simplification of equation (4.16) is possible when considering its application to the data recorded experimentally. The displacement transducers were placed on the outer radius position of the transducer carrier, so it was not possible to determine the number of nodal circles, n , for the disc mode. The values of the radial functions of the forward and backward waves at a particular radius could be determined from the experiment as A and B respectively. Also, for a squealing disc with finite brake

pad area, the relative phases of the opposing waves are unknown and have to be determined experimentally. Consequently, equation (4.16) becomes

$$w = A \sin\{(\omega_j + j\Omega)t - j\theta + \alpha\} + B \sin\{(\omega_j - j\Omega)t + j\theta + \beta\} \quad (4.17)$$

where α and β are the forward and backward wave phase angles.

There are three possible conditions for this equation:-

1. $A > B$, for which the wave will travel forwards (increasing θ),
2. $A < B$, for which the wave will travel backwards (decreasing θ),
3. $A = B$, for which the wave will be stationary in the disc co-ordinate system.

As the disc is rotating, this standing wave is also rotating with the disc. In practice, this type of standing wave is not produced. The standing wave that is produced is aligned with the brake pads and therefore fixed to the calliper co-ordinate system (stationary with respect to the vehicle). Consequently, the development of the stationary wave equation uses the wave equations for a stationary disc.

For a stationary disc, the equations for forward and backward progressive waves are

$$w_f = \frac{A}{2} \sin(\omega_j t - j\theta + \alpha) \quad (4.18)$$

and

$$w_b = \frac{B}{2} \sin(\omega_j t + j\theta + \beta) \quad (4.19)$$

where w_f and w_b are the forward and backward displacements respectively. The superposition of these equations with the assumptions that $w_f = w_b$ and $\alpha = -\beta$ then gives

$$w = \frac{A_s}{2} \sin(\omega_j t - j\theta + \alpha) + \frac{A_s}{2} \sin(\omega_j t + j\theta - \alpha) \quad (4.20)$$

The application of a trigonometry identity to equation (4.20) yields the standing wave equation

$$w = A_s \sin(\omega_j t) \cos(j\theta + \alpha) \quad (4.21)$$

which is for the lateral displacement at a given radius of a standing wave in a disc and is independent of disc rotation speed.

Equation (4.17) for the forward and backward travelling wave and equation (4.21) for the standing wave are those used for performing a least squares fit of the experimental data recorded in the squeal tests.

The equations given for the travelling and standing waves represent a perfect geometric wave form of a homogenous annular disc, perfectly clamped at some inner radius. This is a gross simplification of the physical disc brake. The disc is not homogenous, it is more nearly cyclically symmetric in two respects, there are 37 equally spaced vents between the two disc faces and there are 5 wheel stud positions which are the only means of clamping the inner radius. The action of the brake pads provide localised torsional and compressive forces which can change the behaviour of any waves in the disc. However, these equations provide a basis from which the actual shape of the disc can be compared.

Chapter 5 : Data analysis method

In the analysis of squeal data, the use of the fast Fourier transform (Cooley and Tukey, 1965) to produce a power spectrum of the squeal is of limited use. The phase and amplitude information obtained from a fast Fourier transform of noiseless data can be used to determine wave direction and speed. However, with noisy data, only an approximation to the squeal frequency can be obtained and wave speed and direction information is unreliable. The time domain analysis of small segments of recorded data gave a more detailed understanding of this motion. Least squares fitting of the data to one of the wave equations given in the previous chapter was able to give comparative parameter values for different test data. A fit to equation (4.17) was used for a progressive wave and a fit to equation (4.21) was used for a standing wave.

It is important that the data is appropriate for the analysis, in order that problems of aliasing are removed. The maximum noise frequency of interest in these tests was 8 kHz with a diametral mode in the disc of at least 7 diameters. For the purposes of this thesis, the term 'squeal' will be used for any brake noise between 1 kHz and 8 kHz, i.e. no differentiation will be made between squeal and squeak. For a progressive wave, the speed of the squeal wave on the disc circumference would be $8000 / 7 = 1143$ revolutions per second. As the transducers were spaced at 15 degree intervals, the rate that the progressive wave passed transducers was $1143 \times 24 = 27432$ times per second. Consequently, to prevent aliasing of the signal when plotted against transducer position, a logging frequency greater than 54860 Hz was necessary. The data for the detailed analysis of tests recorded here were logged at 56180 Hz for approximately 0.3 s. Each squeal event record contains enough data

to analyse the development of the squeal wave in the disc. A description of the test method has been given in Chapter 3 (method 3).

Data recorded from the squeal tests were extremely noisy. Many low frequencies were present ranging from disc thickness variation and run-out to bearing rumble and vibration transmitted along the drive train. However, in most cases the presence of a squeal frequency was enough to show a clear indication on the power spectrum, even when it did not last for the full extent of the test.

The following procedures show how simulated and recorded squeal data was processed to give the squeal frequency, amplitude and wave direction.

5.1 Data preparation

Time domain test data from a squeal event was recorded using the LMS system into a binary database and subsequently exported in a standard universal data file format. A Matlab (1995) program was written to convert the data in the universal file into Matlab matrix variables and then save them in a Matlab data file. In this form, the data could easily be accessed by other Matlab programs.

For simulation data, Matlab programs were used to generate data file sets using equations (4.17) for forward and backward travelling waves and equation (4.21) for a standing wave. The simulation data did not include deliberate noise.

5.2 Time domain data

A Matlab program was used to view the time domain test data from any of the recorded channels. It was clear that the recorded data was dominated by low frequency noise from disc run-out, bearing rumble and other extraneous sources.

Figure 5-1 shows a typical series of time domain plots from a recorded squeal event.

The primary sinusoid in the displacement plot is disc run-out at a disc speed of 41 rad s^{-1} . Other noticeable frequencies are bearing rumble and other transmission noise. For example, in Figure 5-1, on the rising face of the displacement plot from 0.05 s through 0.1 s, there is a sinusoid at 656 rad s^{-1} which is 16 times faster than the disc speed. As there are 16 balls in each of the wheel bearing races, it can be assumed that the sinusoid at 656 rad s^{-1} is related to the wheel bearings. The squeal signal is of small amplitude in comparison to the displacements shown.

Temperature, speed and pressure remain constant throughout the test period.

However, the torque fluctuates in a repetitive pattern related to the disc run-out.

There are three possible causes of this fluctuation:-

1. Cyclic variation in the friction coefficient between the pad and disc surface caused by variation in the surface texture of the disc. Reconditioning the disc surface with emery paper did not change this cyclic variation.
2. Disc run-out that either changes the effective radius of the centre of pressure of the brake pads or is insufficient to overcome the stick friction of the pad abutments. Disc run-out at the displacement transducer radius was measured as part of the displacement transducer calibration procedure and is tabulated in Appendix C, Table C-1.
3. Disc thickness variation causing variation in pad contact pressure, but insufficient change to overcome the stick friction of the piston. Disc thickness variation was measured at the outer perimeter of each disc and has been tabulated in Appendix C, Table C-1.

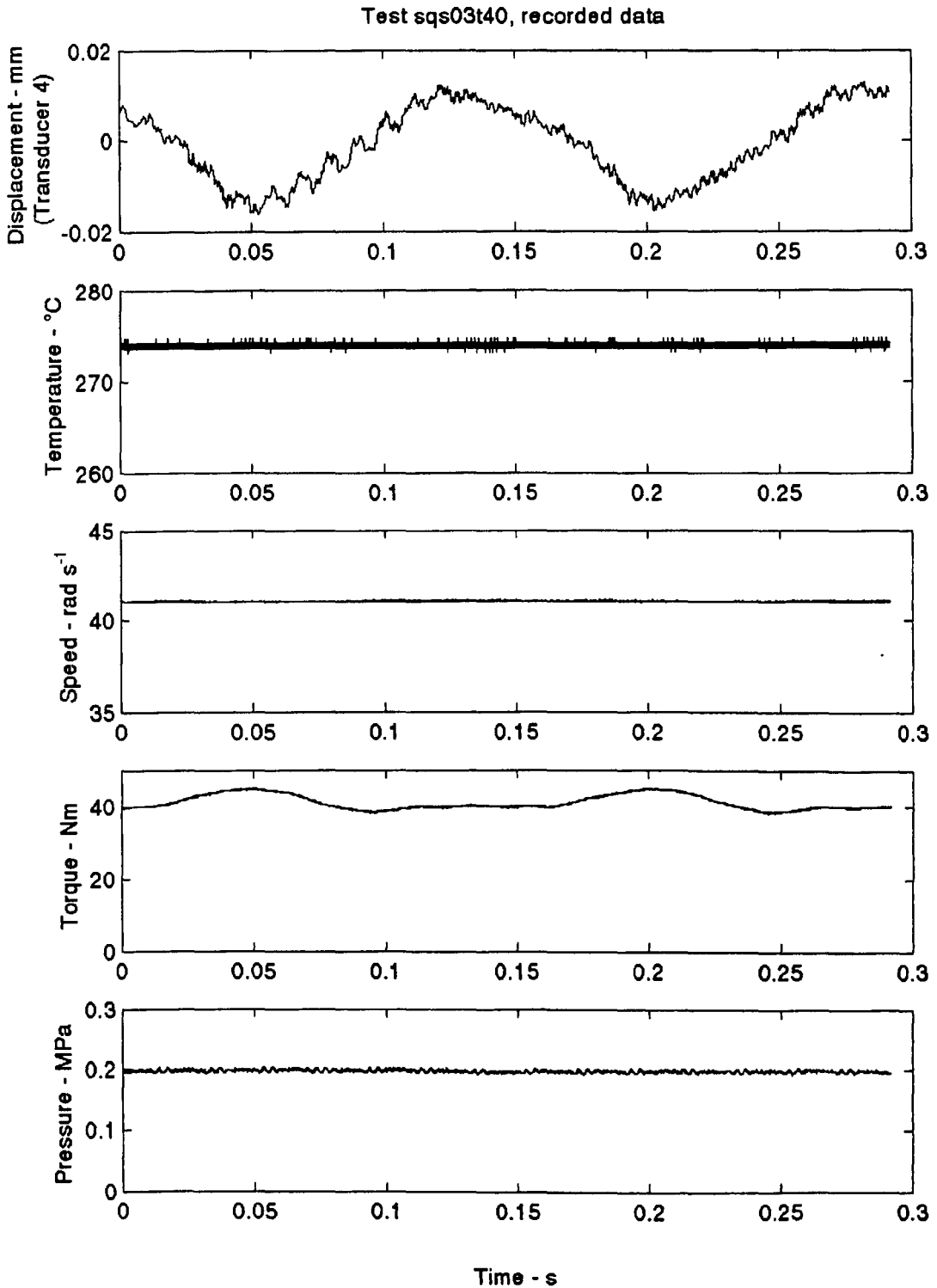


Figure 5-1 : Typical time history of a squeal event

5.3 Squeal frequency estimate

The data recorded from each channel was processed using a fast Fourier transform to produce a power spectrum which was used to give an approximation of the squeal frequencies in the test. The power spectrum in figure 5-2 shows one complete spectrum from test sqs03t05 (Mercedes solid disc). The two labelled frequencies are squeal events that have been analysed and recorded in Chapter 7. The power spectrum shows other spikes (for example, at about 3900 Hz) that, when analysed, have shown either a very short-lived event or an event indistinguishable from the surrounding noise. Figure 5-3 shows a detail of this spectrum for a bandwidth to encompass the 7507.5 Hz squeal frequency analysed from this test.

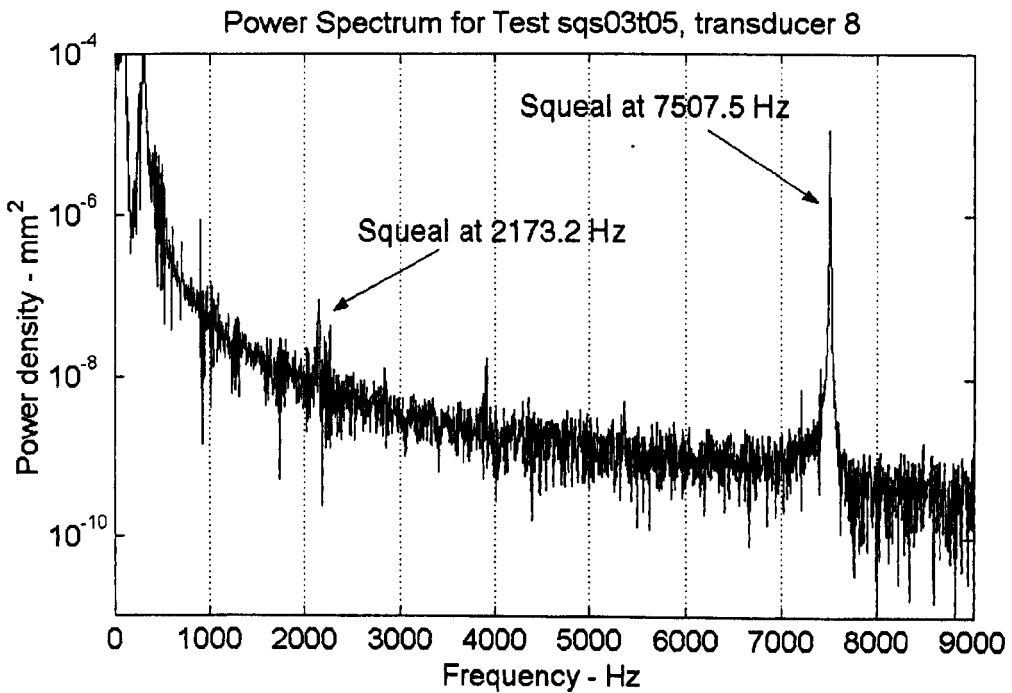


Figure 5-2 : Typical power spectrum plot for the full frequency range

The frequency resolution of the power spectrum is about 3.4 Hz. An approximation of the squeal frequency can be found from this information. In this case the squeal frequency is approximately 7500 Hz.

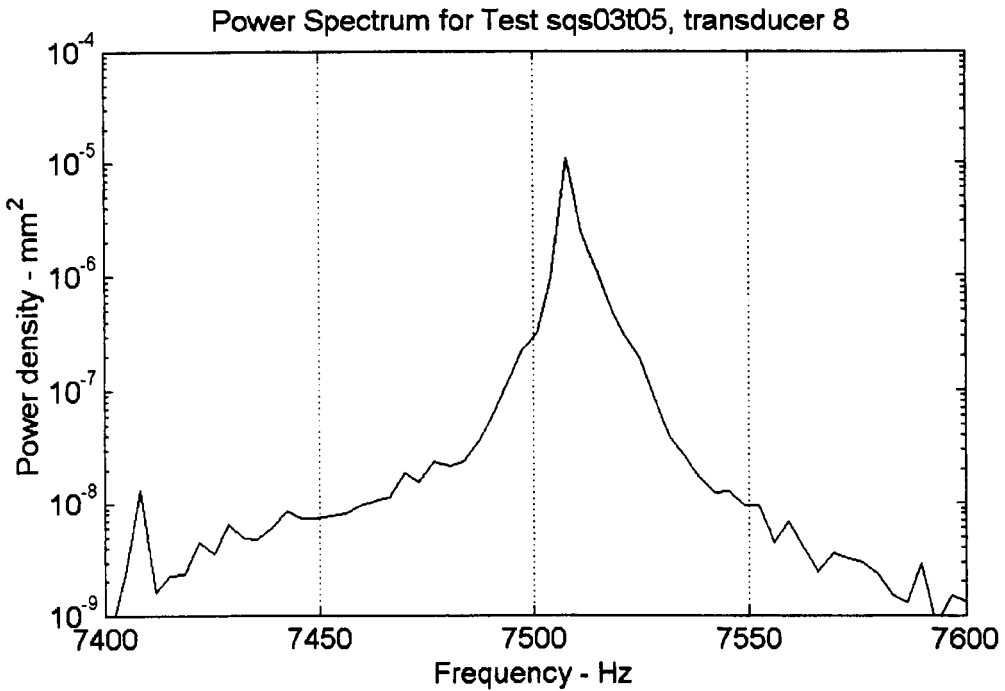


Figure 5-3 : Power spectrum plot of the 7507.5 Hz squeal signal

5.4 Travelling and standing waves

In order to extract more information from the data, it was necessary to remove any extraneous noise by passing it through a digital bandpass filter with a pass band 100 Hz either side of the squeal frequency chosen from the power spectrum. The filtering process was programmed using the Matlab filter toolbox. The filter had a 100 Hz wide rise and fall band and the upper and lower stop bands were set to -80 dB. An FIR type II equiripple filter was used. This filter left a squeal signal that had a clear sinusoidal form, varying in amplitude depending on the squeal volume. Checks made on the pass bandwidth confirmed that there was no loss of signal amplitude with these settings.

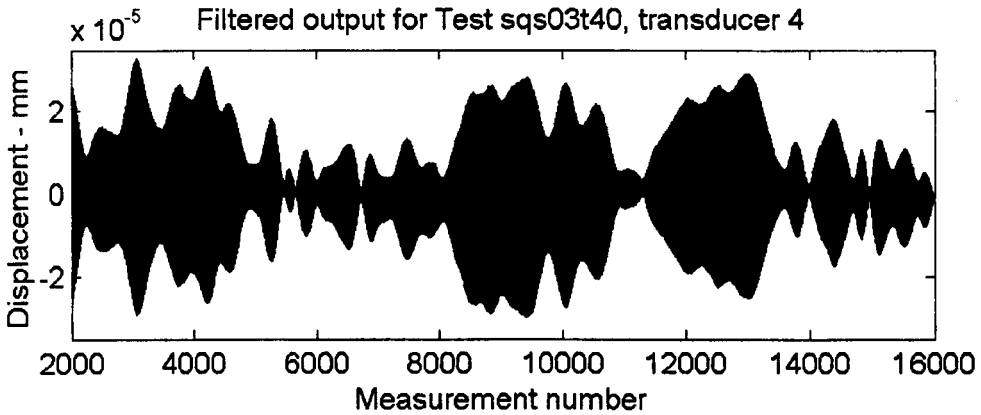


Figure 5-4 : Typical time trace of filtered squeal data

A view of one channel of a typical filtered time domain signal is shown in figure 5-4. This is from test sqs03t40 (Mercedes solid disc) and shows the filtered data for the squeal at 2954.8 Hz (See table 7-5, test name t40a). The axis of abscissae shows the measurement number instead of time to allow data segments to be chosen for analysis (16000 points is equivalent to 0.284 s). For example, in the data shown, a data segment of 410 points, beginning at point 4000, was used to view the forward travelling wave at this frequency.

The wave direction can be determined by plotting sequential displacements of this filtered data for all of the transducers. This is achieved by using a combination of an overlay plot and a contour plot. The equation (4.17) for a forward travelling wave was used to produce simulation data for a typical squeal condition. Figure 5-5 shows this pair of plots from simulation data.

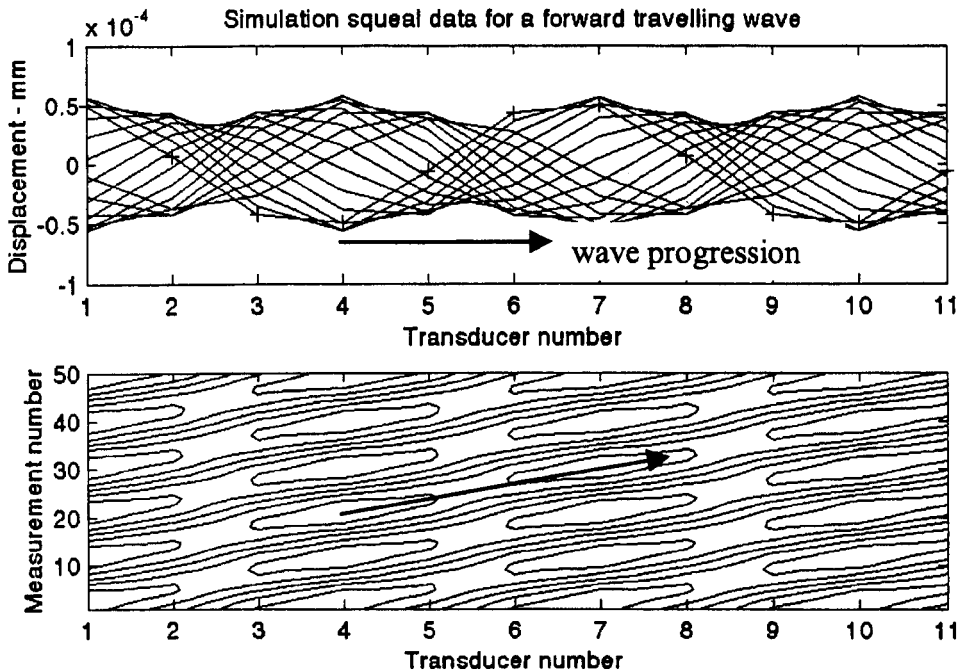


Figure 5-5 : Determination of a forward travelling wave from simulation data

The upper plot in figure 5-5 shows an overlay of sixteen consecutive readings from the eleven transducers, beginning with the plot marked with '+' points. Consecutive plots follow, offset to the right, as indicated by the arrow. The tubular form of the plot indicates that the wave is travelling and the sequential direction, left to right, indicates a forward travelling wave. 'Forward travelling' is defined here as travelling in the same direction as the disc rotation direction, which, in terms of transducer position, is from transducer number 1 towards transducer number 11. In order to reinforce this, the lower contour plot shows contours of constant displacement for fifty consecutive readings from the eleven transducers. The measurement number on the vertical axis is equivalent to a time. The direction of travel of a wave crest (or trough) is travelling in the direction of the arrow, i.e. from left to right with increasing time.

A similar plot, given in figure 5-6, is for the squeal test shown in figure 5-4, for 2954.8 Hz, which shows that for this test and for this small segment of time there is a

forward travelling wave in the disc. Analysis of other segments of data confirm that the forward travelling wave occurs during most of this test at this frequency.

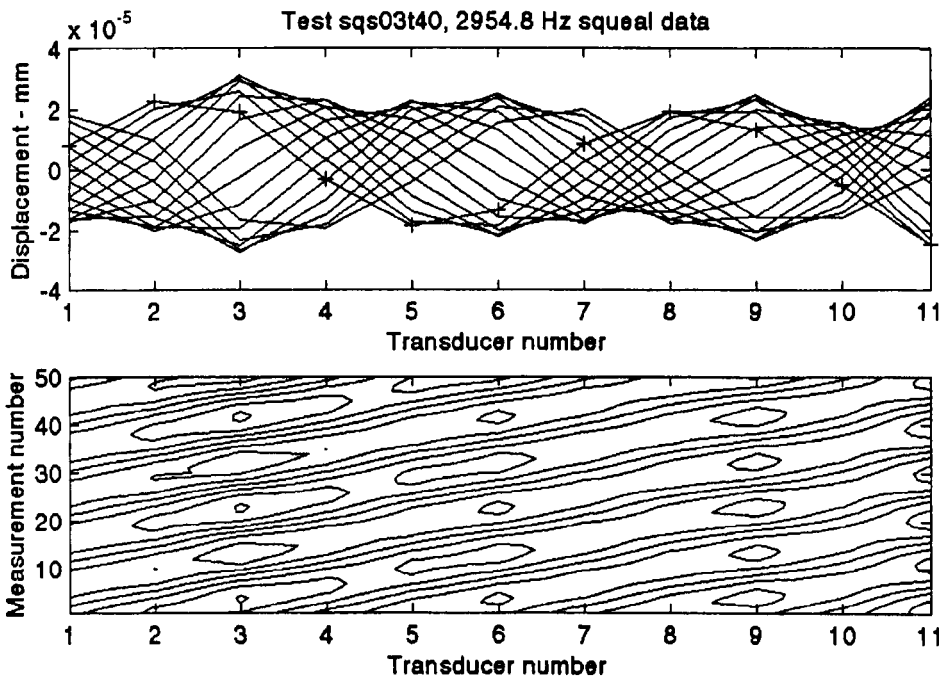


Figure 5-6 : Determination of a forward travelling wave from recorded data

The number of nodal diameters of the wave in the disc can also be determined from the upper plot. In the case shown in figure 5-6, there is a spacing of six transducers for one wavelength of the squeal wave. As the transducer spacing is 15, there are four nodal diameters for this squeal frequency of 2954.8 Hz. However, not all the recorded data gave as clear an indication of nodal diameters as the example shown in figure 5-6. The method used is explained in section 5-5.

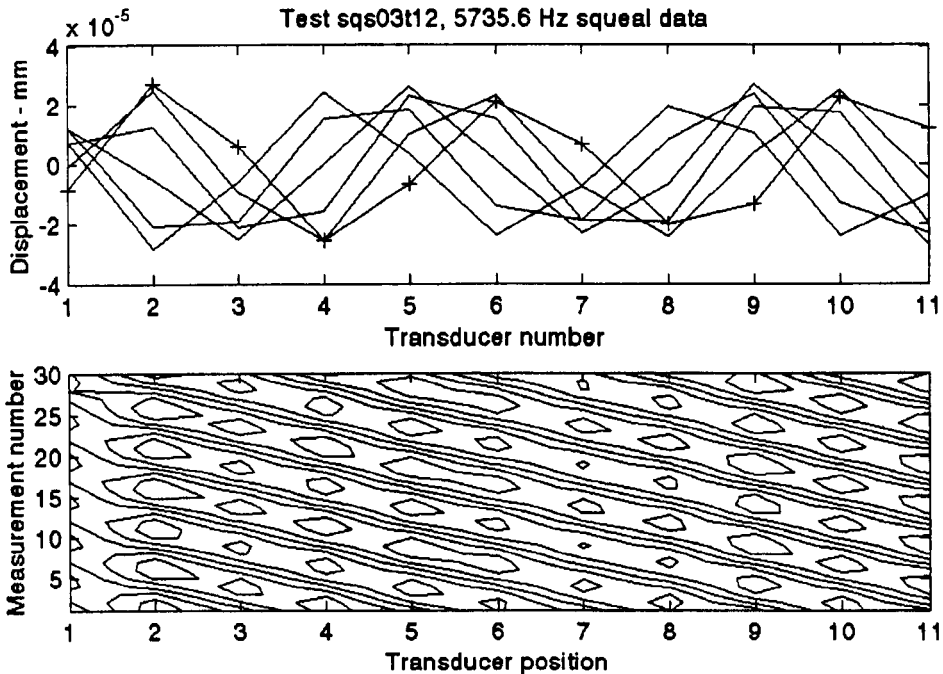


Figure 5-7 : Determination of a backward travelling wave from recorded data

Similarly, analysis of a different squeal event is shown in figure 5-7. This time, the squeal wave is travelling in a backward direction (opposite to the disc rotation), and there are six nodal diameters.

Determination of a standing wave is performed in a similar way. Simulation data was produced using equation (4.21) and from that, overlay and contour plots were made as shown in figure 5-8.

This was by far the most common wave type recorded during the squeal tests on all three brakes. A typical plot from a squeal test is shown in figure 5-9. It is clear that points of zero displacement represent the stationary nodes of the standing wave and the contour plot has a characteristic checker-board configuration. The mode number can be determined from the marked plot in the upper part of Figure 5.8 showing one wavelength in six transducer spacings, hence a mode number of four.

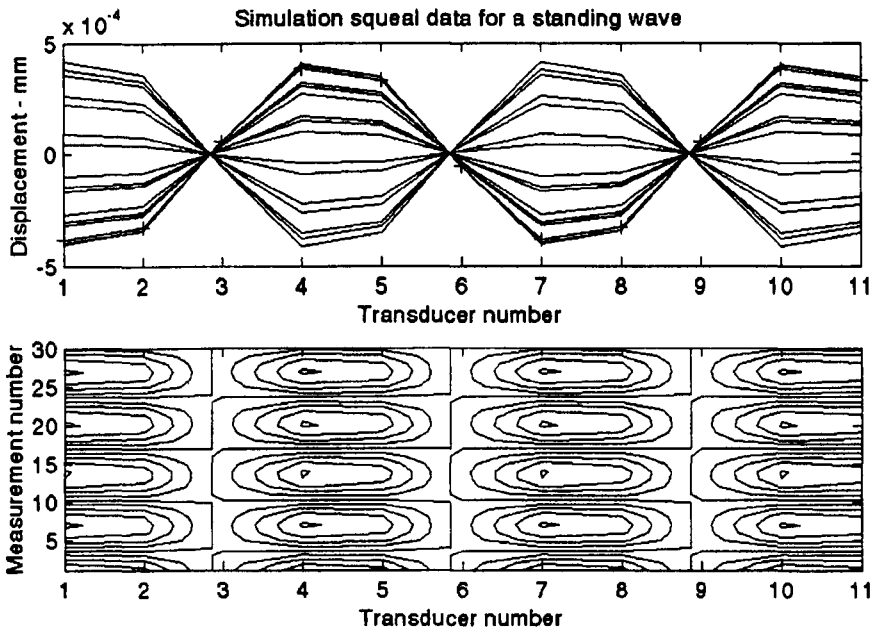


Figure 5-8 : Determination of a standing wave from simulation data

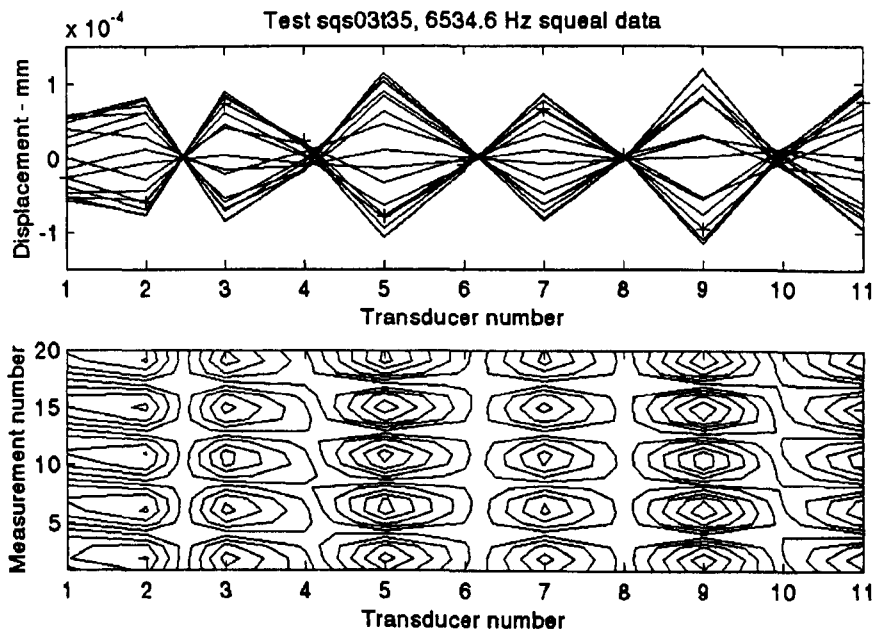


Figure 5-9 : Determination of a standing wave from recorded data

Analysis of the mode number from Figure 5-9 is more difficult, in that there seems to be a non-integer number of waves around the circumference of the disc. The upper part of the Figure shows that there are two wavelengths in a circumferential span of $7\frac{1}{2}$ transducer spacings which indicates 6.4 nodal diameters. For continuity of the

disc, there must be some modification to the wave shape around the pad area, to force the node number to an integer value.

Fosberry and Holubecki (1961) suggested that during a squeal event, the inter-nodal spacing under the brake pad was wider than elsewhere on the disc. However, the laser holography investigations by Fieldhouse and Talbot (2003) showed that there was a reduction in the inter-nodal spacing under the pad and an expansion in the unconstrained part of the disc to give the necessary integer number of nodal diameters for the squeal event.

5.5 Nodal diameter evaluation

The displacement measurements on the brake disc were limited to an arc of 150° with transducer number 11 as near to the pad as possible. The information from these transducers was able to give a good indication of the wave direction, but was not always able to predict the number of nodal diameters for the squeal mode.

The following method of predicting the mode number for a squeal event has been adapted from a proposal by Fieldhouse (1999) using laser holography to view the behaviour of the disc and pads during squeal.

The brake pad acts like a plate in bending and torsion during operation and has a variable pressure distribution over its surface. This pressure is least at the extremes of its circumferential length and consequently the effective length of the pad could be shorter than the full length. It has been found that the effective length of the pad is between 80% and 100% of this circumferential length and for a single piston system the effective length is about 80% of the pad length. Details of brake pad lengths are given in Appendix C, table C-2.

The observed behaviour of a pad pair and disc during squeal has shown that a certain number of antinodes will be 'held' under the pad surface and that these held antinodes will compress their angular pitch. This compression can be between 60% and 90% of the free antinode angular pitch (the antinode angular pitch for the disc

without the brake pads in contact). The majority of the audible squeal noise from the disc emanates from the free surface away from the pads. In this area the remaining antinodes in the disc will elongate to give a system noise frequency that is less than the free mode frequency for the disc. Comparison between the antinode pitch angle in the disc away from the pads to the antinode pitch angle determined from the free mode frequencies of the disc will give the best combination of mode order and number of antinodes under the pad.

A graphical representation of the combination of antinode pitch compression and effective pad length is given in figure 5-10.

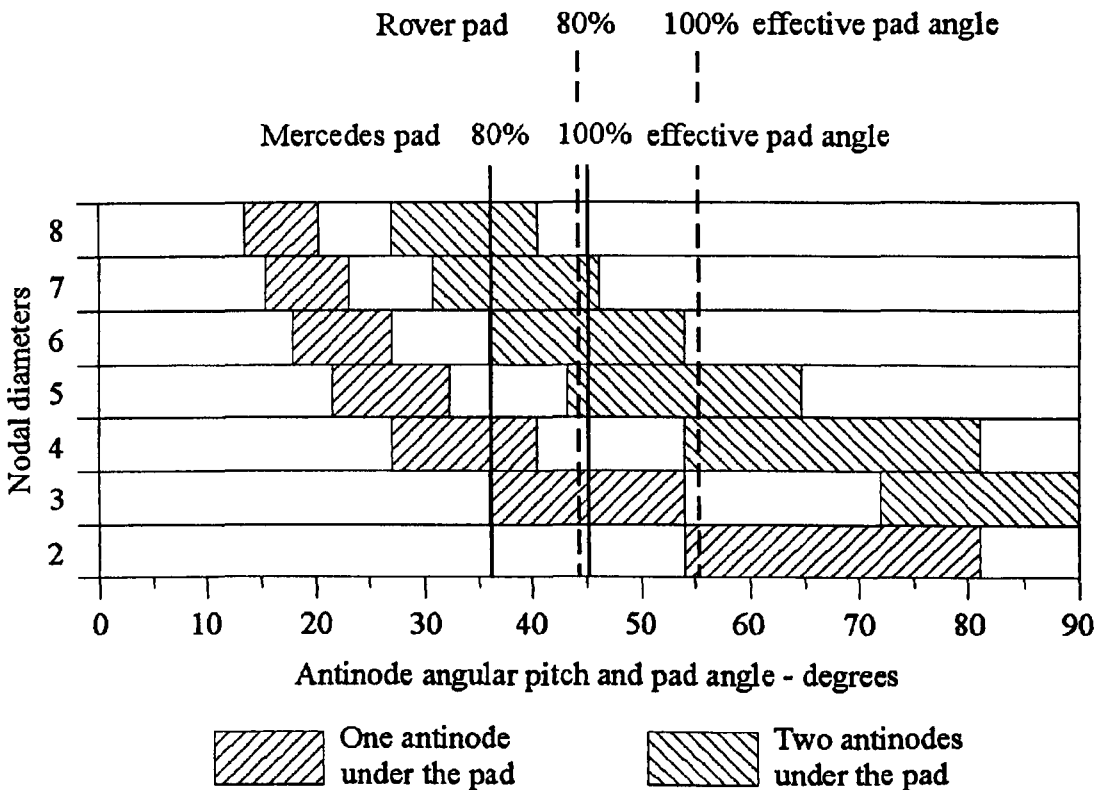


Figure 5-10 : Range of antinode pitch angles for 60% to 90% antinode compression for each disc mode order. These are compared to the effective pad angle.

The range of effective pad length indicated in figure 5-10 shows that, for the Rover pad, the most likely modes with one antinode under the pad are the 3- and 4-diameter modes and the higher modes are likely to have two antinodes under the pad. The 7-diameter mode is likely to be the highest mode with 2 antinodes under the pad. The

Mercedes pads (the same pads are used for the solid and vented discs) have the same modal behaviour with the exception that, with the shorter pad, an 8-diameter mode with 2 antinodes under the pad is possible.

A graphic summary of the free mode frequencies for the three discs is given in figure 5-11. Details of the modal hammer tests to obtain these frequencies is given in Chapter 6.

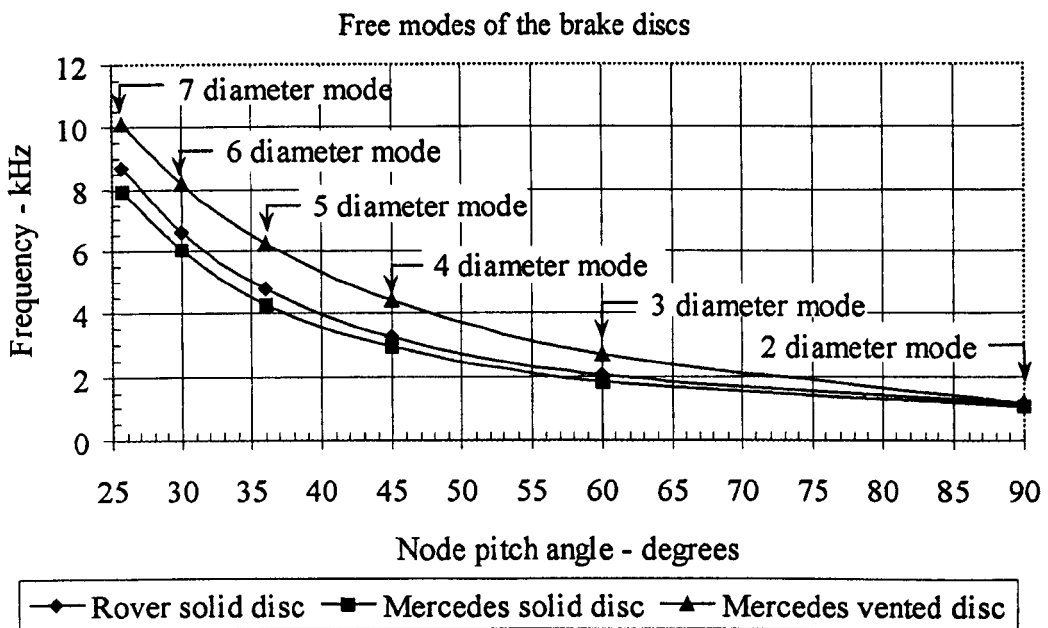


Figure 5-11 : Plot of free mode frequency / node pitch angle for the three discs.

From figure 5-11, the node pitch angle associated with a given squeal frequency can be found for each of the discs and is used as a reference when associating a value for the nodal diameters in the disc.

As an example, for the Mercedes solid disc, test t14 showed a standing wave at a squeal frequency of 7353.6 Hz. By using figure 5-11, this frequency converts to a node pitch angle of 26.8°. It was found that by using a pad effective length of 38° (84% of its total angular length) and 7 nodal diameters with 2 antinodes under the pad, a node pitch angle of 26.8° is obtained in the following expression:

$$\text{node pitch angle} = (360 - 38) / (2 * 7 - 2) = 26.8$$

As a check, from figure 5-10, a 7 order mode with 2 antinodes under the pad has an acceptable compression of about 75% for a pad effective length of 84%.

The analysis of the squeal events using this method has shown that there was a large variation in the calculated pad effective length, between 40% and 90% for mode orders above 3 and greater than 100% for the 3-diameter mode order. Both effects may be explained by the low values of hydraulic pressure used in the tests (typically 0.2 MPa). At this pressure, particularly for a squeal having two nodes under the pad, the nodal pitch compression can be exaggerated to give a relatively small pad effective length, which expands the waves in the remainder of the disc to give a low squeal frequency for the mode number. For the 3- and 4-diameter modes with one node under the pad, the pressure was too light to constrain the node pitch angle under the pad resulting in a squeal frequency close to the free mode frequency indicated in figure 5-11.

This method has been used to record the mode numbers of all the squeal events reported in Chapter 7.

5.6 Squeal parameter determination

The squeal frequency is constantly varying during a squeal event. The amount of variation may be small, but it is measurable over the test time period. It was found that a data sample size of about twenty squeal frequency cycles provided enough information to produce a reliable measure of the wave equation parameters in a least squares analysis of a squeal event.

5.6.1 Travelling wave analysis

The analysis of simulation data highlights a problem with the extraction of the correct squeal frequency. The equation for a travelling wave was given as equation (4.17) and is repeated here:

$$w = A \sin\{(\omega_j + j\Omega)t - j\theta + \alpha\} + B \sin\{(\omega_j - j\Omega)t + j\theta + \beta\} \quad (5.1)$$

The known parameters in this equation are the wave number j , the disc rotation speed Ω and the transducer positions θ . The displacement transducer records signals at two frequencies, that of the forward travelling wave component, $(\omega_j + j\Omega)$ and that of the backward travelling wave component, $(\omega_j - j\Omega)$. The value of ω_j for recorded data is an estimate and the unknown parameters are A , B , α and β . Given an accurate value for ω_j , the unknown parameters can be evaluated by substitution in a least squares analysis. Thus, at any particular value of ω_j , a least squares error can be determined. This process can be repeated for different assumed values of ω_j and a plot of least squares error against frequency can be produced.

The error plots produced by equation (5.1) need further explanation. If it is assumed that the squeal is a backward travelling wave with no forward component, equation (5.1) simplifies to

$$w = B \sin\{(\omega_j - j\Omega)t + j\theta + \beta\} \quad (5.2)$$

in which the displacement transducer is recording a frequency of $(\omega_j - j\Omega)$. In the simulation, $\omega_j = 2400$ Hz, $j = 3$ and $\Omega = 5$ Hz. A plot of the least squares error based on equation (5.2) is shown in figure 5-10.

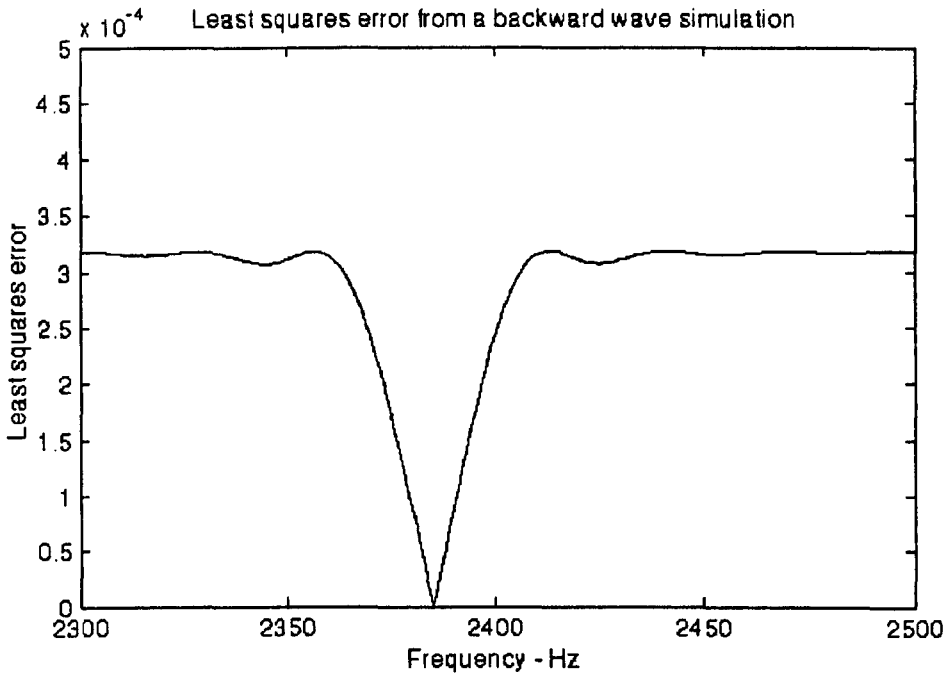


Figure 5-12 : Least squares error for a simulated backward travelling wave (equation 5.2)

The minimum error occurs at 2385 Hz which is $(\omega_j - j\Omega)$, the frequency that a stationary transducer would record. Either side of this minimum the error rises to a high level and remains at this value. However, if the same simulated wave is analysed using equation (5.1) in which it is assumed that there is a forward wave component, the ill-conditioning of the least squares analysis produces a sideband at a lower frequency than $(\omega_j - j\Omega)$, as shown in figure 5-13.

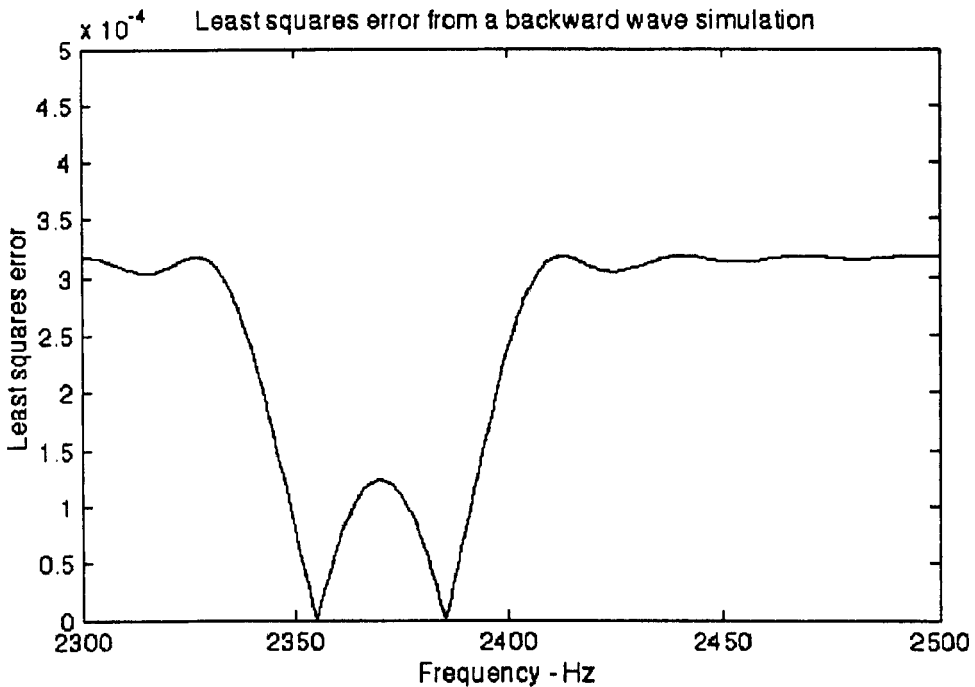


Figure 5-13 : Least squares error for a simulated backward travelling wave (equation 5.1)

This second minimum occurs at a frequency of $(\omega_j - 3j\Omega)$ but does not effect the position of the minimum at $(\omega_j - j\Omega)$. As the amplitude of the forward wave component increases, this second minimum becomes less defined, but a third minimum appears at a frequency of $(\omega_j + 2j\Omega)$ as shown in figure 5-14. For this plot, the forward amplitude was set to 20% of the backward amplitude.

When the forward amplitude is equal to the backward amplitude, the resulting wave is stationary in the disc frame of reference and is not a viable squeal situation. However, using the simulation analysis of a standing wave from equation (5.1), the least squares error is shown in figure 5-15. The two sidebands at frequencies of $(\omega_j - 3j\Omega)$ and $(\omega_j + 2j\Omega)$ can be seen clearly. This situation is not analysed in this way for experimental data, as an experimental standing wave is stationary in the global frame of reference and is analysed using equation (4.21).

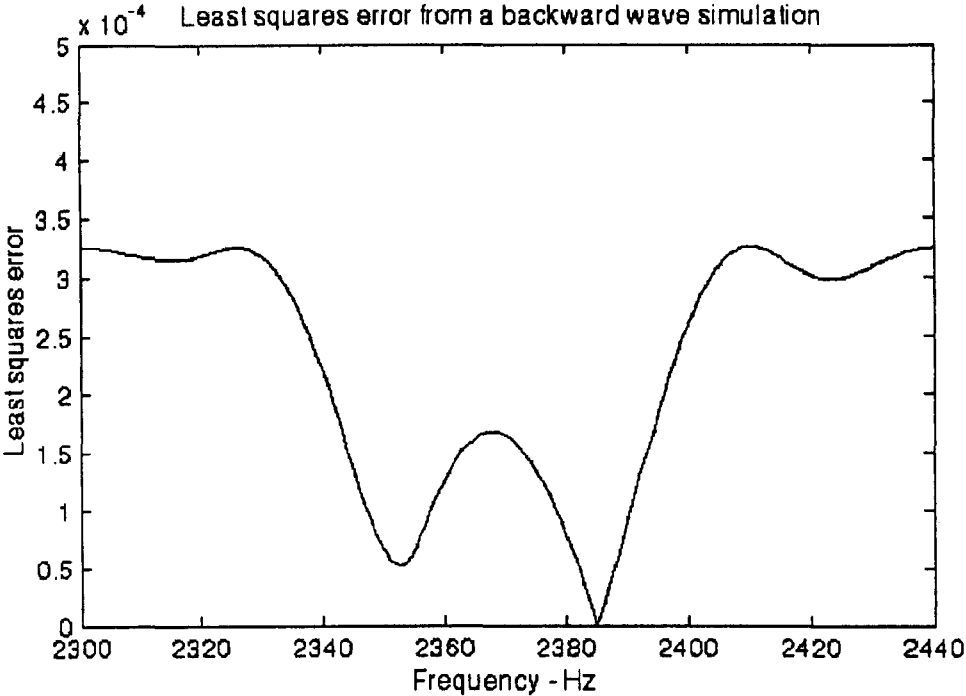


Figure 5-14 : Least squares error for a simulated backward travelling wave (equation 5.1)

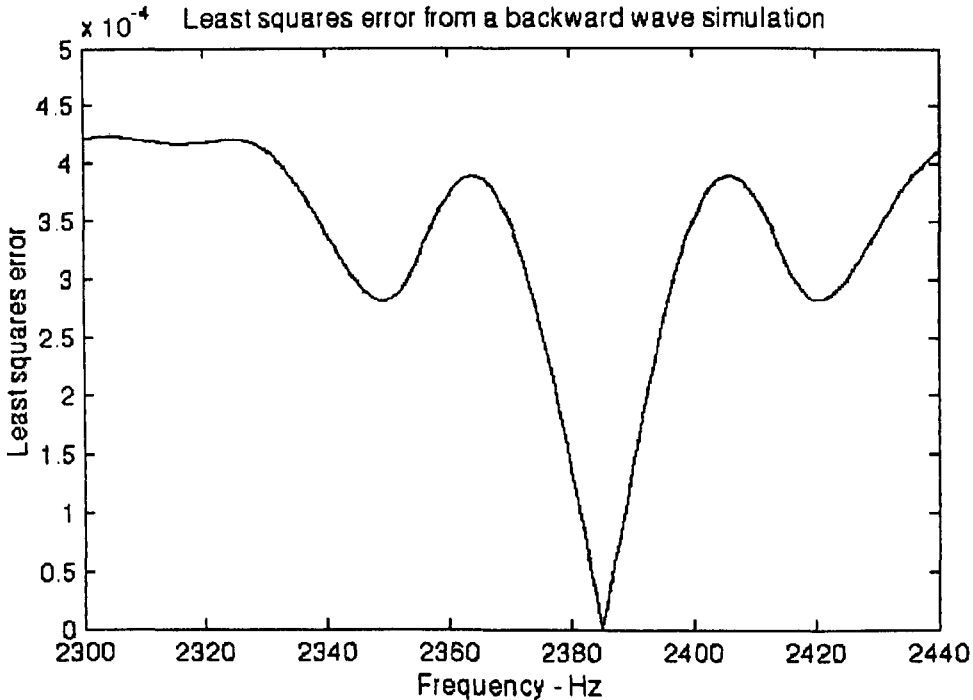


Figure 5-15 : Least squares error for a simulated standing wave (equation 5.1)

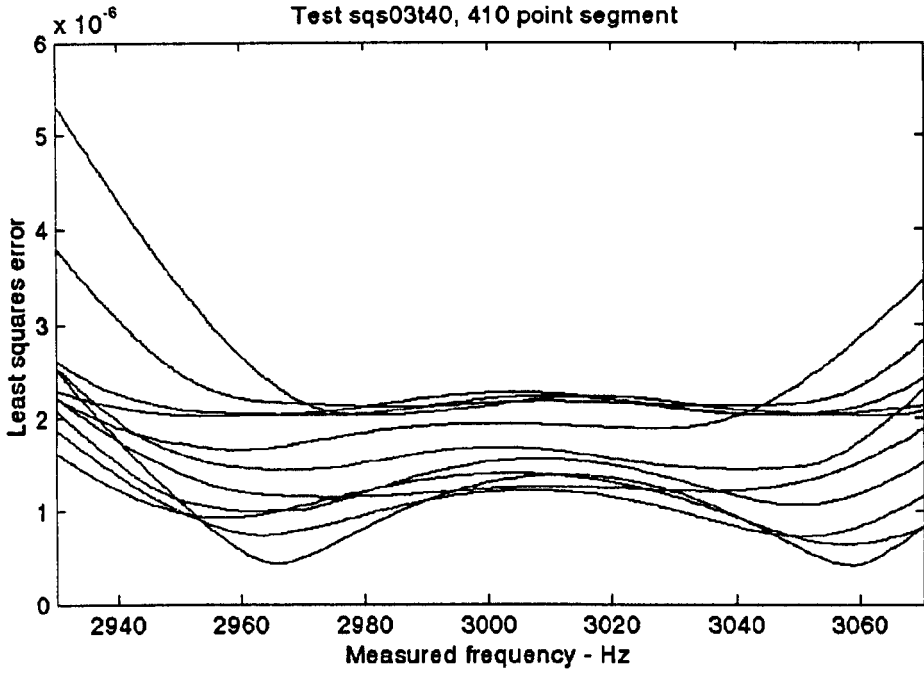


Figure 5-16 : Least squares errors from a recorded forward travelling wave squeal event

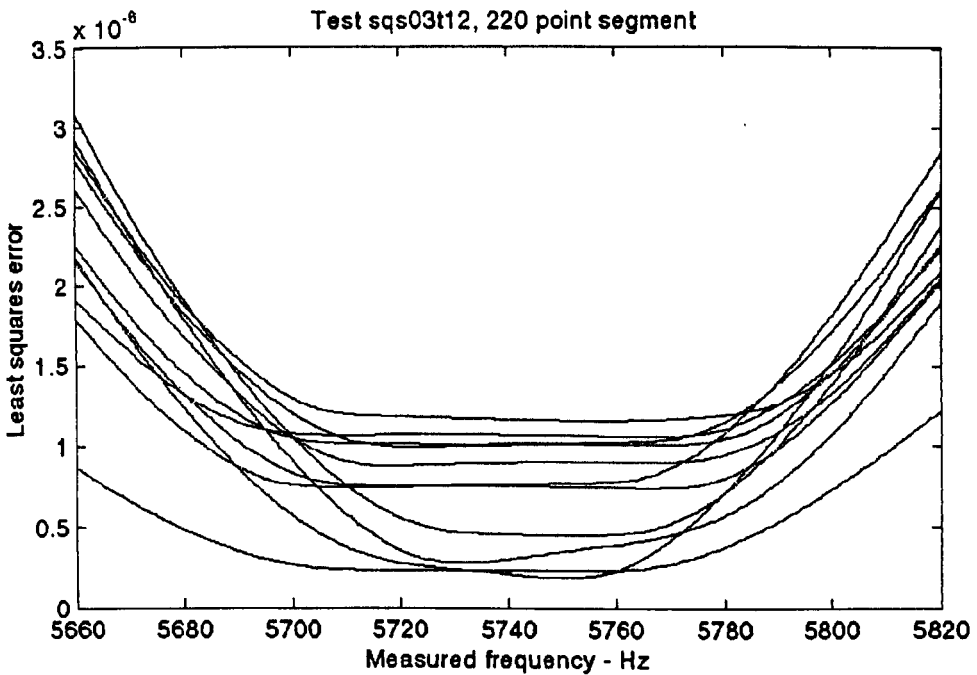


Figure 5-17 : Least squares errors for all channels from a recorded squeal event

The least squares errors from the forward travelling wave recorded from test 'Sqs03t40' are shown in figure 5-16. This data was previously seen in the wave direction plots of figure 5-6. Each curve represents the least squares error for the shown frequency band. Here, the majority of the plots exhibit double minima. As it is known from Figure 5-6 that the wave is forward travelling, a binary search starting from the minimum at the lower frequency (2970 Hz) will find the correct squeal frequency.

If the wave direction is known, a least squares analysis of small data segments, coupled with a binary search for the squeal frequency, will find the appropriate equation to fit the data. Care is needed to ensure that the binary search is operating about the correct minimum least squares error. For simulation data, the definition of the two minima is distinct, but for recorded data their definition is not always so apparent, as figure 5-17 shows. Many of the plots in this figure exhibit a singular minimum and it is not clear what the starting frequency should be. However, as a backward travelling wave was identified for this test, a starting frequency of 5760 Hz would give the correct result. It has been assumed that this lack of definition is caused either by data noise, ill-conditioning in the least squares analysis or a combination of both.

5.6.2 Standing wave analysis

The equation for a standing wave was given as equation (4.21) and is repeated here:

$$w = A_j \sin(\omega_j t) \cos(j\theta + \alpha) \quad (5.3)$$

The known parameters in this equation are the wave number j , measured from the data shown typically in figure 5-9 and the transducer positions θ . The value of ω_j for recorded data is an estimate and the unknown parameters are the amplitude A and the phase angle α . Sequential segments, each about twenty squeal cycles in length, of the data from each transducer were used to tabulate the maximum frequency for each segment. An average frequency was not used as the data contained phase changes

which decreased the value of some of the calculated frequencies, meaning that the true frequency was the upper bound of the calculated frequencies. The phase angle for each segment was found by least squares fitting a sine wave to the data. This had the correct j value and a constant nominal amplitude. It was first fitted by a scan through 180° and followed by a binary search. The amplitude was then found, again by least squares fitting the parameters A and α , using a binary search for the value of A that gave the minimum least squares error, starting from the nominal value of A . The values tabulated in Chapter 7 were the maximum amplitude for the test and the frequency at the point of maximum amplitude, interpolated from the calculated frequencies.

Chapter 6 : Hammer test results

6.1 Introduction

Modal hammer tests were performed on the brake discs of each brake unit to establish the basic mode shapes and related frequencies associated with each disc. These mode shapes and frequencies can be compared to the modes and frequencies that occur during squeal events. The displacement information recorded during a squeal event is from points near the outer radius of the disc. The inner radius was not measured which precludes the determination of the circumferential node number n from the analysis. However, from the pattern of mode shapes and frequencies produced from the squeal events, some of these modes may be found.

Two distinct types of hammer test were performed. The first type of test was a roving hammer test on all three brake discs in which the axial (Z) direction of the disc was excited and measured. This precluded measurement of the radial modes and also modes in the other brake components. The second type of test was on the complete Mercedes vented disc brake assembly in all directions.

For the first type of test two different conditions were used for the modal hammer tests. In the first, the disc was bolted to the knuckle with no brake components present. The knuckle was suspended in a free-free condition during the hammer test. This test is described in section 6.2. In the second, the brake components were attached to the knuckle and a brake hydraulic pressure of 10 bar was applied. The brake assembly was supported in the dynamometer rig during the test. This test is described in section 6.3. Both of the above hammer tests were confined to the axial direction of the disc to measure the modes in the same direction as that of the

displacement transducers. The second type of test on the complete brake structure is described in section 6.5.

6.2 Hammer test on the full disc

The modal hammer test on the full disc was without any brake components present which allowed the measurements to be taken over the full disc surface. A roving hammer test was used in which two accelerometers were attached to the rear surface of the disc and all the node points on the front surface of the disc were hit with the modal hammer. The accelerometers were positioned near the inner and outer disc radii, circumferentially displaced by five node positions (75°). Multiple referencing was used to analyse the mode shapes and frequencies from the LMS system.

Figure 6-1 shows a set of modes produced in a disc from this type of hammer test. The left hand column shows the symbolic representation of the mode shape and the right hand column shows the equivalent three dimensional image from the LMS system. The images shown are from the Mercedes vented disc and are typical of the discs tested. The frequency and damping values for each mode are also indicated.

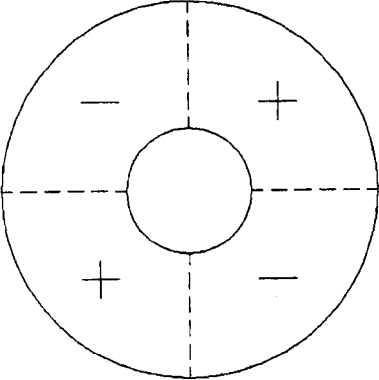
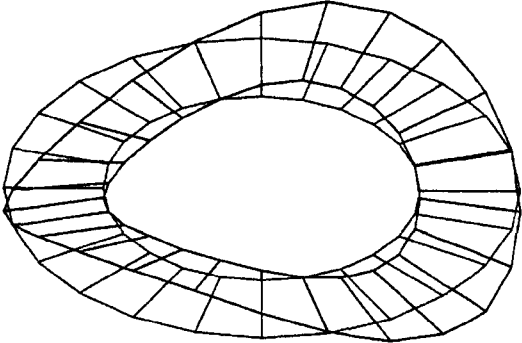
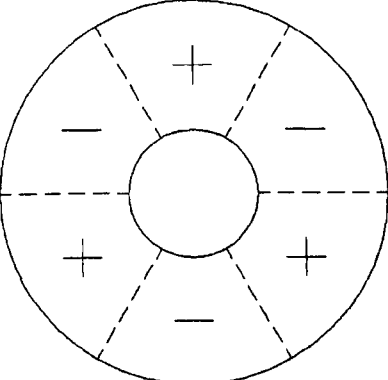
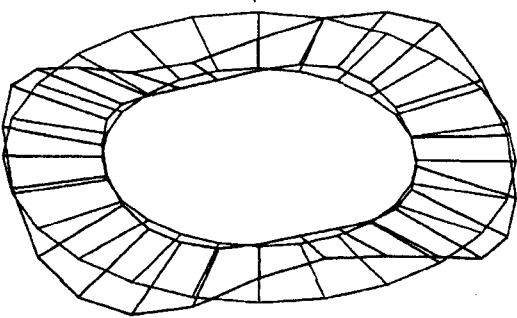
Symbolic mode representation	3-D mode shape from hammer test
<p style="text-align: center;">$j = 2, n = 0$</p> 	<p style="text-align: center;">$j = 2, n = 0$</p>  <p style="text-align: center;">1167 Hz, 0.18%</p>
<p style="text-align: center;">$j = 3, n = 0$</p> 	<p style="text-align: center;">$j = 3, n = 0$</p>  <p style="text-align: center;">2679.7 Hz, 0.38%</p>

Figure 6-1 : Mercedes vented disc – full disc mode shapes

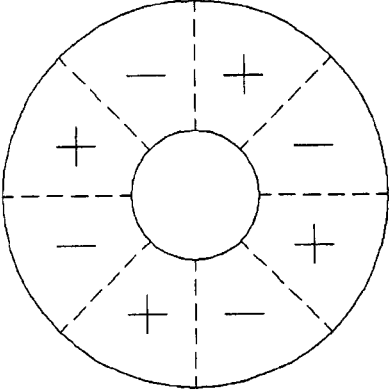
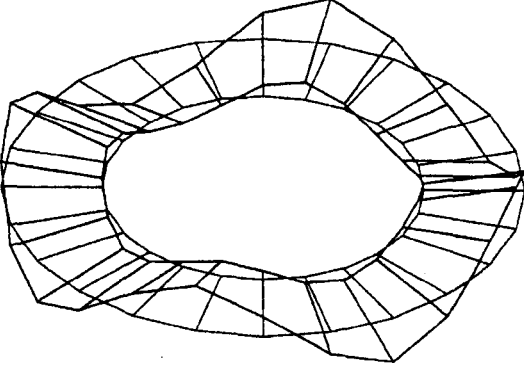
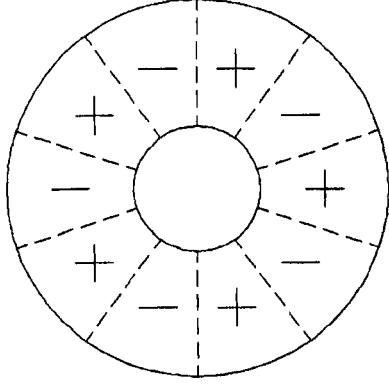
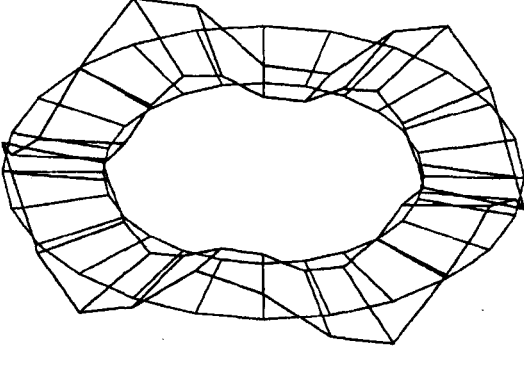
Symbolic mode representation	3-D mode shape from hammer test
<p data-bbox="260 306 411 339">$j = 4, n = 0$</p> 	<p data-bbox="822 306 973 339">$j = 4, n = 0$</p>  <p data-bbox="776 857 1026 890">4425.0 Hz, 0.21%</p>
<p data-bbox="260 948 411 982">$j = 5, n = 0$</p> 	<p data-bbox="822 948 973 982">$j = 5, n = 0$</p>  <p data-bbox="776 1487 1026 1520">6256.3 Hz, 0.15%</p>

Figure 6-1 (continued) : Mercedes vented disc – full disc mode shapes

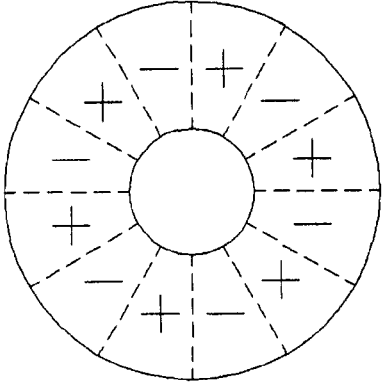
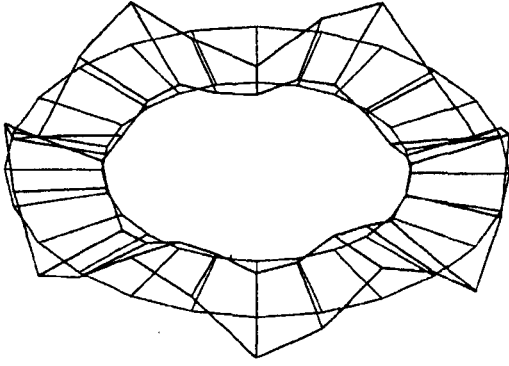
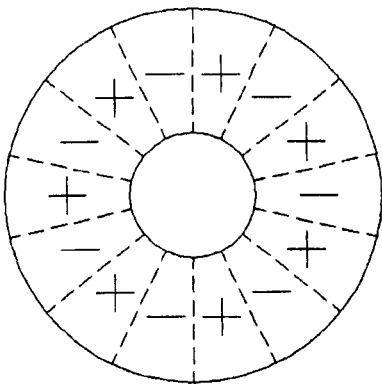
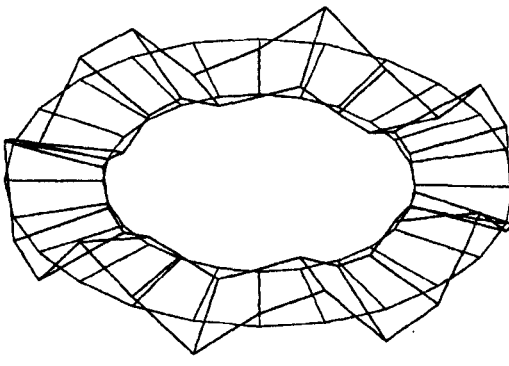
Symbolic mode representation	3-D mode shape from hammer test
<p style="text-align: center;">$j = 6, n = 0$</p> 	<p style="text-align: center;">$j = 6, n = 0$</p>  <p style="text-align: center;">8191.3 Hz, 0.14%</p>
<p style="text-align: center;">$j = 7, n = 0$</p> 	<p style="text-align: center;">$j = 7, n = 0$</p>  <p style="text-align: center;">10124.7 Hz, 0.15%</p>

Figure 6-1 (continued) : Mercedes vented disc – full disc mode shapes

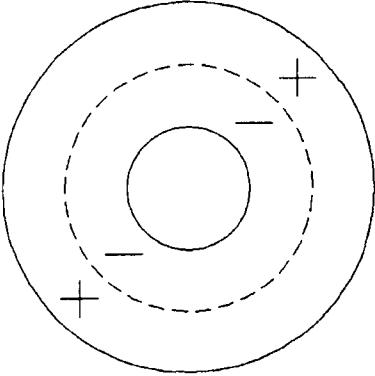
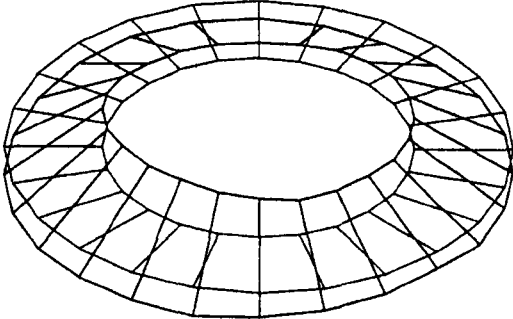
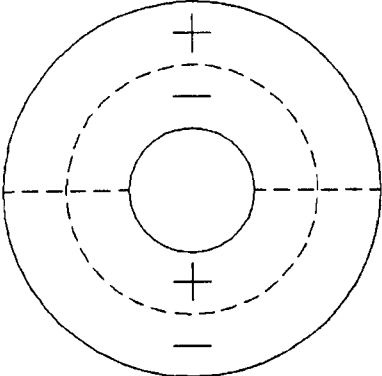
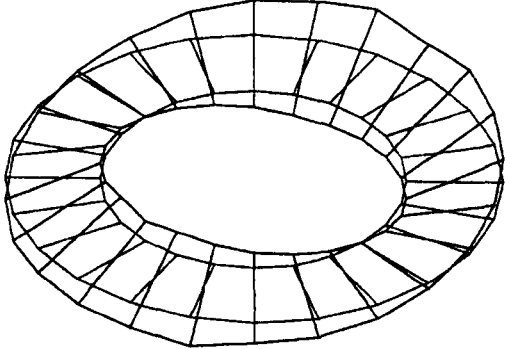
Symbolic mode representation	3-D mode shape from hammer test
<p style="text-align: center;">$j = 0, n = 1$</p> 	<p style="text-align: center;">$j = 0, n = 1$</p>  <p style="text-align: center;">3873.2 Hz, 0.99%</p>
<p style="text-align: center;">$j = 1, n = 1$</p> 	<p style="text-align: center;">$j = 1, n = 1$</p>  <p style="text-align: center;">3066.7 Hz, 0.46%</p>

Figure 6-1 (continued) : Mercedes vented disc – full disc mode shapes

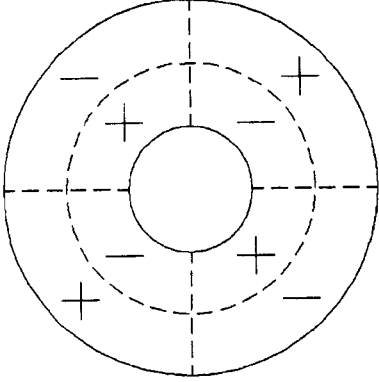
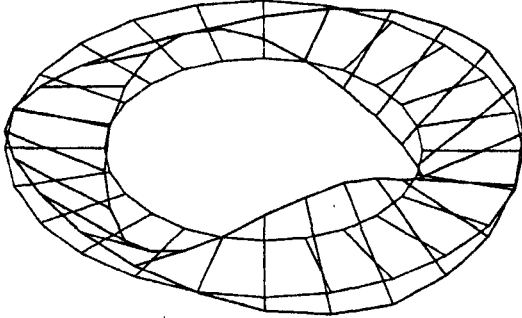
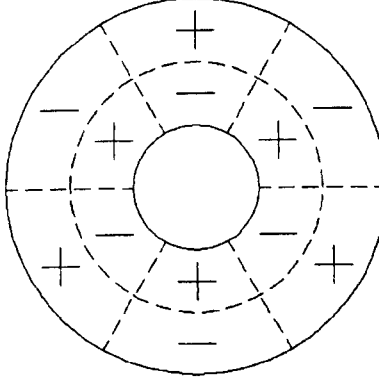
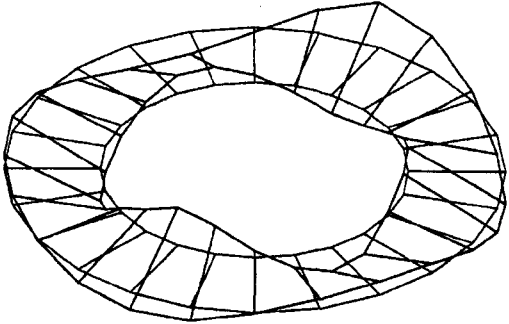
Symbolic mode representation	3-D mode shape from hammer test
<p style="text-align: center;">$j = 2, n = 1$</p> 	<p style="text-align: center;">$j = 2, n = 1$</p>  <p style="text-align: center;">4824.3 Hz, 0.24%</p>
<p style="text-align: center;">$j = 3, n = 1$</p> 	<p style="text-align: center;">$j = 3, n = 1$</p>  <p style="text-align: center;">5769.0 Hz, 0.18%</p>

Figure 6-1 (continued) : Mercedes vented disc – full disc mode shapes

Symbolic mode representation	3-D mode shape from hammer test
<p style="text-align: center;">$j = 4, n = 1$</p>	<p style="text-align: center;">$j = 4, n = 1$</p> <p style="text-align: center;">9105.8 Hz, 0.29%</p>

Figure 6-1 (continued) : Mercedes vented disc – full disc mode shapes

6.3 Hammer test on the disc with the brake applied

The brake pad and calliper occupied about a quarter of the disc circumference which meant that the full surface of the disc could not be hammer tested. However, the information from the remaining area tested (270° of circumference) gave a good indication of the modes in the disc. A roving hammer test was used in which two accelerometers were attached to the rear surface of the disc and all the node points on the front surface of the disc were hit with the modal hammer. The accelerometers were positioned near the inner and outer disc radii, circumferentially displaced by five node positions (75°). Multiple referencing was used to analyse the mode shapes and frequencies from the LMS system.

6.4 Hammer test results

A comparison of the mode shapes and frequencies for the two hammer test formats is given in table 6-1 for the Rover disc, table 6-2 for the Mercedes solid disc and table 6-3 for the Mercedes vented disc. The first circumferential mode, [$j = 0, n = 1$], has one possible frequency. The remaining modes have pairs of modal frequencies produced by the disc symmetry. Possible mode frequencies not found in a hammer test are indicated with a hyphen, '-'. Rigid body combinations are indicated with the comment 'rigid body mode' and modes for which the frequency was too high for the hammer test to resolve are indicated with the comment 'high frequency'.

Rover disc				
Nodal circles	$n = 0$		$n = 1$	
Nodal diameters	Hammer test on full disc	Hammer test with brake	Hammer test on full disc	Hammer test with brake
$j = 0$	rigid body mode		4033.7 (0.34)	-
$j = 1$	rigid body mode		6816.1 (0.70)	7472.8 ¹ (0.39)
			-	7882.0 ² (0.85)
$j = 2$	1174.7 (0.12)	1153.4 (0.45)	2922.9 (0.14)	-
	1189.0 (0.13)	1497.1 (0.53)	3001.3 (0.12)	-
$j = 3$	2044.7 (0.21)	2090.2 (0.49)	5968.1 (0.15)	-
	2048.0 (0.23)	2547.1 (2.01)	-	-
$j = 4$	3256.4 (0.13)	3502.7 (0.71)	9792.3 (0.14)	-
	3256.4 (0.24)	-	10492.1 (0.50)	-
$j = 5$	4799.6 (0.23)	5109.7 (1.02)	high frequency	
	4809.5 (0.12)	-		
$j = 6$	6631.8 (0.14)	6535.5 (1.47)	high frequency	
	6637.7 (0.15)	6894.6 (1.53)		
$j = 7$	8696.3 (0.13)	-	high frequency	
	8710.8 (0.20)	-		
Notes :				
1. The radial node is aligned with the brake pad centre				
2. The radial antinode is aligned with the brake pad centre				

Table 6-1 : Rover disc – comparison of mode shapes and frequencies from hammer tests (Frequencies in Hz, percentage damping in parentheses)

Mercedes solid disc				
Nodal circles	$n = 0$		$n = 1$	
Nodal diameters	Hammer test on full disc	Hammer test with brake	Hammer test on full disc	Hammer test with brake
$j = 0$	rigid body mode		10752.3 (0.52)	-
$j = 1$	rigid body mode		11539.3 (0.44)	-
			-	-
$j = 2$	1087.9 (0.22)	1287.2 (1.17)	-	6373.8 ¹ (0.64)
	1090.9 (0.13)	-	-	-
$j = 3$	1841.3 (0.17)	1750.7 (0.46)	9186.1 (0.22)	9370.1 ¹ (0.54)
	-	2154.9 (1.26)	-	-
$j = 4$	2942.1 (0.26)	2980.4 (1.26)	11026.3 (0.25)	-
	2948.2 (0.17)	-	-	-
$j = 5$	4357.0 (0.36)	4543.7 (0.74)	high frequency	
	-	-		
$j = 6$	6032.5 (0.17)	6159.0 (0.52)	high frequency	
	-	-		
$j = 7$	7931.8 (0.19)	7970.0 (0.66)	high frequency	
	-	-		

Note : The radial node is aligned with the brake pad centre

Table 6-2 : Mercedes solid disc – comparison of mode shapes and frequencies from hammer tests (Frequencies in Hz, percentage damping in parentheses)

Mercedes vented disc				
Nodal circles	$n = 0$		$n = 1$	
Nodal diameters	Hammer test on full disc	Hammer test with brake	Hammer test on full disc	Hammer test with brake
$j = 0$	rigid body mode		3873.2 (0.99)	-
$j = 1$	rigid body mode		3066.7 (0.46) 3161.1 (0.86)	3002.5 ¹ (0.96) 3191.1 ² (0.77)
$j = 2$	1167.0 (0.18) 1168.8 (0.12)	1100.4 (1.12) 1443.5 (1.00)	4824.3 (0.24) -	4844.8 ¹ (0.47) 5031.6 ² (1.82)
$j = 3$	2679.7 (0.38) 2688.8 (0.17)	2412.2 (0.75) -	5769.0 (0.18) 5770.6 (0.15)	7158.4 ² (0.82) 7717.8 ¹ (0.68)
$j = 4$	4410.7 (0.15) 4425.0 (0.21)	4503.9 (1.14) 4617.1 (0.99)	10200.7 (0.23) 10227.3 (0.34)	- -
$j = 5$	6256.3 (0.15) -	6263.9 (0.87) 6784.3 (1.38)	high frequency	
$j = 6$	8176.4 (0.20) 8191.3 (0.14)	7999.3 (0.76) 8481.4 (1.05)	high frequency	
$j = 7$	10124.7 (0.15) 10148.9 (0.24)	- -	high frequency	
Notes :-				
1. The radial node is aligned with the brake pad centre				
2. The radial antinode is aligned with the brake pad centre				

Table 6-3 : Mercedes vented disc – comparison of mode shapes and frequencies from hammer tests (Frequencies in Hz, percentage damping in parentheses)

In a perfectly symmetric disc, each of a mode pair would have the same frequency with the global orientation being arbitrary. The relative orientation between the mode pair is half a circumferential wavelength. For a brake disc, the mode shape orientation is affected by the symmetry of the hub attachment bolts, four in the case of the Rover disc and five for the Mercedes discs. However, the relative orientation of the mode pair remains. For a disc with the brake applied, the mode pair becomes separated in frequency and their orientation is aligned with the brake pad. For the $[n = 0]$ modes, the lower frequency of the pair has its antinode aligned with the centre of the brake pad. With the mode in this orientation, the brake pads and associated calliper are being bodily displaced. This effectively increases the mass at that point on the disc, reducing the natural frequency. Conversely, for the higher frequency, the node is aligned with the brake pad causing the brake pad to rotate to align itself with the disc and increase the effective stiffness of the disc which increases the disc natural frequency. A typical pair of modes for $[j = 2, n = 0]$ is shown in figure 6-2. For modes at higher frequencies than $[j = 3]$, the application of the brake had the overall effect of increasing disc stiffness and consequently increasing the resonant frequencies. The situation is less clear for the $[n = 1]$ modes. Where two frequencies were associated with a mode, usually the lower frequency was associated with a torsional mode of the brake pad and the higher frequency associated with pad rotation about the nodal circle, as in the example given in figure 6-3. An exception to this is for $[j = 3, n = 1]$ for the Mercedes vented disc in which the reverse is true, as shown in figure 6-4.

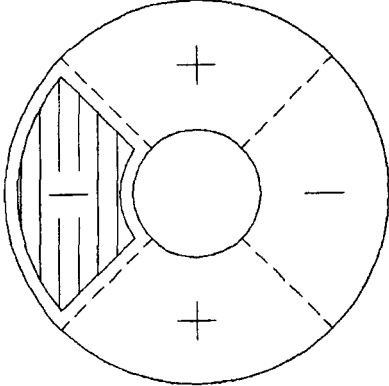
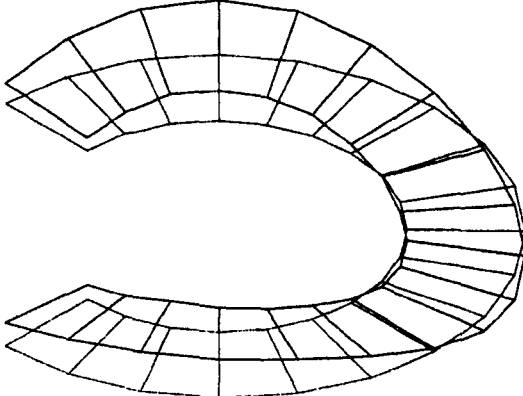
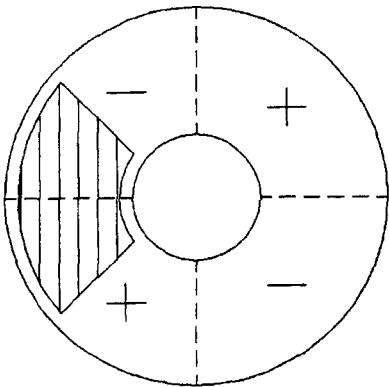
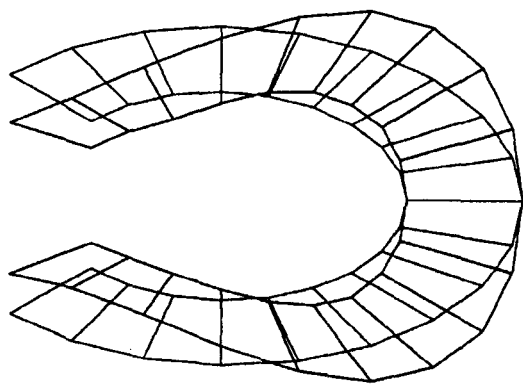
<p>Symbolic mode shape</p> <p>$j = 2, n = 0$</p>	<p>3-D mode shape from hammer test</p> <p>$j = 2, n = 0$</p>
	 <p data-bbox="786 870 1041 911">1100.4 Hz, 1.12%</p>
	 <p data-bbox="786 1419 1041 1460">1443.5 Hz, 1.00%</p>

Figure 6-2 : Mercedes vented disc – mode alignment for $[j = 2, n = 0]$

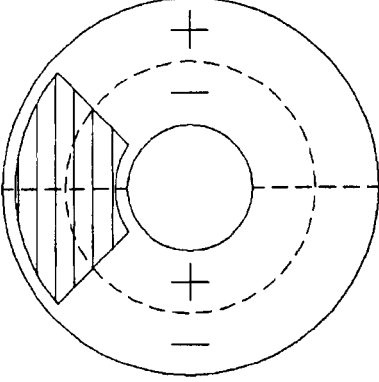
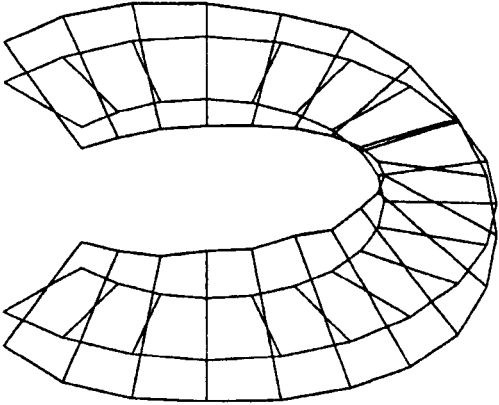
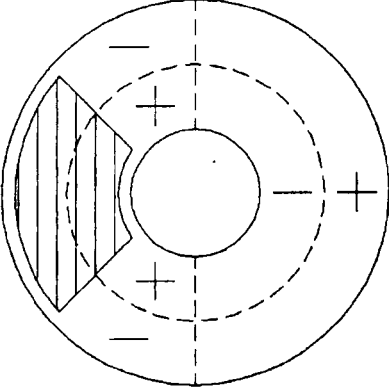
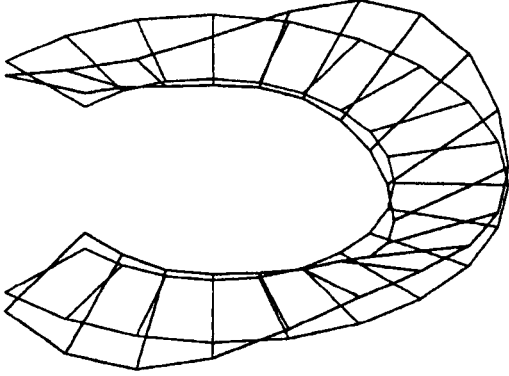
Symbolic mode shape $j = 1, n = 1$	3-D mode shape from hammer test $j = 1, n = 1$
	 <p data-bbox="790 899 1042 934">3002.5 Hz, 0.96%</p>
	 <p data-bbox="790 1458 1042 1493">3191.1 Hz, 0.77%</p>

Figure 6-3 : Mercedes vented disc – mode alignment for $[j = 1, n = 1]$

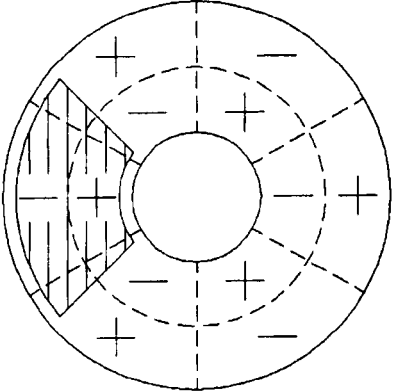
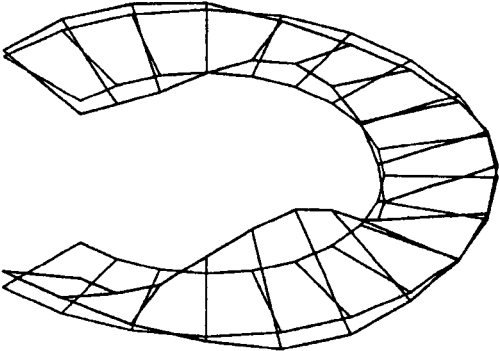
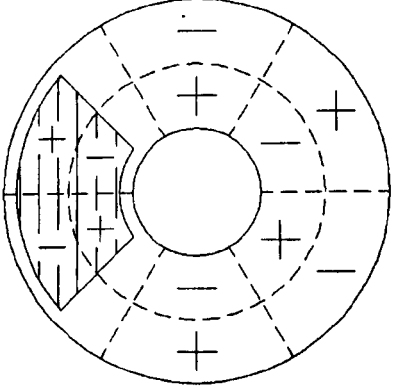
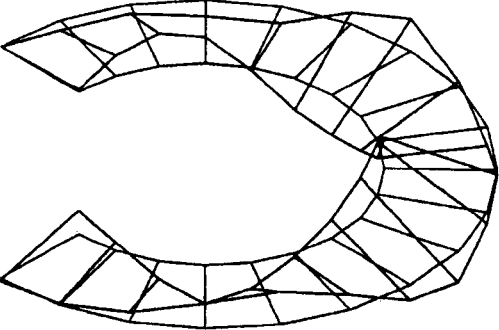
<p>Symbolic mode shape</p> <p>$j = 3, n = 1$</p>	<p>3-D mode shape from hammer test</p> <p>$j = 3, n = 1$</p>
	 <p data-bbox="794 820 1045 855">7158.4 Hz, 0.82%</p>
	 <p data-bbox="798 1328 1041 1363">7717.8 Hz, 0.68%</p>

Figure 6-4 : Mercedes vented disc – mode alignment for $[j = 3, n = 1]$

6.5 Full brake hammer tests

The procedure for testing the full brake assembly was different to the previous hammer tests. The brake was assembled in a similar fashion as before with the following exceptions:

1. The steering arm was attached to the support bracket with a stiff link.
2. The drive flange was bolted to the hub with spacer washers between it and the disc to simulate the contact areas at the wheel studs.
3. Before measurements were taken, a torque was applied to the brake at low brake pressure to ensure that the pads had seated against their abutments in the cage. The pressure was then increased to 90 bar to compress the pads onto the disc. The torque was then removed and the pressure reduced to 40 bar for the hammer test.

The brake assembly was tested in this condition as four components; the disc, hub, cage and calliper. The disc had 41 nodes, 36 on the disc annulus and five at the bolt positions. Each was measured in the axial (Z) and radial (R) directions. Two non-orthogonal nodes were used for the fixed hammer test in the axial (Z) and radial (R) directions giving four reference degrees of freedom for the test. Tangential modes of the disc could not be measured. The hub (knuckle) had 9 nodes, the cage (carrier) had 10 nodes and the calliper (fist) had 11 nodes. A fixed hammer test was used for each, measured in the three orthogonal directions (X, Y, Z) with three orthogonal reference degrees of freedom.

The measurements in R and Z on the disc revealed some radial modes within the squeal frequency range as well as the expected axial modes. Figure 6-5 shows the disc modes for this test in order of increasing frequency.

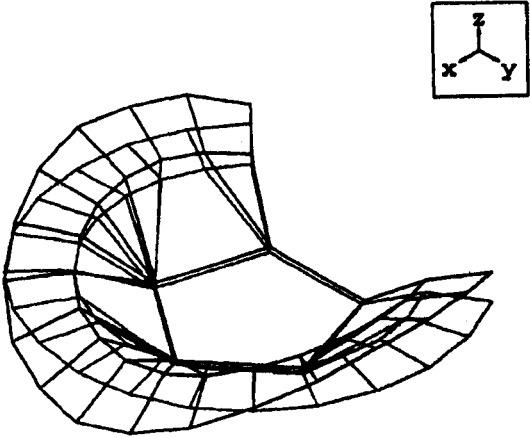
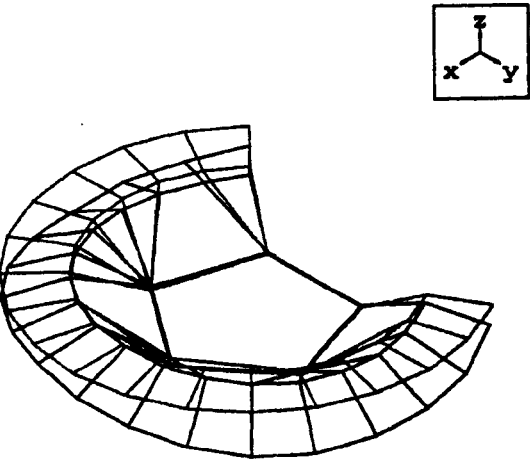
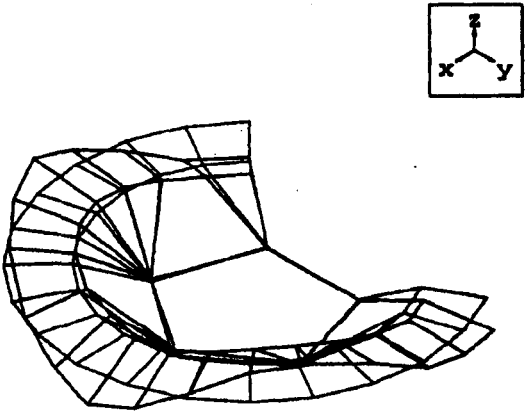
Mercedes vented disc modes – full brake hammer test	
	<p>Frequency : 1233.8 Hz</p> <p>Damping : 1.44%</p> <p>Mode shape :</p> <p style="padding-left: 40px;">Z – mode</p> <p style="padding-left: 40px;">2 diameters [$j = 2, n = 0$]</p> <p>Antinode aligned with brake pad</p>
	<p>Frequency : 1419.8 Hz</p> <p>Damping : 3.19%</p> <p>Mode shape :</p> <p style="padding-left: 40px;">Z – mode</p> <p style="padding-left: 40px;">0 diameters [$j = 0, n = 0$]</p> <p>Diaphragm mode (not an [$n = 1$] mode)</p>
	<p>Frequency : 2601.1 Hz</p> <p>Damping : 1.03%</p> <p>Mode shape :</p> <p style="padding-left: 40px;">Z – mode</p> <p style="padding-left: 40px;">3 diameters [$j = 3, n = 0$]</p> <p>Antinode aligned with brake pad</p>

Figure 6-5 : Mercedes vented disc mode shapes from the full brake hammer test

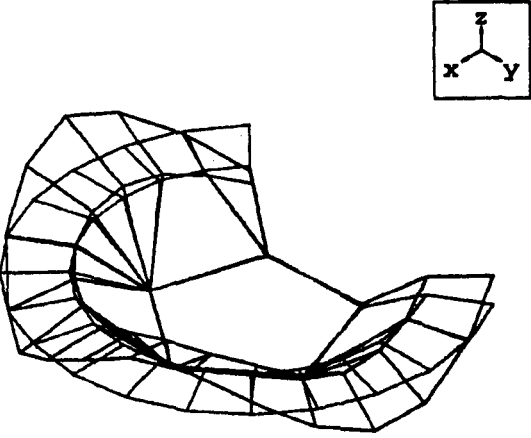
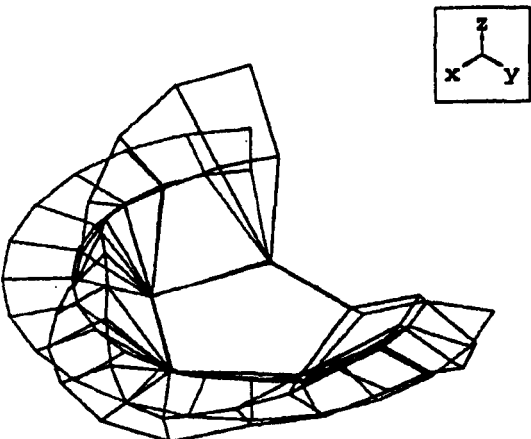
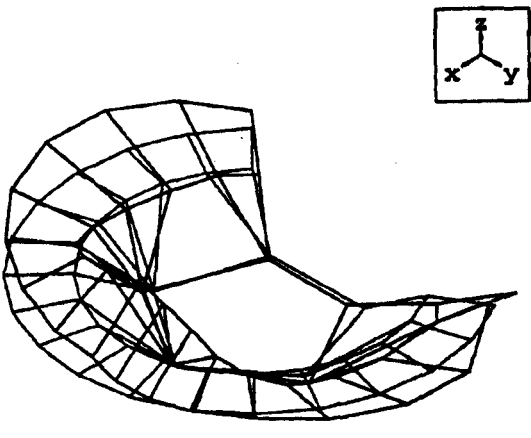
Mercedes vented disc modes – full brake hammer test	
	<p>Frequency : 3135.3 Hz</p> <p>Damping : 0.87%</p> <p>Mode shape :</p> <p style="padding-left: 40px;">Z – mode</p> <p style="padding-left: 40px;">3 diameters [$j = 3, n = 0$]</p> <p>Node aligned with brake pad</p>
	<p>Frequency : 3507.1 Hz</p> <p>Damping : 1.24%</p> <p>Mode shape :</p> <p style="padding-left: 40px;">R – mode</p> <p style="padding-left: 40px;">2 diameters</p> <p>Node aligned with brake pad</p>
	<p>Frequency : 3720.1 Hz</p> <p>Damping : 1.04%</p> <p>Mode shape :</p> <p style="padding-left: 40px;">R – mode</p> <p style="padding-left: 40px;">2 diameters</p> <p>Antinode aligned with brake pad</p>

Figure 6-5 (continued) : Mercedes vented disc mode shapes from the full brake hammer test

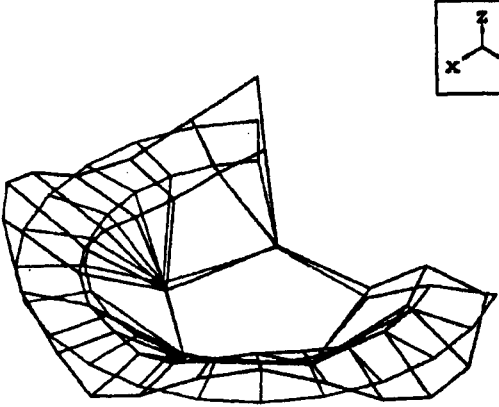
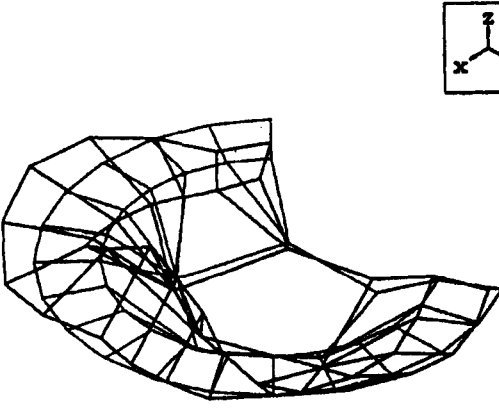
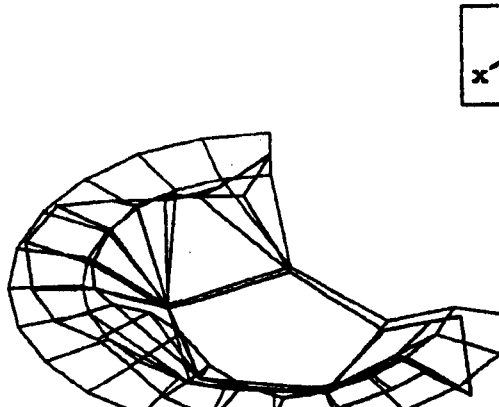
Mercedes vented disc modes – full brake hammer test	
	<p>Frequency : 3918.1 Hz</p> <p>Damping : 1.49%</p> <p>Mode shape :</p> <p>Z – mode</p> <p>4 diameters [$j = 4, n = 0$]</p> <p>Antinode aligned with brake pad</p>
	<p>Frequency : 5845.3 Hz</p> <p>Damping : 1.17%</p> <p>Mode shape :</p> <p>R – mode</p> <p>3 diameters</p> <p>Antinode aligned with brake pad</p>
	<p>Frequency : 6247.1 Hz</p> <p>Damping : 0.88%</p> <p>Mode shape :</p> <p>R – mode</p> <p>0 diameters</p> <p>Radial 'breathing' mode</p>

Figure 6-5 (continued) : Mercedes vented disc mode shapes from the full brake hammer test

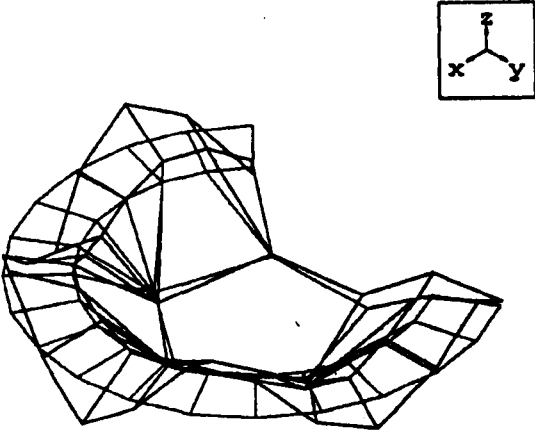
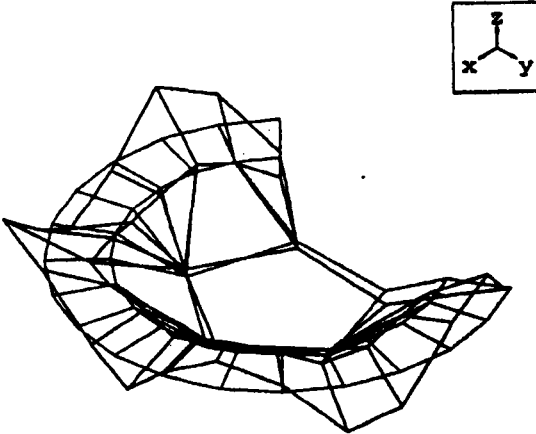
Mercedes vented disc modes – full brake hammer test	
	<p>Frequency : 6386.1 Hz</p> <p>Damping : 0.76%</p> <p>Mode shape :</p> <p style="padding-left: 40px;">Z – mode</p> <p style="padding-left: 40px;">5 diameters [$j = 5, n = 0$]</p> <p>Antinode aligned with brake pad</p>
	<p>Frequency : 6499.3 Hz</p> <p>Damping : 0.57%</p> <p>Mode shape :</p> <p style="padding-left: 40px;">Z – mode</p> <p style="padding-left: 40px;">5 diameters [$j = 5, n = 0$]</p> <p>Node aligned with brake pad</p>

Figure 6-5 (continued) : Mercedes vented disc mode shapes from the full brake hammer test

The appearance of a mode in the hub, cage or calliper at or near the same frequency as a Z directional mode in the disc would indicate that the brake component was assisting in the development of resonance at that frequency. In table 6-4 a comparison is made for the recognisable [$n = 0$] Z direction modes in the disc with an indication of similar frequencies in other brake components.

Mercedes vented disc – Full brake assembly hammer test				
Nodal diameters	Disc	Hub	Cage	Calliper
$j = 2$	1233.8 (1.44)	1244.4 (0.97)	1245.1 (3.40)	1246.6 (1.39)
$j = 3$	2601.1 (1.03)	2609.4 (0.36)	-	-
	3135.3 (0.87)	3138.3 (0.48)	3113.0 (2.73)	3025.8 (1.30)
$j = 4$	3918.1 (1.49)	4003.3 (0.41)	3970.74 (1.57)	3938.2 (1.52)
$j = 5$	6386.1 (0.76)	6480.1 (0.18)	-	-

Table 6-4 : Mercedes vented disc – Z direction [$n = 0$] disc modes compared with other brake component modes (Frequencies in Hz, percentage damping in parentheses)

For the [$j = 2$] mode, all the brake components have a resonant frequency close to that of the disc which may indicate that the whole structure has a mode at this frequency. There is also good correlation for both [$j = 3$] modes between the disc and the hub, but not for the other components. The comparison for the other modes is less clear, with large differences in frequency between the disc and the other components. It is unlikely that they are influencing the disc at these frequencies.

Mercedes vented disc		
Nodal diameters	Mean squeal frequency	Full brake assembly hammer test – disc modes
$j = 2$	1351 (1323.0 – 1378.0)	1233.8 (1.44)
$j = 3$	2401 (2089.3 – 2713.3)	2601.1 (1.03)
$j = 4$	4203 (4139.0 – 4266.1)	3918.1 (1.49)
$j = 5$	6139 (5599.3 – 6678.8)	6386.1 (0.76)

Table 6-5 : Mercedes vented disc – comparison of squeal modes with disc modes from the full brake assembly hammer test (Frequency range shown in parentheses under the squeal frequencies, percentage damping in parentheses after the disc mode frequencies)

Table 6-5 compares these disc frequencies with experimental squeal frequencies found on the Mercedes vented disc. It can be seen from this table that the correlation between the recorded squeal frequencies and the mode frequencies from the full brake assembly hammer test is good for the $[j = 3]$ and $[j = 5]$ modes. For the $[j = 2]$ and $[j = 4]$ modes the hammer test frequency was lower than for the equivalent squeal mode. The higher frequency $[j = 3]$ mode given in table 6-4 was not included in table 6-5 as it did not match any definite squeal mode.

Chapter 7 : Squeal test results

7.1 Recording squeal events

Disc brake squeal events on the dynamometer used for this research were unpredictable. Very often there would be no squeal noise from the brake for hours, followed by a short period when several events could be recorded before reverting to quiet running. However, there were some actions which seemed to promote the occurrence of squeal. The brake pads were not fitted with any form of squeal suppression device in any of the tests. The anti-squeal shims which were glued to the back plate of the Mercedes pads were removed. None of the brakes would squeal from a cold start. Each had to be warmed up by a bedding-in process lasting about half an hour in which the disc was run at low speed (about 6 rad s^{-1}) with a brake pressure of between 3 and 10 bar. This process warmed the disc to about $250 \text{ }^\circ\text{C}$ and also warmed the pads through. After about a hour, the whole of the calliper system was hot to the touch. After this warming session, the brake would be more likely to squeal as the temperature of the disc was dropped to about $150 \text{ }^\circ\text{C}$. If squeal started, testing would usually increase the temperature again and it would stop squealing. Obviously, the tests at high pressures and speeds increased the temperature very quickly and so had to be of short duration. Tests performed with initially wet pads and the use of water spray on the discs did not promote squeal. As squeal generally occurred when the discs were at a temperature of at least $100 \text{ }^\circ\text{C}$, it is unlikely that moisture or humidity is an important factor in the generation of brake squeal on this dynamometer.

For each disc brake, the testing procedure followed much the same form. After the initial warming, a matrix of running conditions was imposed where the disc speed, the brake pressure and the disc temperature were varied. For each speed setting, the pressure was slowly changed over the full range available (limited by the maximum torque of 400 Nm). If a squeal event occurred, it was usually as pressure was increasing, and it would occur over a limited pressure range. The event was recorded with the pressure set to produce the loudest (and usually most consistent) audible squeal noise. The sequence of disc speeds was not usually incremental, and was different for each speed cycle to ensure a variation in disc temperature and pad bedding-in conditions before each test sequence. In this way, the complete set of combinations of speed, pressure and temperature were covered many times and squeal events recorded when they occurred.

Each recorded event lasted for about 0.3 s. Consequently, for disc rotation speeds of less than 20 rad s^{-1} , the time of the recorded event was less than one revolution of the disc. Manual triggering of the recording process was not always successful in capturing the best data at these slow speeds if the squeal event was intermittent or highly variable. In these cases, where the squeal lasted for long enough, several recordings were taken using different trigger timings.

7.2 Squeal test results

The results of the squeal tests are shown in tabulated and graphical form. In the tabulated form, the test names for a given disc are in chronological order by number, i.e. test t27 was recorded before test t46. Test names with the suffix a, b, etc. have more than one squeal frequency recorded in the same test. For example, in the table for the Mercedes solid disc results, the analysis of test t05 indicated that two squeal frequencies were present. One frequency was named t05a, the other was named t05b. In the graphical form of the results, symbols are used to represent different squeal frequency wave types, as shown in table 7-1.

Symbol	Wave type
○	Standing wave
□	Forward travelling wave
Δ	Backward travelling wave

Table 7-1 : Symbols used in the graphic results

The results are for the three disc brake types tested; the Rover brake, the Mercedes brake with a solid disc and the Mercedes brake with a vented disc. The results for each brake type are in separate sections as follows:-

7.2.1 Rover brake with a solid disc

Tables 7-2 and 7-3 show the results for the tests on the Rover brake. There were no recorded tests that contained forward travelling waves. The test conditions were measured during the test and the average value of each has been tabulated. The values of squeal frequency, maximum displacement and the number of nodal diameters given in the tables are those calculated with the procedures given in Chapter 5.

Figure 7-1 shows the displacement amplitude normal to the disc related to squeal frequency and the mode order as the number of nodal diameters. Squeal frequencies for this disc tend to be polarised about the two lower frequencies of 3 kHz (4 nodal diameters) and 4 kHz (5 nodal diameters) with a few tests showing squeals at 6 kHz (6 nodal diameters) and 8 kHz (7 nodal diameters). Of the 44 tests which gave data that could be analysed, 27 were standing waves (shown as ○) and 17 were backward travelling waves (shown as Δ). Although the three tests at 6 kHz showed backward travelling waves, this does not appear significant; there seems to be no wave type preference relating to squeal frequency.

standing wave squeal tests							
test conditions					squeal parameters		
test name	temp.	speed	torque	pressure	freq.	max. amp.	nodal dia.'s ¹
	°C	rad s ⁻¹	Nm	MPa	Hz	mm	
t02b	96.7	3.193	219.25	1.0225	8167.4	9.18E-06	7(2)
t03	105.5	3.220	223.29	1.0273	4055.9	1.94E-04	5(2)
t06b	144.8	6.358	179.11	0.8184	7967.0	1.87E-05	7(2)
t09b	188.0	10.409	140.86	0.5951	3865.5	2.82E-04	5(2)
t10b	201.0	10.412	150.46	0.5991	3870.3	3.27E-04	5(2)
t11	247.5	10.468	173.77	0.6462	3937.0	9.65E-05	5(2)
t13a	269.0	10.504	131.81	0.4852	3452.1	4.08E-05	4(1)
t13b	269.0	10.504	131.81	0.4852	3747.7	1.88E-04	5(2)
t14b	274.9	10.483	132.84	0.4966	3718.5	2.70E-04	5(2)
t15	234.8	20.667	134.20	0.5988	3846.0	2.71E-04	5(2)
t21	193.2	3.260	129.42	0.5956	2924.2	2.75E-04	4(1)
t23	195.3	3.247	183.83	0.7853	2950.3	4.77E-04	4(1)
t24	208.1	3.232	313.18	1.2297	3045.4	4.45E-04	4(1)
t25	224.4	3.194	363.38	1.3785	3057.9	5.19E-04	4(1)
t26	231.7	3.212	236.46	0.9429	2991.8	7.32E-05	4(1)
t30	116.2	6.345	172.64	0.7519	3000.3	8.15E-04	4(1)
t31	128.3	6.337	199.93	0.8543	3008.2	8.15E-04	4(1)
t32	141.0	6.343	245.25	1.0366	3043.3	4.42E-04	4(1)
t33	158.2	6.331	291.35	1.1784	3048.5	8.50E-04	4(1)
t34	179.0	6.281	348.66	1.4077	3061.1	6.01E-04	4(1)
t35	205.4	6.305	286.46	1.1734	3052.1	4.20E-04	4(1)
t36	217.4	6.357	179.11	0.7868	2894.6	8.79E-04	4(1)
t37	221.9	6.380	135.66	0.5836	2888.3	4.01E-04	4(1)
t39a	202.2	6.365	201.90	0.7625	2905.0	8.93E-04	4(1)
t43	221.9	10.468	135.30	0.5359	2899.8	1.03E-04	4(1)
t45	212.8	10.452	137.46	0.5204	2895.2	3.32E-04	4(1)
t51	182.2	3.263	242.12	0.8253	2960.9	5.66E-04	4(1)

Note : 1. the number of antinodes under the pad is in parentheses

Table 7-2 : Rover brake – test results with standing waves

backward travelling wave squeal tests							
test conditions				squeal parameters			
test name	temp.	speed	torque	pressure	freq.	max. amp.	nodal dia.'s ¹
	°C	rad s ⁻¹	Nm	MPa	Hz	mm	
t02a	96.7	3.193	219.25	1.0225	4034.6	9.28E-04	5(2)
t04	119.5	3.229	181.12	0.8165	3953.0	4.50E-04	5(2)
t05	135.4	6.342	157.51	0.7263	3931.5	3.42E-04	5(2)
t06a	144.8	6.358	179.11	0.8184	3969.4	1.08E-03	5(2)
t07	155.8	6.367	169.28	0.7533	3958.4	6.92E-04	5(2)
t09a	188.0	10.409	140.86	0.5951	3571.6	2.43E-04	5(2)
t10a	201.0	10.412	150.46	0.5991	3576.4	1.21E-04	5(2)
t14a	274.9	10.483	132.84	0.4966	3423.7	1.04E-04	4(1)
t22	192.9	3.244	158.69	0.6920	2946.0	6.24E-04	4(1)
t38	189.4	6.345	58.34	0.2671	5899.9	1.17E-04	6(2)
t39b	202.2	6.365	201.90	0.7625	5812.2	5.97E-05	6(2)
t40	210.5	6.353	149.29	0.5540	2860.2	2.08E-03	4(1)
t42	209.5	10.526	97.71	0.4391	6164.5	1.18E-04	6(2)
t44	220.4	10.466	179.09	0.6938	2928.2	3.46E-04	4(1)
t46	149.1	3.228	117.27	0.4886	8234.6	6.13E-05	7(2)
t50	177.3	3.259	279.50	0.9657	3013.3	1.53E-04	4(1)
t52	185.3	3.242	182.60	0.6271	2928.3	1.64E-03	4(1)

Note : 1. the number of antinodes under the pad is in parentheses

Table 7-3 : Rover brake – test results with backward travelling waves

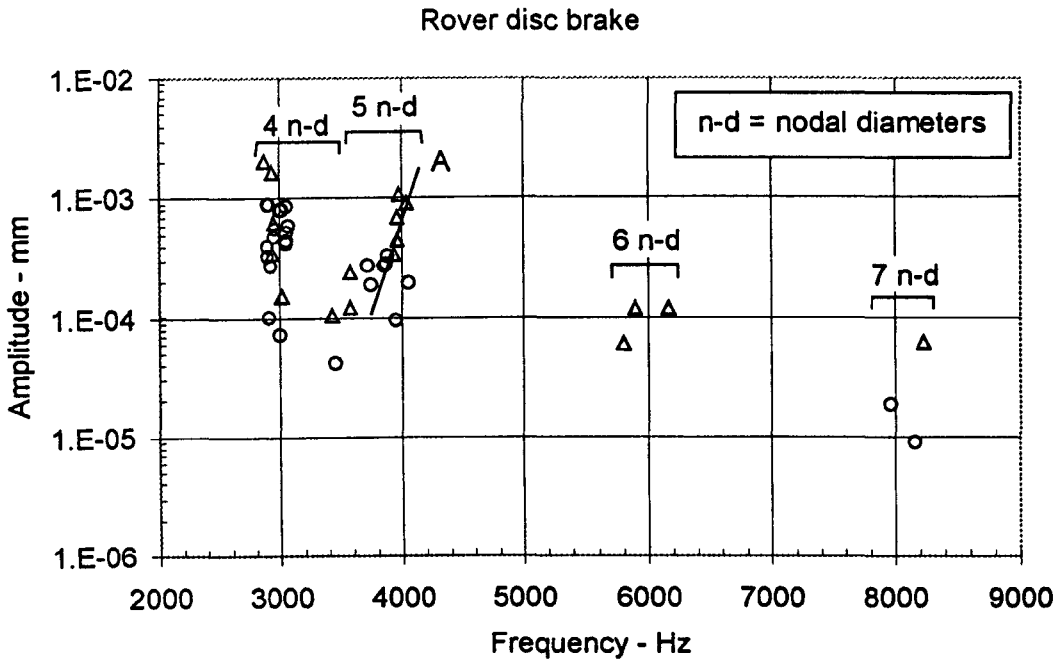


Figure 7-1 : Amplitude / frequency plot for the Rover disc brake

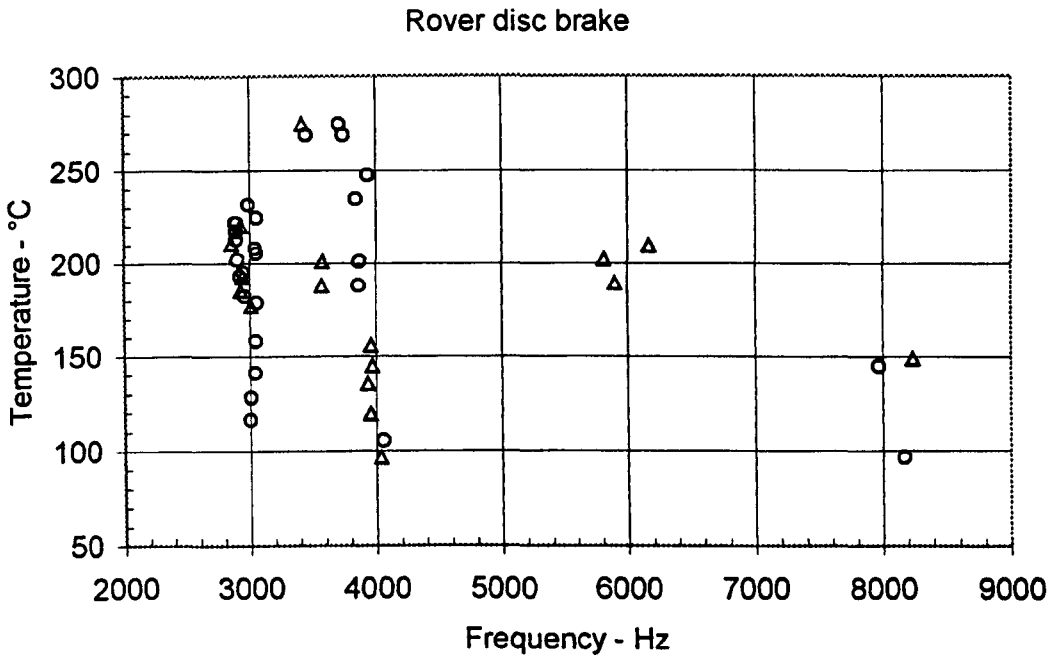


Figure 7-2 : Temperature / frequency plot for the Rover disc brake

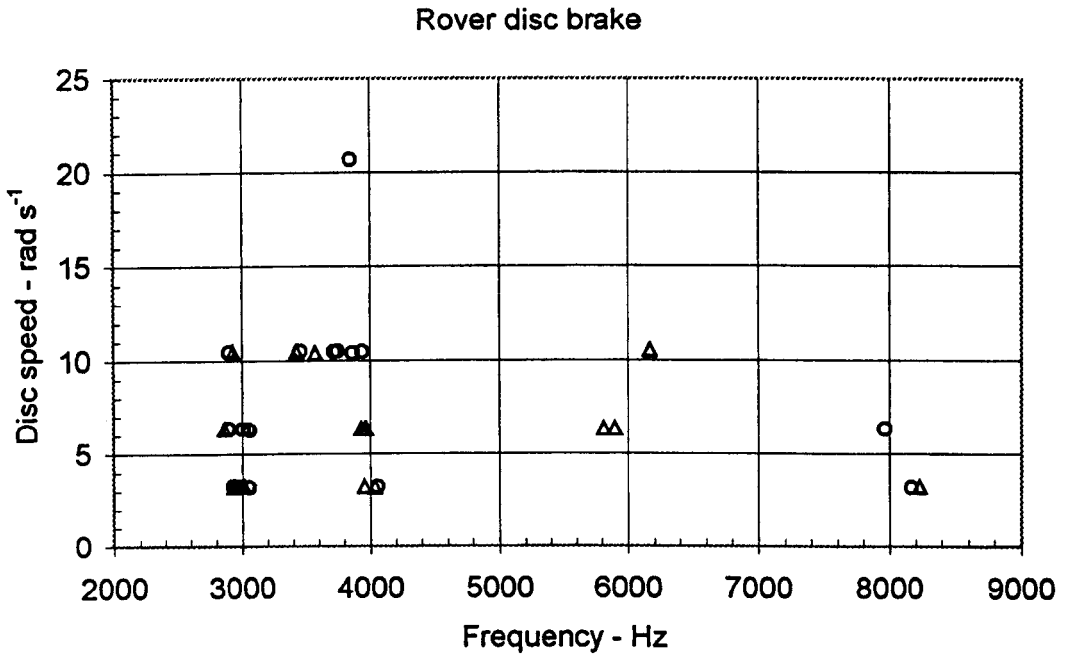


Figure 7-3 : Disc speed / frequency plot for the Rover disc brake

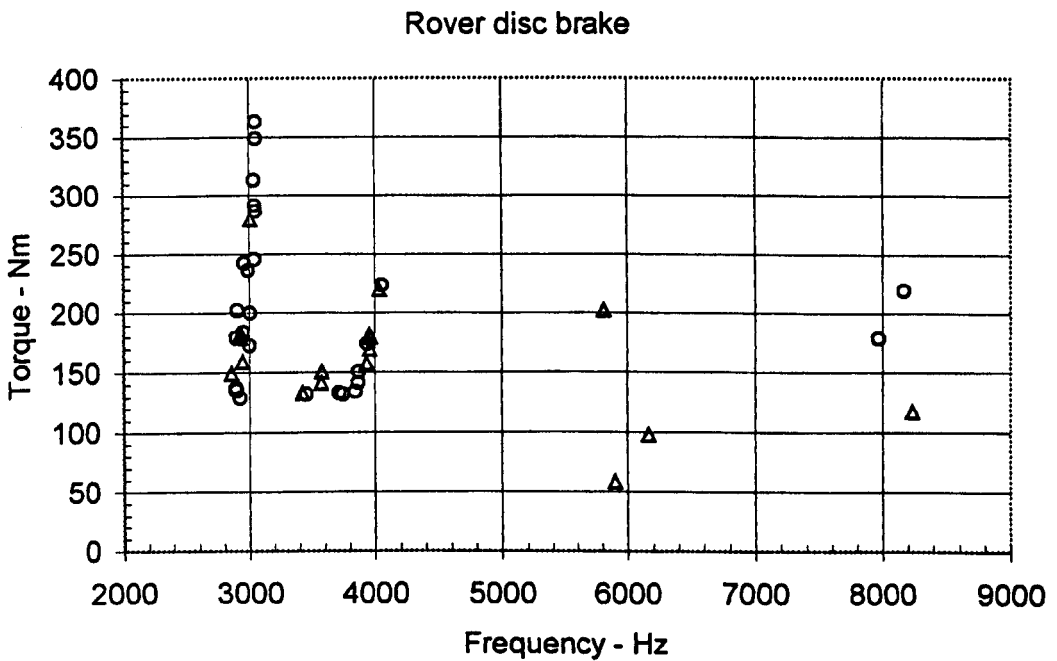


Figure 7-4 : Torque / frequency plot for the Rover disc brake

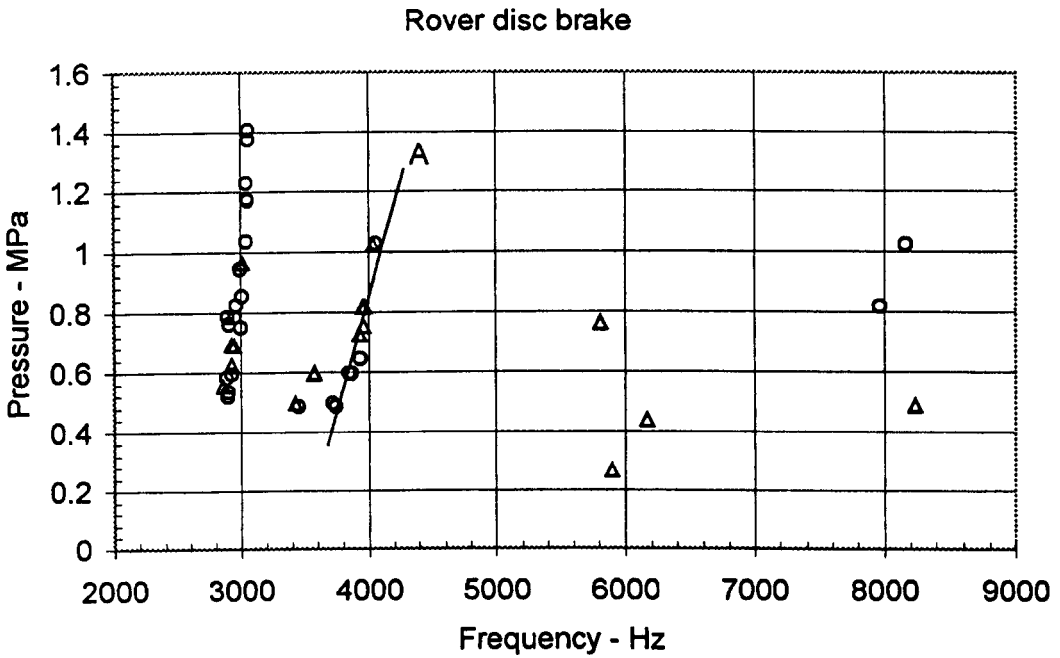


Figure 7-5 : Pressure / frequency plot for the Rover disc brake

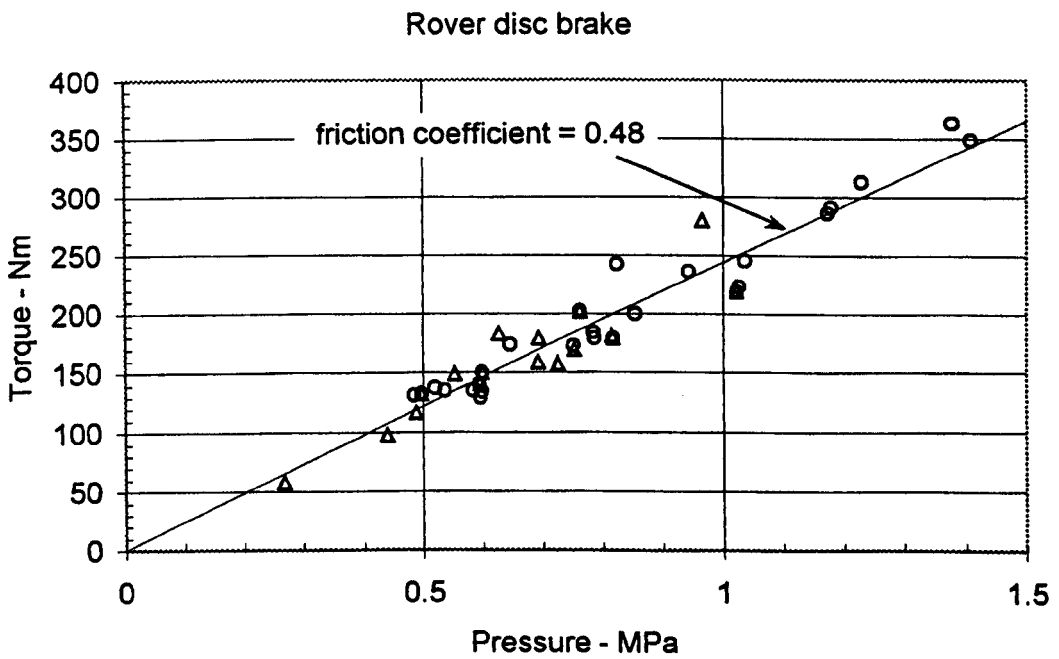


Figure 7-6 : Torque / pressure plot for the Rover disc brake

There is a tendency for the 5-order mode to increase frequency with an increase in amplitude, as indicated by the trend line 'A' in figure 7-1. This is markedly different from most of the 4-order mode squeals which do not change frequency with amplitude. The difference between the two modes is that the 4-order mode squeals have one antinode under the pad and the 5-order mode squeals have two antinodes under the pad. If these two antinodes are compressed under the pad and the inter-nodal spacing is longer under the pad for a larger squeal amplitude, then the inter-nodal spacing will be shorter away from the pad, where the squeal noise is generated, giving a higher noise frequency. The single antinode under the pad for the 4-order mode squeals did not perform this compression variation.

Figures 7-2 to 7-5 show the relationship between squeal frequency and the test conditions of disc temperature, speed, shaft torque and hydraulic pressure. No squeal events were recorded at disc speeds greater than 21 rad s^{-1} .

Of some interest here are the tests showing squeal frequencies between the 3 kHz and the 4 kHz clusters. These tests all occurred at temperatures above $180 \text{ }^\circ\text{C}$, at a disc speed of 10 rad s^{-1} and at torque levels below 150 Nm . This may indicate that there is a coupling effect between a disc mode and some brake structural mode during these squeal tests, whereas the wide parameter range of the 3 kHz and 4 kHz squeal events indicate modes related only to the disc. There may also be some significance to the 6 kHz cluster occurring at $200 \text{ }^\circ\text{C}$, but is not conclusive as there was an insufficient number of squeal events at this frequency.

Figure 7-5 shows the effect of hydraulic pressure on frequency. The trend line indicated as 'A' on this plot shows that for the 5-order mode with two antinodes under the pad, an increase in pressure causes an increase in noise frequency. The increase in pressure forces the compressed antinode spacing under the pad to expand a little and the antinode spacing away from the pad must compress, causing an increase in noise frequency.

Figure 7-6 shows the relationship between shaft torque and hydraulic pressure during the squeal event. This shows a linear trend with very little zero offset. The trend line

in this plot is a least squares fit to the data, the slope being used to calculate the coefficient of friction (0.48). System values used in the calculation were the hydraulic piston diameter of 54 mm and the effective pad radius of 110 mm (given by BBA Friction). The effect of brake piston seal friction was not taken into account.

7.2.2 Mercedes brake with solid disc

standing wave squeal tests							
test conditions					squeal parameters		
test name	temp. °C	speed rad s ⁻¹	torque Nm	pressure MPa	freq. Hz	max. amp. mm	nodal dia.'s ¹
t01b	33.0	3.221	77.78	0.3341	6599.4	1.38E-05	6(1)
t03	119.5	6.292	37.51	0.2087	4275.1	7.27E-05	5(1)
t05a	64.3	6.291	225.73	0.8504	7507.5	1.51E-04	7(2)
t05b	64.3	6.291	225.73	0.8504	2173.2	8.44E-05	4(2)
t06	83.7	6.317	210.93	0.8329	7540.2	1.31E-04	7(2)
t07	180.2	10.374	33.85	0.1929	4200.7	8.17E-05	5(1)
t08	174.2	10.394	34.77	0.2077	4217.6	6.97E-05	5(1)
t09	190.9	15.470	52.71	0.2741	4303.2	5.13E-05	5(1)
t10	203.7	15.476	58.50	0.2881	7092.8	1.41E-05	7(2)
t14	170.5	20.602	41.30	0.1958	7353.6	2.41E-05	7(2)
t15	227.1	20.624	28.45	0.1802	4199.4	7.60E-05	5(1)
t16	221.0	20.629	33.44	0.2015	4210.2	7.64E-05	5(1)
t17	252.4	20.614	30.73	0.1880	4204.3	1.24E-04	5(1)
t18	219.6	25.734	28.63	0.1717	7077.1	5.44E-05	7(2)
t19a	255.8	25.754	25.22	0.1554	6797.1	3.75E-05	6(1)
t25	216.7	3.253	87.43	0.4016	7409.0	3.19E-05	7(2)
t27	131.7	3.234	182.26	0.6581	7112.3	3.24E-05	7(2)
t29a	269.7	100.282	18.32	0.1221	5681.6	2.51E-05	6(1)
t29b	269.7	100.282	18.32	0.1221	4167.2	1.94E-05	5(1)
t35	168.2	61.481	35.15	0.2304	6534.6	1.35E-04	6(1)
t36	177.0	61.469	36.38	0.2279	6645.3	1.38E-04	6(1)
t38	271.1	41.033	36.82	0.1821	4189.3	1.15E-04	5(1)
t39	278.1	41.024	34.55	0.1748	4172.7	8.97E-05	5(1)
t40b	274.1	41.039	41.26	0.1976	1681.5	6.30E-05	3(1)
t42	287.6	41.033	100.28	0.3695	6952.9	7.38E-05	7(2)
t43a	60.3	3.224	28.73	0.1720	2807.4	3.68E-05	4(1)
t43b	60.3	3.224	28.73	0.1720	1892.3	3.36E-05	3(1)
t44	63.7	3.211	83.90	0.3401	1755.1	1.54E-04	3(1)
t46b	197.0	15.508	30.01	0.1778	4292.4	1.82E-05	5(1)
t47	232.2	3.278	95.46	0.3780	8201.1	1.63E-04	7(1)

Note : 1. the number of antinodes under the pad is in parentheses

Table 7-4 : Mercedes solid disc brake – test results with standing waves

forward travelling wave squeal tests							
test conditions					squeal parameters		
test name	temp. °C	speed rad s ⁻¹	torque Nm	pressure MPa	freq. Hz	max. amp. mm	nodal dia.'s ¹
t19b	255.8	25.754	25.22	0.1554	2944.4	2.13E-05	4(1)
t21	263.0	30.900	18.95	0.1281	8090.9	5.37E-05	7(1)
t40a	274.1	41.039	41.26	0.1976	2954.8	2.32E-05	4(1)
t46a	197.0	15.508	30.01	0.1778	3054.8	4.01E-05	4(1)

Note : 1. the number of antinodes under the pad is in parentheses

Table 7-5 : Mercedes solid disc brake – test results with forward travelling waves

backward travelling wave squeal tests							
test conditions					squeal parameters		
test name	temp. °C	speed rad s ⁻¹	torque Nm	pressure MPa	freq. Hz	max. amp. mm	nodal dia.'s ¹
t01a	33.0	3.221	77.78	0.3341	3516.1	3.30E-04	5(2)
t02	43.3	3.231	74.41	0.3230	3519.2	2.46E-04	5(2)
t04	120.2	6.302	41.10	0.2223	4282.9	1.19E-04	5(1)
t12	196.8	15.488	24.28	0.1624	5735.6	4.03E-05	6(1)
t45	76.2	3.220	231.60	0.8062	7420.5	4.61E-05	7(2)

Note : 1. the number of antinodes under the pad is in parentheses

Table 7-6 : Mercedes solid disc brake – test results with backward travelling waves

Tables 7-4 to 7-6 show the results for the Mercedes solid disc brake. In these tests all three types of wave were found (standing, forward travelling and backward travelling), although the majority were standing waves (30 from 39 tests).

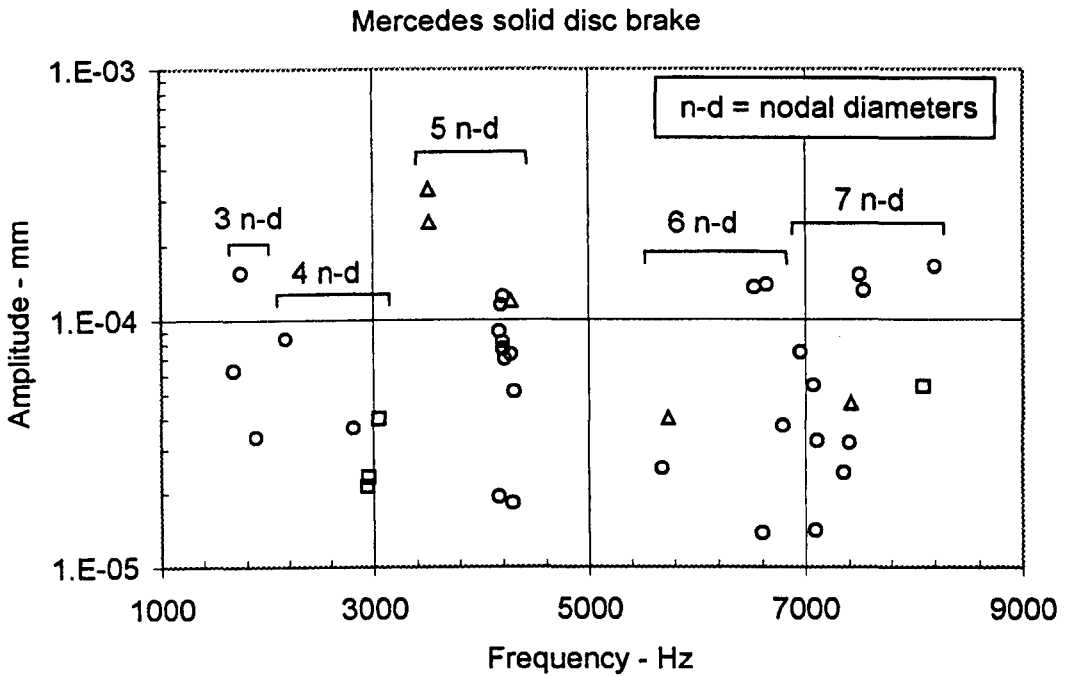


Figure 7-7 : Amplitude / frequency plot for the Mercedes solid disc brake

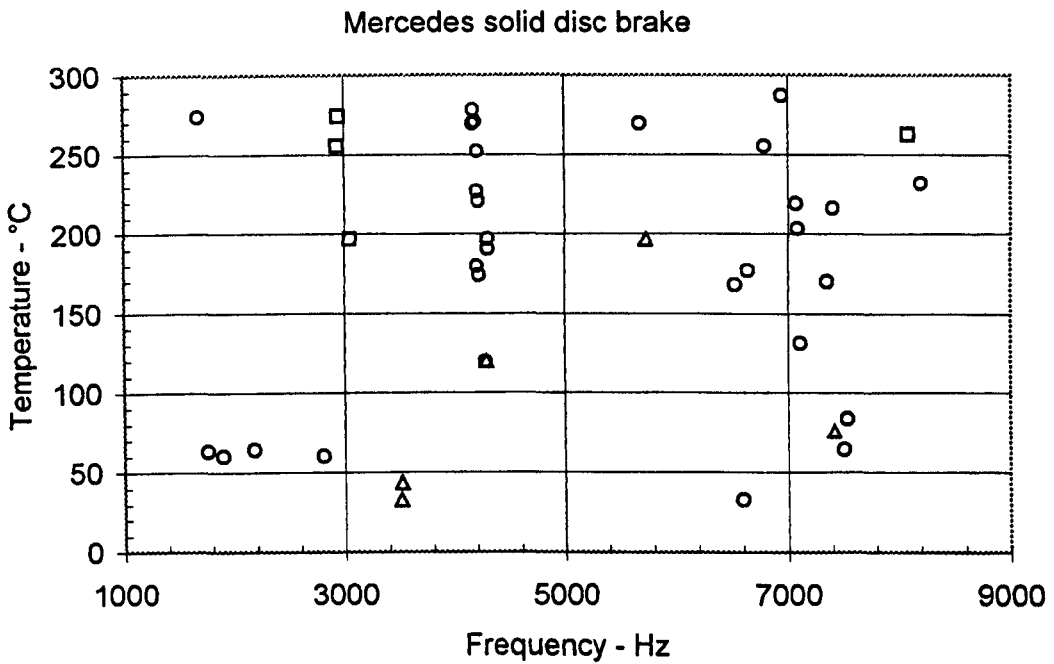


Figure 7-8 : Temperature / frequency plot for the Mercedes solid disc brake

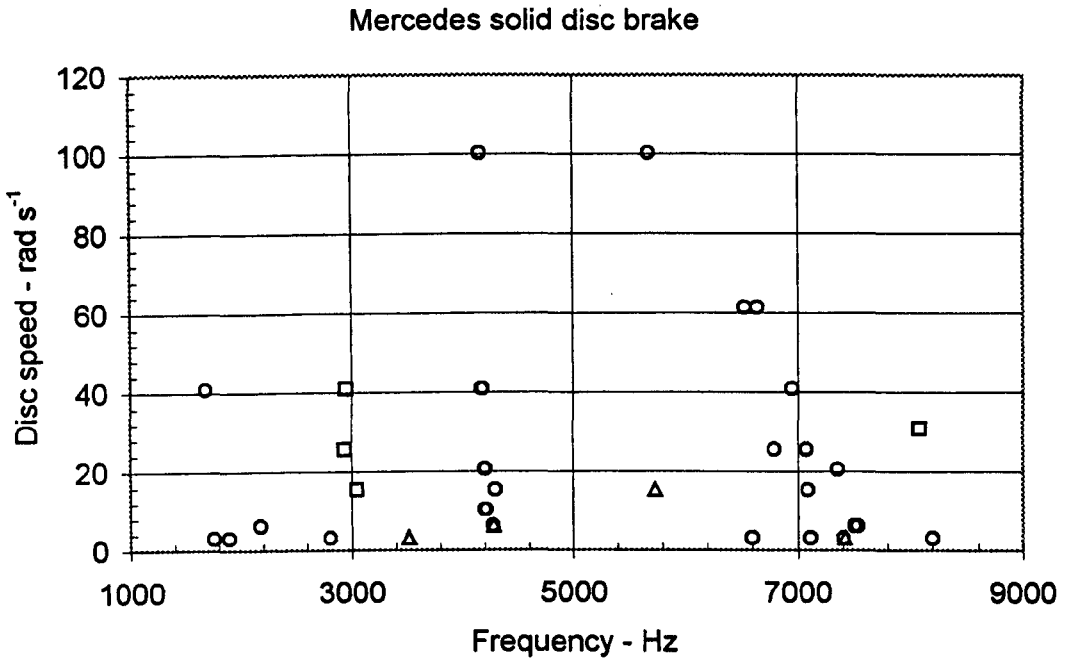


Figure 7-9 : Disc speed / frequency plot for the Mercedes solid disc brake

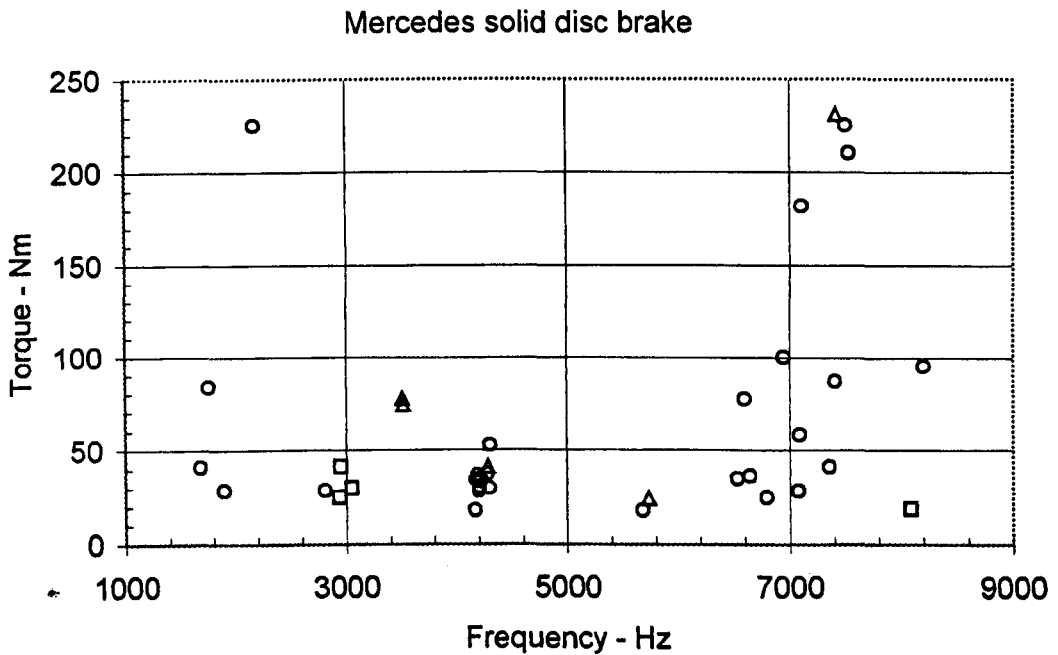


Figure 7-10 : Torque / frequency plot for the Mercedes solid disc brake

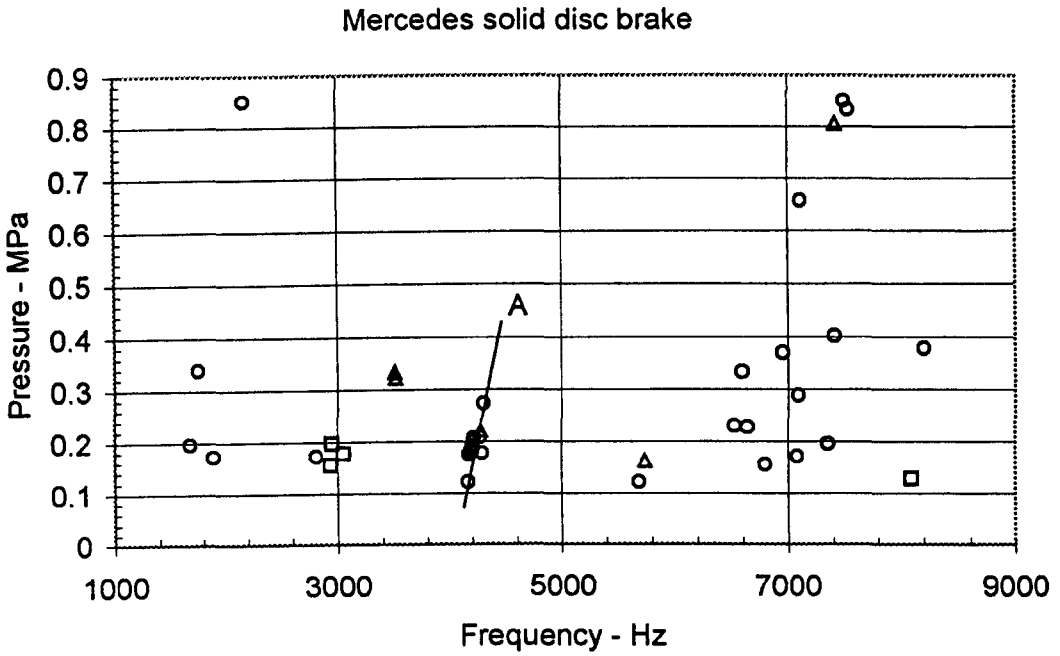


Figure 7-11 : Pressure / frequency plot for the Mercedes solid disc brake

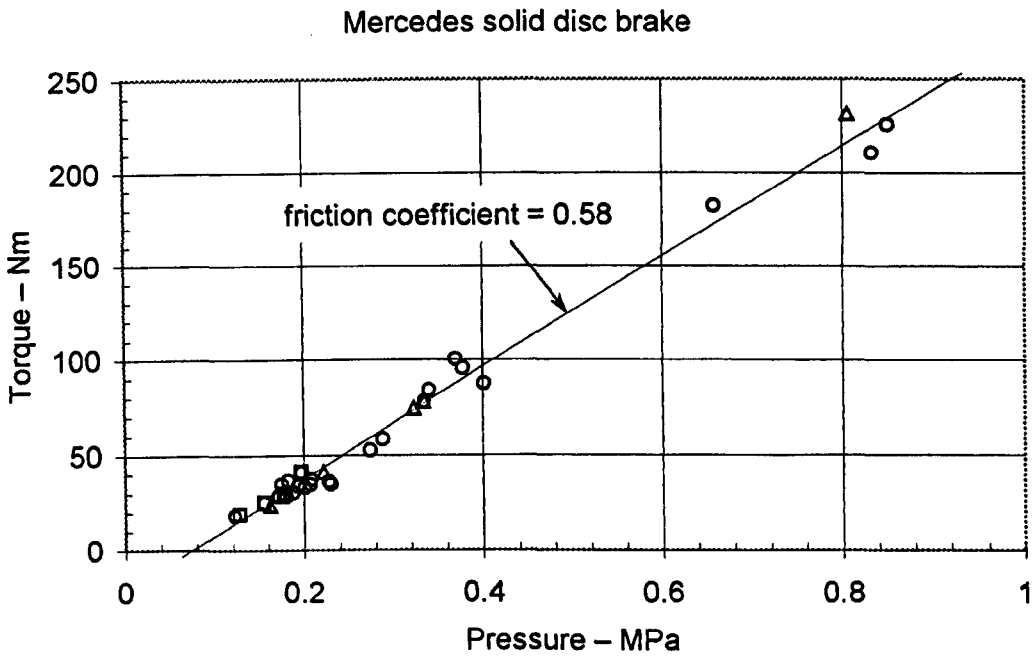


Figure 7-12 : Torque / pressure plot for the Mercedes solid disc brake

The plot of disc amplitude shown in figure 7-7 shows that this disc resonated at many frequencies in the range of interest. However, the main cluster of squeal events occurred at 4.2 kHz and were predominantly standing waves. The wide frequency gap between the 4-order mode in test t05b at 2173.2 Hz is due to there being two antinodes under the pad instead of one for the other 4-order mode tests. The presence of two antinodes compresses the inter nodal spacing under the pad and expands the inter nodal spacing for the remaining part of the disc. This larger spacing gives a lower noise frequency.

Figures 7-8 to 7-11 show the test conditions related to squeal frequency. Figure 7-8 indicates that all the 4.2 kHz cluster of squeal events occurred at temperatures above 110 °C and that the three forward travelling wave events at 3 kHz occurred at temperatures above 180 °C. For this disc there were a few squeal events recorded at high disc speeds as shown in figure 7-9 and these events were coupled with low values of shaft torque. No squeal events for this disc were recorded with torque values greater than 240 Nm and the main cluster of 4.2 kHz tests had torque values below 60 Nm.

Figure 7-11 shows similar behaviour to the Rover disc for the 5-order mode, as indicated by the trend line marked 'A'.

Figure 7-12 shows the expected linear trend of torque with pressure, but with a zero offset. The reasons for this offset have not been investigated here, but are thought to be the result of seal friction in the hydraulics, and friction between the pad backing plate and the spring supports and guides in the calliper. The least squares trend line shows a friction coefficient of 0.58, using an effective pad radius of 111 mm (given by TRW) and a hydraulic piston diameter of 54 mm.

7.2.3 Mercedes brake with vented disc

standing wave squeal tests							
test conditions					squeal parameters		
test name	temp. °C	speed rad s ⁻¹	torque Nm	pressure MPa	freq. Hz	max. amp. mm	nodal dia.'s ¹
t01	65.6	3.322	51.32	0.3116	2155.8	1.95E-05	3(1)
t05a	98.6	3.286	382.68	1.2544	2126.9	2.70E-05	3(1)
t05b	98.6	3.286	382.68	1.2544	7759.0	1.06E-04	6(1)
t09a	178.3	6.439	114.03	0.5079	2104.5	9.61E-05	3(1)
t09b	178.3	6.439	114.03	0.5079	6922.4	5.20E-05	6(2)
t10a	179.5	6.408	119.75	0.5235	2124.9	6.58E-05	3(1)
t10b	179.5	6.408	119.75	0.5235	2485.7	5.51E-05	3(1)
t10c	179.5	6.408	119.75	0.5235	6977.3	5.32E-05	6(2)
t12b	166.3	10.473	111.81	0.5274	2442.8	5.59E-05	3(1)
t12c	166.3	10.473	111.81	0.5274	3384.3	2.48E-05	4(2)
t13a	171.0	10.494	112.94	0.5314	2121.7	3.75E-05	3(1)
t13b	171.0	10.494	112.94	0.5314	2439.6	3.16E-05	3(1)
t13c	171.0	10.494	112.94	0.5314	3363.6	3.77E-05	4(2)
t16a	152.0	20.706	23.03	0.1717	1323.0	3.69E-05	2(1)
t16c	152.0	20.706	23.03	0.1717	3336.1	1.48E-05	4(2)
t27	137.0	6.480	241.83	0.8993	2119.3	8.05E-05	3(1)
t40a	180.8	3.262	27.78	0.1974	1378.0	3.60E-05	2(1)
t41	159.5	6.423	48.46	0.3130	6348.7	1.94E-05	5(1)
t42	174.7	6.375	117.50	0.5281	6979.5	1.88E-05	6(2)
t44b	148.0	10.497	33.82	0.2397	6921.7	3.80E-05	6(2)
t45a	151.1	10.490	60.69	0.3306	3018.8	2.40E-05	4(2)
t45b	151.1	10.490	60.69	0.3306	3966.0	1.22E-05	4(1)
t49	171.0	3.298	168.55	0.6533	2174.0	4.49E-05	3(1)
t50	174.2	3.225	302.72	1.1437	2166.5	2.34E-05	3(1)

Note : 1. the number of antinodes under the pad is in parentheses

Table 7-7 : Mercedes vented disc brake – test results with standing waves

backward travelling wave squeal tests							
test conditions				squeal parameters			
test name	temp.	speed	torque	pressure	freq.	max. amp.	nodal dia.'s ¹
	°C	rad s ⁻¹	Nm	MPa	Hz	mm	
t12a	166.3	10.473	111.81	0.5274	2089.3	1.68E-04	3(1)
t15	150.5	20.707	19.58	0.1632	6421.6	2.05E-05	5(1)
t16b	152.0	20.706	23.03	0.1717	2713.3	2.76E-05	3(1)
t16d	152.0	20.706	23.03	0.1717	4145.4	3.06E-05	4(1)
t16e	152.0	20.706	23.03	0.1717	6678.8	6.55E-05	6(2)
t17	181.1	20.702	17.98	0.1488	4139.0	6.51E-05	4(1)
t21	194.3	6.385	36.07	0.2259	5903.3	1.09E-04	5(1)
t24	95.8	6.407	46.83	0.2975	4207.6	2.79E-04	4(1)
t25	100.0	6.445	77.72	0.3804	4260.0	5.60E-04	4(1)
t26	103.7	6.447	81.58	0.3768	4266.1	4.97E-04	4(1)
t40b	180.8	3.262	27.78	0.1974	5913.9	8.41E-05	5(1)
t43a	147.8	10.511	32.87	0.2469	4211.0	1.99E-05	4(1)
t43b	147.8	10.511	32.87	0.2469	5599.3	5.56E-05	5(1)
t44a	148.0	10.497	33.82	0.2397	5882.8	4.14E-05	5(1)

Note : 1. the number of antinodes under the pad is in parentheses

Table 7-8 : Mercedes vented disc brake – test results with backward travelling waves

Tables 7-7 and 7-8 show the results for the Mercedes vented disc brake. No forward travelling waves were recorded from this brake. Of the 38 test results analysed, 24 were of standing waves and 14 were backward travelling waves.

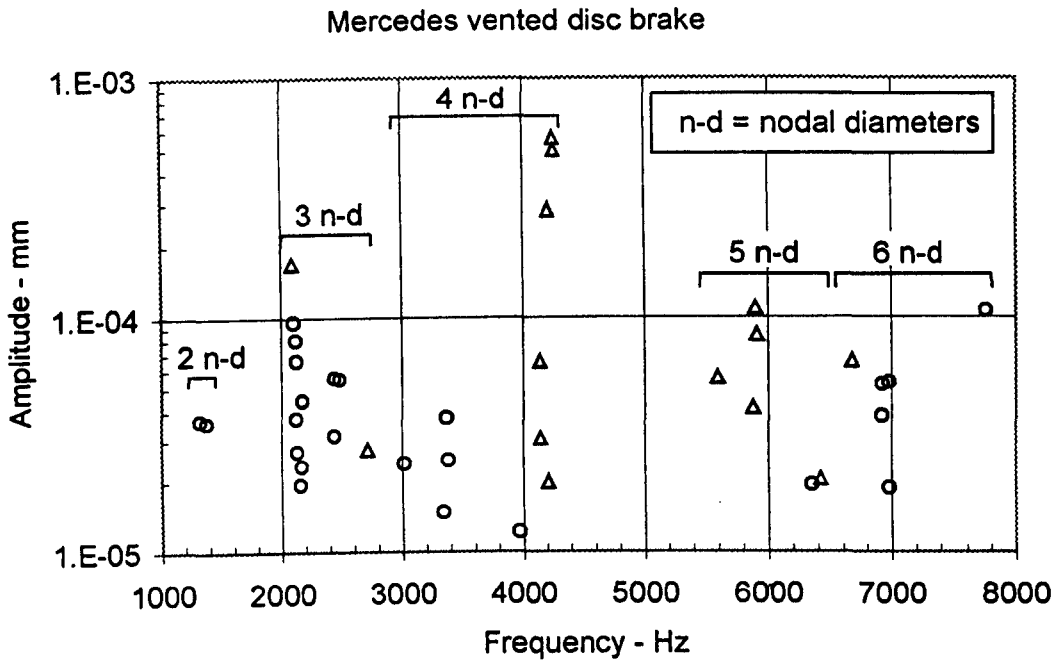


Figure 7-13 : Amplitude / frequency plot for the Mercedes vented disc brake

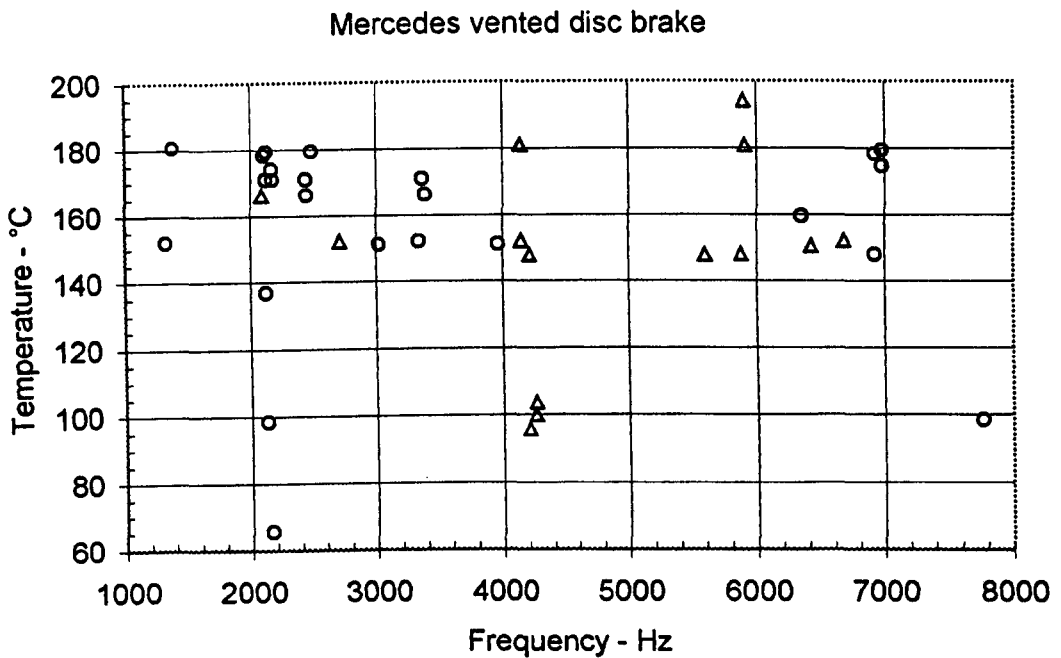


Figure 7-14 : Temperature / frequency plot for the Mercedes vented disc brake

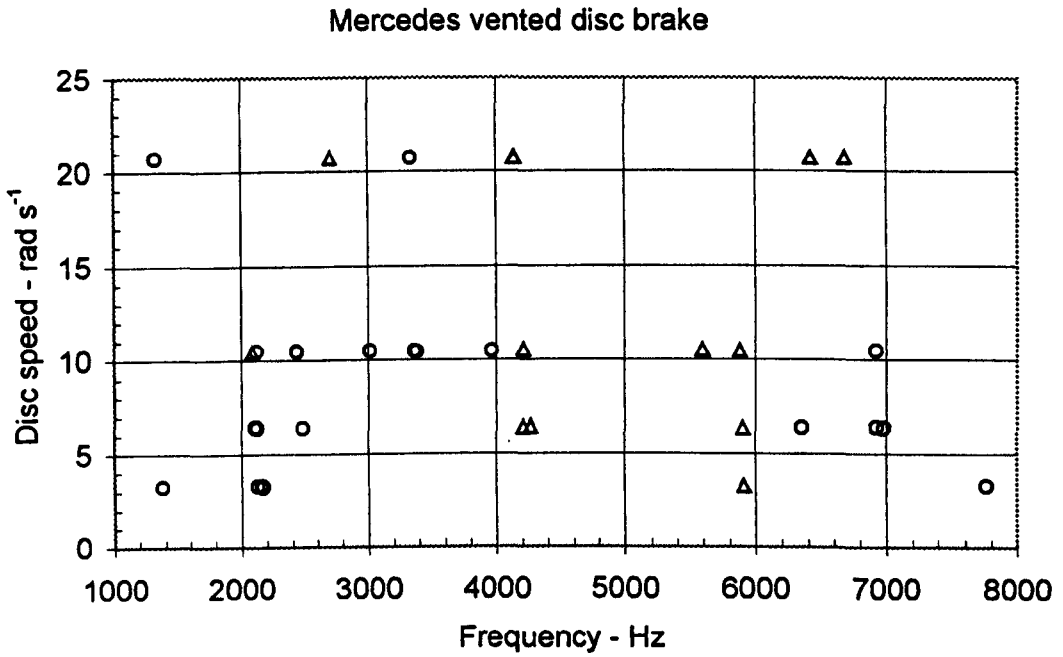


Figure 7-15 : Disc speed / frequency plot for the Mercedes vented disc brake

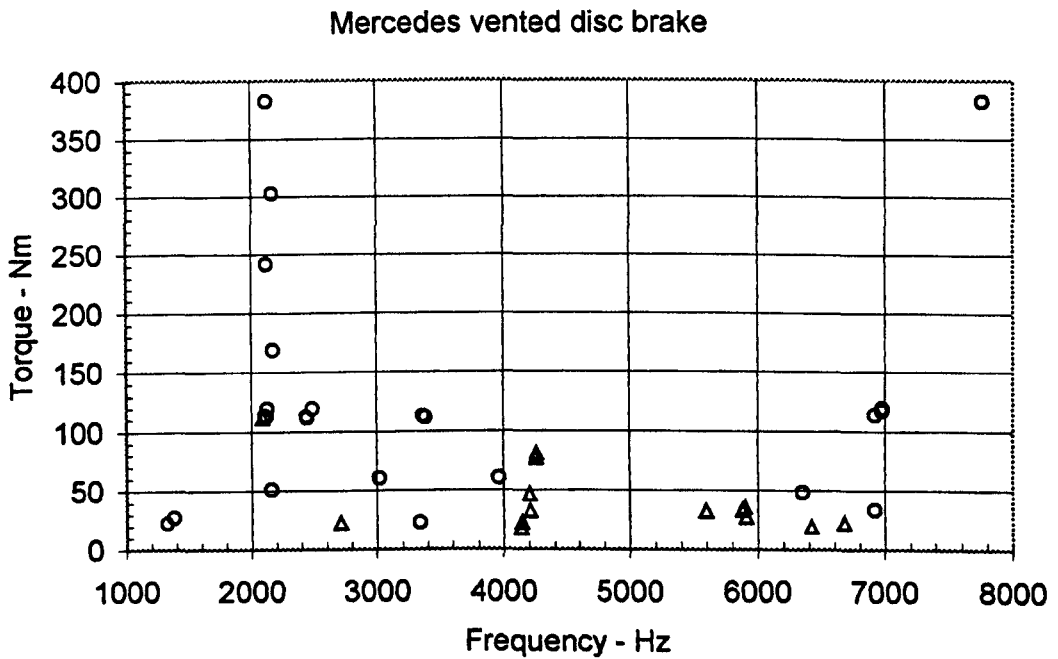


Figure 7-16 : Torque / frequency plot for the Mercedes vented disc brake

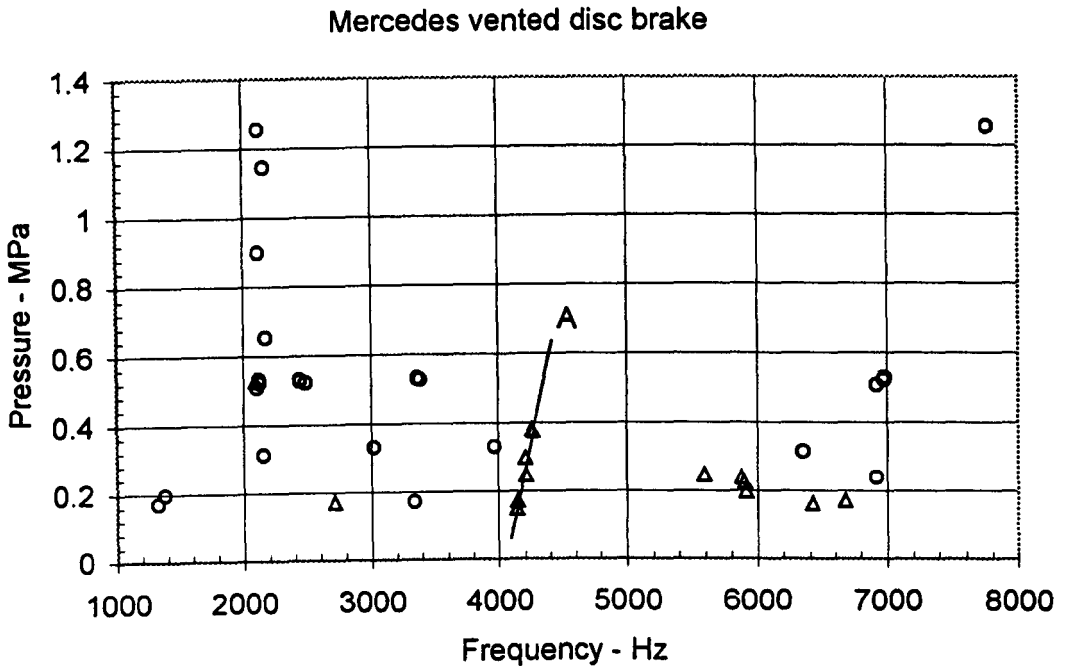


Figure 7-17 : Pressure / frequency plot for the Mercedes vented disc brake

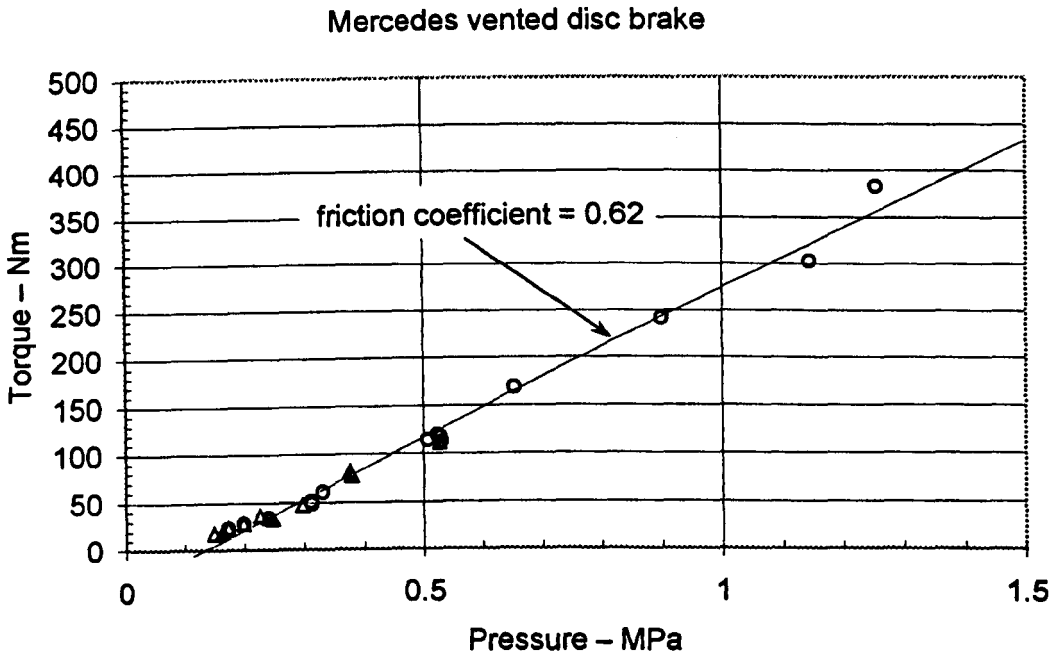


Figure 7-18 : Torque / pressure plot for the Mercedes vented disc brake

Figure 7-13 shows the relationship between disc displacement amplitude and squeal event frequency. Mode orders are also indicated. As with the Mercedes solid disc, there were many resonant frequencies present, but primarily at 2.1 kHz, 2.4 kHz and 4.2 kHz. Earlier tests indicated that the 2.4 kHz squeal frequency was more common than appears from this data. These earlier tests were not included here either because the data logging frequency was not high enough or insufficient data was recorded for analysis. Most of the 2.1 kHz cluster were standing waves and most of the 4.2 kHz cluster were backward travelling waves, as were those between 5.6 kHz and 6 kHz.

Figures 7-14 to 7-18 show the relationship between the test conditions and squeal frequency. Figure 7-14 shows that most of the squeal events occurred at temperatures above 140 °C. Figure 7-15 shows that no squeal events occurred at disc speeds of 16 rad s⁻¹ or above 21 rad s⁻¹. Figure 7-16 shows that although most squeal events occurred at torque levels less than 150 Nm, the cluster at 2.1 kHz could be excited over the whole torque range available.

Figure 7-17 shows the same frequency increase with increasing pressure as for the other discs for the 5-order mode, as indicated by the trend line 'A'.

Figure 7-18 shows a similar relationship between pressure and torque as for the Mercedes solid disc, for which the same arguments apply. The calculated friction coefficient of 0.62 is close to that of the Mercedes solid disc, as the same pads were used in both tests.

The 121 squeal events recorded here represent the culmination of many months of squeal test development on the dynamometer. Hundreds of squeal events were recorded during that time, used to improve either the measurement techniques or the analysis methods. There is now a workable system in place for conducting tests with the dynamometer and for analysing squeal results from those tests. A summary of this test and analysis methodology is given in James et al. (2003).

Chapter 8 : Finite element results

8.1 Finite element analysis of brakes at Liverpool

Recent research at Liverpool on the development of a finite element (FE) model of the Mercedes brake with a vented disc has been conducted by Mottershead, Ouyang and Cao in co-operation with sponsors TRW. In particular, Ouyang et al. (1999, 2000) explained the methodology of the FE analysis of disc brake squeal. The initial FE model provided by TRW was primarily used for stress analysis in the brake design. Development of the model was necessary to achieve realistic dynamic analysis coupled with efficient use of computation time, the main effort being applied to the many contact and friction surfaces in the structure. At Liverpool, FE analysis has been used for the vibration analysis of both the stationary brake system and the brake system in which the disc is rotating in the brake assembly.

A schematic of a brake assembly is given in figure 8-1 in which the various parts of the brake assembly are shown. The FE model used for the Liverpool analysis was that of the Mercedes vented disc brake. Photographs of this assembly are shown in figure 8-2 and a smooth rendered FE model is shown in figure 8-3. From these, it can be seen that the knuckle and carrier are fixed, the calliper is constrained to move only in the axial (Z) direction and the action of hydraulic pressure to the piston produces an equal axial force to both brake pads either side of the rotating disc.

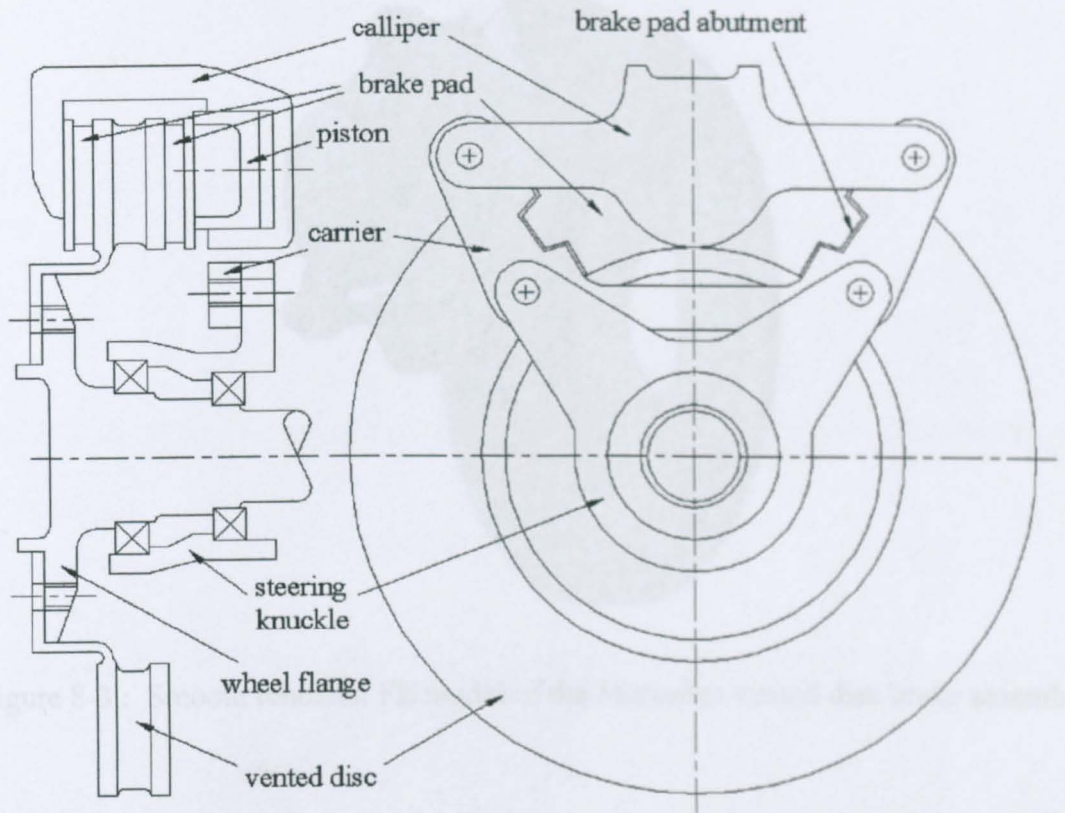


Figure 8-1 : Schematic brake assembly for a vented disc



Figure 8-2 : Photographs of the Mercedes vented disc brake assembly

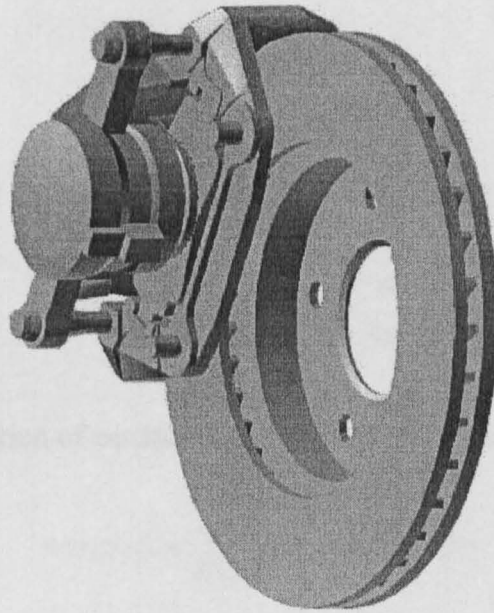


Figure 8-3 : Smooth rendered FE model of the Mercedes vented disc brake assembly

8.1.1 The combined FE and analytical model

The brake structure consists of several parts; the disc, the two brake pads made of friction material with steel backing plates, the calliper with the two guide pins, the carrier and the steering knuckle. Elements representing the contact surfaces between the brake parts were inserted into the FE model to make an assembled FE structure. Various conditions of the brake were then modelled by modifying these contact elements. For example, the pad to disc contact surface was represented by a layer of elements with high stiffness in the axial direction (normal to the disc) and very low stiffness in the other two directions.

FE analysis of the structure with a stationary disc was achieved by assuming an analytical model for the vented disc which is cyclically symmetric combined with an FE model for the other brake parts. The benefit of this approach is that of reduced computation time. The analysis of the disc given by Ouyang (2000) uses the equation of free transverse vibration of a thin annular disc given as

$$\rho h \frac{\partial^2 w}{\partial t^2} + D \nabla^4 w = 0 \quad (8.1)$$

where h is now the full disc thickness and

$$\nabla^4 = \left(\frac{\partial^2}{\partial r^2} + \frac{1}{r} \frac{\partial}{\partial r} + \frac{1}{r^2} \frac{\partial^2}{\partial \theta^2} \right)^2 \quad (8.2)$$

The free vibration solution of equation (8.1) can be given using a modal expansion as

$$w(r, \theta, t) = \sum_{j=-\infty}^{\infty} \sum_{n=0}^{\infty} \psi_{jn}(r, \theta) q_{jn}(t) \quad (8.3)$$

where q_{jn} is the modal co-ordinate for j nodal diameters and n nodal circles in the disc and

$$\psi_{jn}(r, \theta) = \frac{1}{\sqrt{\rho h b^2}} R_{jn}(r) \exp(ij\theta) \quad (8.4)$$

The complex form of the Fourier series has been used here. In this the sine and cosine doublet diametral modes appear as negative and positive values of j , hence the appearance of $j = -$ to $j =$ in the summation.

The hammer test of the full disc bolted to the hub without the brake applied was used to modify the boundary conditions of the analytical disc at its inner radius, as the physical disc was bolted to the hub at five discrete points. This modified disc model was also used to analyse the modes of the brake assembly with the brake applied.

The static components consisted of the brake pads, retaining springs, calliper, piston, guide pins and carrier. The carrier was assumed fixed at its connection with the knuckle. The original FE model of the static parts consisted of about 100,000 degrees of freedom. A reduced (super-element) model of 2,300 degrees of freedom was constructed using the Craig-Bampton dynamic reduction technique. This

technique was optimised to retain nodes at the contact surfaces between the stationary components and the friction surfaces of the pads.

The equations of motion of the static parts were expressed in the form

$$M\ddot{x} + C\dot{x} + Kx = f \quad (8.5)$$

The nodal displacement vector and the nodal force vector were divided into two parts. One part was for the disc / pad interfaces and the other part was for the remaining nodes. In this way the parameters associated with the friction behaviour of the brake can be isolated in the analysis. From this can be derived an expression for the nodal force, p , in the axial direction at the disc / pad interfaces in terms of the nodal displacements at those positions, x_w , as

$$p(t) = X_{\mu}^{-T} \left(I \frac{d^2}{dt^2} + 2\text{diag}[\beta_c, \omega^2] \frac{d}{dt} + \text{diag}[\omega^2] \right) X_p^{-1} x_w(t) + n \quad (8.6)$$

The force vector n is due to the static pressure. The vector p is the overall force vector which includes both the vibration pressure and the static pressure. The dynamics of the pads, calliper and mounting is contained in the terms X , $\text{diag}[\beta, \omega^2]$ and $\text{diag}[\omega^2]$ which are obtained using commercial software.

The primary source of disc brake noise emanates from the friction behaviour between the brake disc and the brake pads. The frictional contact surface between these two components is an important influence on squeal generation in a disc brake. It is very difficult to determine experimentally the detailed conditions of this contact, and the physics of the frictional contact surface is not fully understood. However, the static pressure distribution for the piston-side pad and the finger-side pad is known, and estimates can be made for the shift in pressure distribution caused by the relative movement of the disc and pads. A non-linear contact analysis has been used to introduce shell elements at the friction layer with the Young's modulus of each element dependent on the local pressure given by the contact analysis.

Other contact surfaces in the disc brake structure are also important in that they can effect the local damping and non-linearity of the structure in its vibrational behaviour. These contacts undergo through-zero relative motion with variable contact pressures, in which the friction behaviour can be a mixture of stick-slip and sliding contact, even though the displacements are small.

These contact points are:-

1. the piston head to the piston-side pad back plate,
2. the calliper fingers to the finger-side pad back plate,
3. the piston seal contact with the piston,
4. the piston boot contact with the piston,
5. the trailing edge pad abutment to the retaining springs,
6. the leading edge pad abutment to the retaining springs,
7. the retaining spring abutment to the carrier,
8. the guide pin contact with the carrier.

Other parts of the assembly that may contribute a small amount of damping are the guide pin boots, the bolted joints between the calliper and the guide pins and the bolted joints between the carrier and the knuckle.

Using this combined approach, it was possible to investigate the variation of dynamic stability of the brake system in several ways. Firstly, when changing the disc rotation speed, it was found that some modes became more stable, some became less stable and others did not change their degree of stability with increasing speed. Some modes were very sensitive to disc speed. The second set of tests varied the damping characteristics of the pad material. It was found that a small increase in damping could increase the stability of the disc. The third set changed the stiffness of the stationary components by modifying the Young's modulus. This had a mixed effect, as an increase in stiffness made some stable modes unstable and some unstable modes more stable.

8.1.2 The full FE model

For the comparative analysis between the FE model and the experimental hammer tests on the complete brake system, a full FE model of the brake, including the disc, was used. A drawback to the use of a mixture of analytic and FE structures has been the difficulty in determining the squeal mode shapes of the disc with their phase relationship to the brake structure. The analysis of the disc vibrations uses a linear, complex-valued, asymmetric eigenvalue routine. The eigenvalues and their corresponding eigenvectors are extracted by an in-house FORTRAN code using a standard NAG library QZ algorithm. The squeal frequencies are assumed to be the imaginary part of an eigenvalue in which the real part is positive. The mode shapes were plotted using PATRAN to show the squeal modes in the disc. It is assumed that these modes are stationary in space, as there can be no indication of travelling waves with this analysis.

8.2 Comparison of FE results with hammer tests

A comparison between the FE analysis of the Mercedes vented disc and the hammer test on the full disc with no brake installed is given in table 8-1. Modes of the disc with up to one nodal circle and up to seven nodal diameters were recognised as valid disc modes in both the hammer tests and the FE analysis. An FE model of the complete structure, including the disc, was used which meant that the modes in the disc were stationary.

There was no brake structure present for the full disc analysis, and the orientation of the modes was assumed to be linked to the wheel stud holes in the top-hat section of the disc. In the hammer tests on this disc, the relative orientation of the top-hat stud holes to the mesh nodes was not recorded. In most of the modes, each mode shape had two frequencies, one separated circumferentially by a half wavelength from the other. In table 8-1 which compares the full disc modes, the lower frequency mode from the hammer test was compared to the lower frequency mode from the FE

analysis, and similarly for the higher modal frequencies. In two cases, $[j = 5, n = 0]$ and $[j = 2, n = 0]$, only one mode frequency was found from the hammer test and this was compared to both the mode frequencies found from the FE analysis. It is interesting to note the anomaly for modes $[j = 1, n = 1]$ and $[j = 2, n = 1]$. The comparison of frequencies in the table has been made from a match between their mode shapes and this has given rise to large discrepancies between the hammer test and the FE analysis for these two modes.

For the static comparison of modes with the brake applied, as given in table 8-2, the physical phase relationship with the brake structure was evident from the FE output and could be directly compared with that from the hammer tests. As was noted in Chapter 8, for each mode pair of $[n = 0]$ modes, the antinode of the mode shape was aligned with the brake pad centre for the lower frequency mode and the node of the mode shape was aligned with the brake pad centre for the higher frequency mode. Again, there is an anomaly in the comparison for modes $[j = 1, n = 1]$ and $[j = 2, n = 1]$ with the exception that the FE analysis did produce a mode at 2406.2 Hz for the antinode aligned $[j = 1, n = 1]$ mode.

Mercedes vented disc						
Nodal circles	$n = 0$			$n = 1$		
Nodal diameters	Hammer test on full disc	Finite element analysis	F.E. difference percent	Hammer test on full disc	Finite element analysis	F.E. difference percent
$j = 0$	rigid body mode			3873.2	3505.8	9.5
$j = 1$	rigid body mode			3066.7	4094.5	+ 33.5
				3161.1	4129.4	+ 30.6
$j = 2$	1167.0	1195.6	+ 2.5	4824.3	3174.7	34.2
	1168.8	1202.0	+ 2.8	4824.3	3191.5	33.8
$j = 3$	2679.7	2607.8	2.7	5769.0	5844.1	+ 1.3
	2688.8	2609.6	2.9	5770.6	5878.5	+ 1.9
$j = 4$	4410.7	4220.4	4.3	10200.7	9210.5	9.7
	4425.0	4225.8	4.5	10227.3	9223.9	9.8
$j = 5$	6256.3	5902.7	5.7			
	6256.3	5910.0	5.5			
$j = 6$	8176.4	7651.1	6.4			
	8191.3	7653.3	6.6			
$j = 7$	10124.7	9438.9	6.8			
	10148.9	9441.9	7.0			

Table 8-1 : Mercedes vented disc - comparison of mode shapes and frequencies between the hammer test on the full disc and the equivalent finite element analysis
(Frequencies in Hz)

Mercedes vented disc						
Nodal circles	$n = 0$			$n = 1$		
	Hammer test with brake	Finite element analysis	F.E. difference percent	Hammer test with brake	Finite element analysis	F.E. difference percent
$j = 0$	rigid body mode			3873.2 (full disc)	3535.8	8.7
$j = 1$	rigid body mode			3002.5 ¹ 3191.1 ²	2406.2 4283.4	19.9 + 34.2
$j = 2$	1100.4 1443.5	1181.6 1403.0	+ 7.4 2.8	4844.8 ¹ 5031.6 ²	3169.1 3190.0	34.6 36.6
$j = 3$	2412.2 -	2471.3 2794.5	+ 2.5 -	7158.4 ² 7717.8 ¹	7670.5 7736.3	+ 7.2 + 0.2
$j = 4$	4503.9 4617.1	3969.0 4086.5	11.9 11.5	Notes :- 1. The radial node is aligned with the brake pad centre 2. The radial antinode is aligned with the brake pad centre		
$j = 5$	6263.9 6784.3	5949.7 6549.1	5.0 3.5			
$j = 6$	7999.3 8481.4	7453.1 8009.1	6.8 5.6			

Table 8-2 : Mercedes vented disc - comparison of mode shapes and frequencies between the hammer test with the brake and the equivalent finite element analysis (Frequencies in Hz)

8.3 Comparison of FE results with squeal tests

Table 8-3 shows the comparison between the experimental squeal frequencies and the FE results for squeal analysis. The experimental squeal frequencies given are the mean values of the squeals that appear close to the nodal diameter trend line in figure 7-17. The values in parentheses under these frequencies are the results from the hammer test on the disc with the brake applied, as given in table 8-2. It is unclear from figure 7-17 that any squeal events produced a 6-diameter mode. Consequently the figures in table 8-3 are for 2 to 5 diameter modes only. All the modes in the table are for $[n = 0]$, as the limitations of the measurement positions precluded the inclusion of any $[n = 1]$ modes.

It can be seen from table 8-3 that the squeal frequencies derived from the FE analysis are in reasonable agreement with those from the squeal tests. The FE analysis frequencies for the lowest three modes are slightly higher than those for the experimental squeal. If the mass of the brake components is similar for both the experimental brake and the FE model, then it can be assumed that the overall stiffness of the FE model is higher than that of the experimental brake. This may be an effect of elemental component stiffness as given by a material Young's modulus, or could be explained by the stiffnesses of the interface elements being higher than those existing in the experimental brake. The comparison for the $[j = 5]$ mode may be suspect due to the uncertainty of the mode shape match in the experimental results. However, the mean squeal frequencies given in this table are a close match to those given in table 8-2 for the hammer test of the disc with the brake applied.

Mercedes vented disc			
Nodal circles	$n = 0$		
Nodal diameters	Mean squeal frequency	Finite element analysis	F.E. difference percent
$j = 2$	1351 (1100.4 – 1443.5)	1428	+ 5.7
$j = 3$	2401 (2412.2)	2499	+ 4.1
$j = 4$	4206 (4503.9 – 4617.1)	4499	+ 7.0
$j = 5$	6139 (6263.9 – 6784.3)	5225	14.9

Table 8-3 : Mercedes vented disc - comparison of mode shapes and frequencies between the mean squeal frequency and the equivalent finite element analysis (Frequencies in Hz, values in parentheses are Z direction hammer modes from table 8-2)

Chapter 9 : Conclusions and future work

9.1 Conclusions

A dynamometer can be used to produce squeal in a disc brake and the out of plane displacements of the disc can be measured to give useful detailed information about the behaviour of the squeal frequency waves in the disc.

Data recording speeds need to be high enough for aliasing not to occur and allow the wave direction to be observed. Typically, a recording speed of 56180 samples per second was used in these tests to analyse squeal frequencies up to 8 kHz.

The discs exhibited four (Rover disc) or five (both Mercedes discs) primary squeal frequency diametral modes between 1 kHz and 8 kHz with close correlation to equivalent hammer test diametral modes and, for the Mercedes vented disc, diametral modes produced using finite element analysis.

Analysis of the squeal events using least squares methods on short time-slices of data showed that within a squeal event, a squeal mode could consist of a stationary wave in the disc, fixed relative to space co-ordinates, or a travelling wave, either backward travelling (against the disc rotation direction) or forward travelling. Most common were stationary waves. Although the audible squeal frequency sounded constant and stable to the ear, this was not the case when measured in detail. Large variations in amplitude were measured.

Squeal events on the dynamometer were not readily forthcoming. Normally, squeal would not occur when the disc and brake assembly was cold (<50°C). It would usually occur at temperatures above 100°C. As the temperature is so high for squeal to develop, it is unlikely that changes in humidity have any effect on squeal

behaviour. The squeal tests were performed by setting a constant speed and varying the hydraulic pressure to the brake piston. When a squeal event did occur, it would sound within a limited pressure range and measurements were taken at several pressures if the event lasted long enough to record them. On many occasions, the squeal event was too short lived to record more than one reading. Reproduction of apparently identical values of speed, temperature, pressure and torque did not guarantee reproduction of a squeal event.

9.2 Future work

9.2.1 Drive parameter variation

The dynamometer was designed for a disc speed range of 0 to 100 rad s⁻¹. However, the squeal test results show that squeal events are prevalent at comparatively low speeds. In the case of the Rover disc and the Mercedes vented disc, no squeal was recorded for disc speeds above 23 rad s⁻¹ and for the Mercedes solid disc, there were very few squeal events at disc speeds in excess of 41 rad s⁻¹.

A useful modification to the dynamometer would be a change of drive pulleys to utilise the 42 kW from the motor to drive the shaft at a maximum speed of 40 rad s⁻¹. The torque transducer and probably the drive shafts would need to be replaced to accommodate 1000 Nm, but this modification would enable squeal tests with brake pressures up to 50 bar to be performed. This would also enable a greater variety of conditions to be used during the brake pad bedding-in process necessary before squeal tests could begin. Reversal of the existing pulley system already enables shaft speeds of 315 rad s⁻¹ to be achieved but the torque is limited to 130 Nm, equivalent to about 6.5 bar hydraulic pressure.

9.2.2 Mounting stiffness

The hub and steering knuckle are mounted in a rigid fashion to minimise extraneous movement of the disc at the displacement transducers. It is likely that this arrangement can change the squeal behaviour of the brake due to the interaction between the mounting structure and the brake components.

Some elasticity could be achieved in the knuckle mounting by using compressed rubber shims as shown in figure 3-9. These would effectively isolate the brake mechanism from the support structure at high frequencies without allowing the disc to move too far relative to the static displacement transducers. The air gap between the transducers and the disc is 1 mm for the current tests and this allows a fine displacement resolution to be used. If the elastic supports were such that no more than 0.5 mm of axial disc displacement could be guaranteed, then the existing 1 mm gap could be retained.

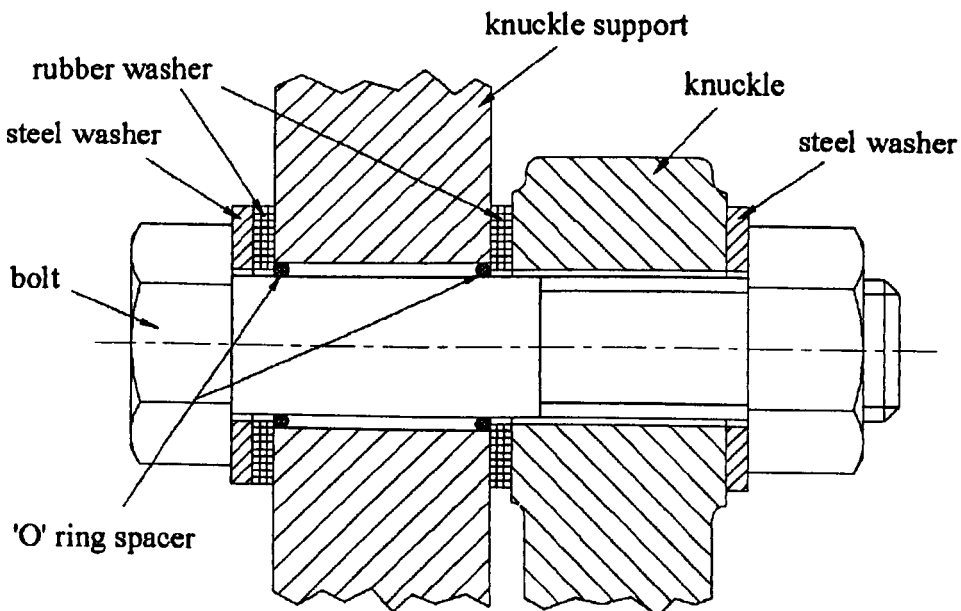


Figure 9-1 : Proposed flexible knuckle mounting

A complication to this procedure lies in the transducer calibration. The displacement transducers do not have a linear calibration function. The sensitivity is proportional

to the inverse of the square of the air gap. With such a flexible mounting system it may be necessary to monitor the actual air gap and adjust the transducer output calibration accordingly. However, this is a procedure that could be developed in the post processing software used in future tests.

9.2.3 High speed recording

A built-in limitation to the data logging rate is the number of channels being simultaneously recorded. The more channels that are recorded, the slower is the maximum logging rate. In the present experimental configuration, 11 or 12 displacement transducers, a microphone, disc temperature, disc speed, shaft torque and hydraulic pressure were recorded which would use up to a total of 17 channels on the data logger. Of these, only the 11 or 12 displacement channels and the microphone needed to be recorded at high speed. The other channels could have been recorded at 100 Hz without loss of information, so long as a time link was recorded to synchronise their data with that of the displacement channels. Future development of the instrumentation could provide this modification to allow 12 transducers and a microphone to be recorded at high speed and the other channels recorded by another computer at low speed.

At low disc speeds (less than 20 rad s^{-1}) the time for a squeal event record is shorter than one complete rotation of the disc. A further modification to the data logging control is needed to allow a recorded squeal event to start at different disc rotation positions. This would allow the capture of data for a complete revolution of the disc using several tests.

The test control has been entirely manual in the existing set-up. A further development could be to increase the level of automation used in the capture of squeal data, particularly with regard to running the dynamometer for multiple stop matrix testing as is presently carried out by the brakes industry. This dynamometer would use software controlled simulated inertia, whereas the commercial

dynamometers use a flywheel. However, this development may provide a useful comparison between the two methods.

9.2.4 Analysis development

The analysis given in Chapter 5 is a useful simulation of the nature of the mode shapes of the disc and represents a simplification which is useful in a comparative sense. The equations used are for mode shapes in a perfect axisymmetric disc without any interference from a brake.

As well as the variation in frequency, other wave parameters are constantly changing during a squeal event. Squeal amplitude can vary between zero and maximum in only a few cycles in some cases. It is also possible for the squeal wave parameters to change from, say, a travelling wave to a standing wave, also within a few squeal frequency cycles. For these reasons, a power spectrum obtained from the complete test data represents an amalgam of the information available, whereas analysis of small time slices can be used to view the changing nature of a squeal event.

Programs developed using Matlab have been used to perform this detailed analysis and further development of these programs is required to simplify the analysis procedure. Analysis of consecutive time-slices of data from a test may be used to generate an animation of the wave motion in the disc. This animation could be used to show how the modal waves in the disc change over longer periods of time to allow engineers to gain a better insight into the disc behaviour during a squeal event.

9.2.5 Squeal test development

Three methods of recording squeal were used in the experimental procedure. The most successful method was that of high frequency recording. This allowed small samples of time domain data to be analysed using a least squares technique and gave an overall picture of the behaviour of the squeal wave in the disc. Fifteen channels

of data were recorded at 56 kHz, the limiting frequency of the hardware for this number of channels. It is proposed that, by recording the four non-displacement channels by other (slower) methods, the eleven displacement channels could be recorded at a faster speed. A further modification would be to use a variable trigger point for squeal events in which the recording time was less than one complete revolution of the disc.

The squeal events were successfully analysed using a variety of Matlab (1995) programs. Fast Fourier transforms were used on the raw data to determine the approximate squeal frequencies present in the squeal event. For each frequency to be analysed, filtered data was used to determine the nature of the wave in the disc (either stationary in space, forward travelling or backward travelling). Finally small time-slices of the filtered data (about 20 cycles per time-slice) were analysed using least squares methods to provide the parameters for a 'best fit' equation. It is accepted that the 'best fit' equations presented here are not a true representation of the wave shapes existing during squeal events, but give an approximation used for comparison.

9.2.6 Finite element development

The future of disc brake design lies with the increasing use of finite element techniques, as has been identified by Kinkaid (2002). It will be increasingly necessary to use non-linear modelling methods for the complex instability behaviour of these structures. Much work has yet to be done in refining the prediction accuracy of finite element models of brake assemblies to give brake design engineers appropriate tools with which to design quiet brakes. The techniques given in this experimental study can be used to verify improvements to these finite element models and test new designs of quieter brakes.

References

Abendroth H., "Advances in brake NVH test equipment", *Automotive Engineering International*, pp. 60-63, February 1999.

Akay A., "Acoustics of friction", *J. Acoust. Soc. Am.* Vol. 111, No. 4, pp. 1525-1548, April 2002.

Bergman F., Eriksson M., Jacobson S., "The effect of reduced contact area on the occurrence of disc brake squeals for an automotive brake pad", *Proc. I. Mech. E.*, Vol. 214, *Journal of Automobile Engineering*, pp. 561-568, 2000.

Bracken W. J., Sakioka J. K. Jr., "A method for the quantification of front disc brake squeal", S.A.E. Technical Paper 820037, 1982.

Brooks P. C., Crolla D. A., Lang A. M., Schafer D. R., "Eigenvalue sensitivity analysis applied to disc brake squeal", *I. Mech. E. Paper C444/004/93*, pp. 135-143, 1993

Butcher I., Ewins D. J., "Multidimensional decomposition of time-varying vibration response signals in rotating machinery", *Mechanical Systems and Signal Processing*, Vol. 11, No. 4, pp. 577-601, 1997.

Chan S. N., "Analysis of discs with friction loading", Ph.D. thesis, University of Liverpool, December 1993.

Chan S. N., Mottershead J. E., Cartmell M. P., "Parametric resonances at subcritical speeds in discs with rotating frictional loads", *Proc. I. Mech. E.*, Vol. 208, *Journal of Mechanical Engineering Science*, pp. 417-425, 1994

- Chen J. S., Bogy D. B., "Effects of load parameters on the natural frequencies and stability of a flexible spinning disk with a stationary load system", *Trans. of the ASME, Journal of Applied Mechanics*, Vol. 59, pp. 230-235, June 1992.
- Chen J. S., Bogy D. B., "The effects of a space-fixed friction force on the in-plane stress and stability of transverse vibrations of a spinning disk", *Trans. of the ASME, Journal of Applied Mechanics*, Vol. 60, pp. 646-648, September 1993.
- Cooley J. W., Tukey J. W., "An algorithm for the machine calculation of complex Fourier series", *Mathematics of Computation*, Vol. 19, pp. 297-301, 1965.
- Dixon G. L., "Speckle techniques map deformation and displacement", *Laser Focus World*, pp. 75-81, June 1998.
- Dunlap K. B., Riehle M. A., Longhouse R. E., "An investigative overview of automobile disc brake noise", S.A.E. Technical Paper 1999-01-0142, 1999.
- Earles S. W. E., Badi M. N. M., "Oscillatory instabilities generated in a double-pin and disc undamped system: a mechanism of disc-brake squeal", *Proc. I. Mech. E.*, Vol. 198, *Journal of Mechanical Engineering Science*, No. 4, pp. 43-50, 1984.
- Earles S. W. E., Chambers P. W., "Disc brake squeal noise generation: predicting its dependency on system parameters including damping", *Int. Journal of Vehicle Design*, Vol. 8, Nos. 4/5/6, pp. 538-552, 1987.
- Earles S. W. E., Chambers P. W., "Disc brake squeal - some factors which influence its occurrence", *I. Mech. E.*, Paper C454/88, pp. 39-46, 1988.
- Felske A., Hoppe G., Mattai H., "Oscillations in squealing disc brakes – analysis of vibration modes by holographic interferometry", S.A.E. Technical Paper 780333, 1978.
- Fieldhouse J. D., Newcomb T. P., "An investigation into disc brake noise using holographic interferometry", *3rd Int. EAEC conference on vehicle dynamics and powertrain engineering*, EAEC No.91084, pp. 568-578, June 1991.

- Fieldhouse J. D., Newcomb T. P., "The application of holographic interferometry to the study of disc brake noise", S.A.E. *10th annual colloquium on brakes and engineering display*, Oct 1992.
- Fieldhouse J. D., "A proposal to predict the noise frequency of a disc brake based on the friction pair interface geometry", S.A.E. Brake Colloquium and Engineering Display, Paper no. 1999-01-3403, 1999.
- Fieldhouse J. D., Talbot C. J., "Visualising brake noise – from holographic investigations to 3D animated images of real brakes generating noise", Proc. I.M.A.C., *21st Int. Modal Analysis Conf.*, Paper No. 306, pp. 1-8, 2003.
- Fosberry R. A. C., Holubecki Z., "Interim report on disc brake squeal", M.I.R.A. Technical Report No. 1959/4, 1959.
- Fosberry R. A. C., Holubecki Z., "Disc brake squeal – its mechanism and suppression", M.I.R.A. Technical Report No. 1961/2, 1961.
- Ghesquiere H., "Brake squeal noise analysis and prediction", I. Mech. E., Paper C389/257, No. 925060, pp. 175-181, 1992.
- Harding P. R. J., Wintle B. J., "Flexural effects in disc brake pads", Proc. I. Mech. E., Vol. 192, *Automobile Division*, pp. 1-7, 1978.
- Huang F. Y., Mote C. D. Jr., "Mathematical analysis of stability of a spinning disk under rotating, arbitrarily large damping forces", Trans. of the ASME, *Journal of Vibration and Acoustics*, Vol. 118, pp. 657-662, 1996.
- Iwan W. D., Stahl K. J., "The response of an elastic disk with a moving mass system", Trans. of the ASME, *Journal of Applied Mechanics*, Vol. 40, pp. 445-451, June 1973.
- Iwan W. D., Moeller T. L., "The stability of a spinning elastic disk with a transverse load system", Trans. of the ASME, *Journal of Applied Mechanics*, Vol. 43, No. 3, pp. 485-490, September 1976.

- James S., Brookfield D. J., Mottershead J. E., Ouyang H., "An experimental study of disc brake squeal generation", in preparation for Proc. I. Mech. E., *Journal of Mechanical Engineering Science*, (2003).
- Jarvis R. P., Mills B., "Vibrations induced by dry friction", Proc. I. Mech. E., Vol. 178, Part 1, No. 32, pp. 847-866, 1963/4.
- Kinkaid N. M., O'Reilly O. M., Papadopoulos P., "Automotive disc brake squeal: a review", *Journal of Sound & Vibration*, accepted for publication, (2002).
- Lamb H., Southwell R. V., "The vibrations of a spinning disk", Proc. Royal Soc., London, No. 99, pp. 272-280, 1921.
- Lang A. M., Smales H., "An approach to the solution of disc brake vibration problems", I. Mech. E., Paper C37/83, pp. 223-231, 1983.
- Lee C.-W., Kim M.-E., "Identification of travelling wave modes in rotating disk using wave dFRFs", Proc. I.M.A.C., *14th Int. Modal Analysis Conf.*, pp.1403-1408, February 1996.
- Lee D., Waas A. M., "Stability analysis of a rotating multi-layer annular plate with a stationary frictional follower load", *Int. Journal of Mechanical Science*, Vol. 39, No. 10, pp. 1117-1138, 1997.
- Longley J. W., Gardner R., "Some compositional effects in the static and dynamic properties of commercial vehicle disc brakes", Proc. I. Mech. E., C453/88, pp. 31-38, 1988.
- MATLAB, "High-performance numeric computation and visualization software - Reference Guide", The MathWorks, Inc., April 1995.
- McLellan R. G., "Requirements of friction materials in commercial vehicle disc brake applications", I. Mech. E., Paper C451/88, pp. 9-13, 1988.

Millner N., "An analysis of disk brake squeal", S.A.E. Technical paper 780332, 1978.

Mottershead J. E., Chan S. N., "Flutter instability of circular discs with frictional follower loads", Trans. of the ASME, *Journal of Vibration and Acoustics*, Vol. 117, pp. 161-163, 1995.

Mottershead J. E., Ouyang H., Cartmell M. P., Friswell M. I., "Parametric resonances in the annular disc, with a rotating system of distributed mass and elasticity; and the effects of friction and damping", Proc. Royal Soc., London, No. 453, pp. 1-19, 1997.

Mottershead J. E., "Vibration- and friction-induced instability in discs", *The Shock and Vibration Digest*, Vol. 30, No. 1, pp. 14-31, 1998.

Murakami H., Tsunada N., Kitamura T., "A study concerned with a mechanism of disc brake squeal", S.A.E. Technical paper 841233, 1984.

Nishiwaki M., "Generalized theory of brake noise", Proc. I. Mech. E., Vol. 207, *Journal of Automobile Engineering*, pp. 195-202, 1993.

North M. R., "Disc brake squeal", I. Mech. E., Paper C38/76, pp. 169-176, 1976.

Ouyang H., Mottershead J. E., Brookfield D. J., James S., Cartmell M. P., Kaster T., Treyde T., Hirst B., Allen R., "Dynamic instabilities in a simple model of a car disc brake", S.A.E. Technical paper No. 1999-01-3409, 1999.

Ouyang H., Mottershead J. E., Brookfield D. J., James S., Cartmell M. P., "A methodology for the determination of dynamic instabilities in a car disc brake", *Int. Journal of Vehicle Design*, special edition on "Brake Roughness, Noise, Vibration and Dynamics", Vol. 23, Nos. 3/4, pp. 241-262, 2000.

Reeves M., Taylor N., Edwards C., Williams D., Buckberry C. H., "A study of brake disc modal behaviour during squeal generation using high speed electronic speckle pattern interferometry and near-field sound pressure measurements", Proc. I. Mech. E., Vol. 214, *Journal of Automobile Engineering*, pp. 285-296, 2000.

- Richmond J. W., Holton T. R., Smith A. C., Beckett P. B., Hodges T., "The development of an integrated experimental and theoretical approach to solving brake noise problems", *Advances in Automotive Braking Technology, Design Analysis and Materials Developments*, pp. 3-23, 1996.
- Samie F., Sheridan D. C., "Contact analysis for a passenger car disc brake", S.A.E. Technical paper 900005, pp. 37-43, 1990.
- Schwartz H. W., Hayes W. D., Tarter J. H., "A systematic approach to the analysis of brake noise", S.A.E. Technical paper 850990, pp. 267-275, 1985.
- Shen I. Y., Mote C. D. Jr., "On the mechanisms of instability of a circular plate under a rotating spring-mass-dashpot system", *Journal of Sound and Vibration*, Vol. 148, pp. 307-318, 1991.
- Shen I. Y., "Response of a stationary, damped, circular plate under a rotating slider bearing system", *Trans. of the ASME, Journal of Vibration and Acoustics*, Vol. 115, pp. 65-69, 1993.
- Southwell R. V., "On the free transverse vibrations of a uniform circular disc clamped at its centre; and on the effects of rotation", *Proc. Royal Soc., London*, Vol. 101, pp. 133-153, 1921.
- Spurr R. T., "A theory of brake squeal", *Proc. I. Mech. E., Automobile Division*, No. 1, pp. 33-40, 1961/2.
- Stanbridge A. B., Ewins D. J., "Using a continuously-scanning laser doppler vibrometer for modal testing", *Proc. of I.M.A.C., 14th Int. Modal Analysis Conf.*, pp. 816-822, February 1996.
- Talbot C., Banawi K. A., Fieldhouse J. D., "Three-dimensional animation of a real disc brake generating noise", *Proc. of I.S.M.A. 25*, pp. 1113-1118, 2000.
- Tarter J. H., "Disc brake squeal", S.A.E. Technical paper 830530, 1983.

Tirovic M., Day A. J., “Disc brake interface pressure distributions”,
Proc. I. Mech. E., Vol. 205, *Journal of Automobile Engineering*, pp. 137-146, 1991.

Yu R. C., Mote C. D. Jr., “Vibration and parametric excitation in asymmetric circular
plates under moving loads”, *Journal of Sound and Vibration*, Vol. 119(3), pp. 409-
427, 1987.

Appendix A : Measurement method

A.1 Data logging instrumentation

Data collection for squeal events was implemented with a Scadas II synchronous 20-channel data logger driven by LMS (Leuven Measurement Systems) Cada-X software, version 3.5.D. The system is a sophisticated modal testing and analysis package capable of many different test formats. Those used in this research were the General Applications Monitor, the Throughput Acquisition and Processing Monitor and the Impact Testing Monitor in the Fourier Monitor module. The Geometry module was used to display the mode shapes from the hammer tests.

The General Applications Monitor (GAM) was used to record time domain data from all the transducer channels. The maximum recording speed was limited by the number of channels being recorded and the record length was limited by the internal memory of the data logger. The squeal tests recorded here were logged at 56 kHz and acquired about 0.5 s of data per recorded event. The LMS software provided a file export facility to convert the measured time domain data into a universal file format (ascii). A Matlab (1995) program was written to transfer this data to a Matlab data file (.mat) which was more readily imported into other Matlab programs for analysis.

The Throughput Acquisition Monitor was used to record longer test times than were achievable in GAM. As the name suggests, data is streamed directly to computer storage instead of being held in local RAM. The penalty for this facility is that for the number of channels being recorded, the maximum recording frequency was 16 kHz, too slow to recognise travelling waves without aliasing. Once collected, the

data had to be post-processed with the Throughput Processing Monitor to convert it to recognisable data files. This could only be done in 2 s time slices which meant that four processed files had to be concatenated to make up an 8 s record.

Impact testing was used for all the hammer tests on the brake components. For the Z only hammer tests, a roving hammer type of test was used and for the multi-dimensional hammer tests a fixed hammer type of test was used. All the impact tests used a logging frequency of 16 kHz which gave a maximum frequency response of 8 kHz. A metallic hammer tip was used throughout. Single axis type 356B16 ICP accelerometers were used in all of the hammer tests. Each brake component geometry was entered using the Geometry module. The LMS software related the measured modes to the geometry to produce the mode shape images shown in Chapter 8.

A.2 Monitoring instrumentation

A PC with LabView software (from National Instruments) was used to monitor the disc brake parameters during squeal events. A permanent front-end display of disc temperature, disc rotation speed, shaft torque and hydraulic pressure was updated 5 times per second to allow full monitoring of the brake systems during a test. These values were also fed to the Scadas II data logger and recorded during a squeal event.

Also present on the test rig were a digital display of disc temperature and a bourdon type pressure gauge for measuring the hydraulic pressure.

Disc speed and hydraulic pressure were both manually controlled throughout.

Appendix B : Calibration procedures

Calibration of all the experimental instrumentation was carried out before testing could begin. Re-calibration of some transducers was necessary at various times, particularly the displacement transducers. These needed re-calibrating whenever they were moved on the rig.

The following sections explain the calibration procedures for each of the transducers used in the experimentation.

B.1 Temperature calibration

The temperature of the brake disc was measured using a copper faced thermocouple probe supplied by BBA Friction. The probe face was set in contact with the brake disc at a point near the outer radius of the brake contact and just after the disc had passed the brake pads. Thus it was measuring the temperature of the hottest accessible point on the disc.

A Jenco Model 765 Thermometer, digital and analogue indicator was used to both show the measured temperature and feed an analogue voltage to the data logger. Initial calibration with ice and boiling water was used to check the digital output at 0°C and 100°C. The analogue output voltage was compared to the digital indicator.

A calibration value of $105.27\text{ }^{\circ}\text{CV}^{-1}$ was used throughout the tests.

B.2 Speed calibration

The Mentor motor controller has a digital display for motor speed with a minimum value of -1000 (full speed in reverse) through 0 (stationary) to a maximum value of $+1000$ (full speed forward). The controller receives its information from an encoder on the motor shaft. The output voltage from this is linear from -950 to $+950$ as indicated on the digital display. The analogue output from the encoder was set to give 0 V for the stationary shaft and 7 V for an indicated -700 . The reverse motor direction drives the brake disc in the forward direction.

Speed calibration on the brake shaft used the SPDCAL2.BAS program in QuickBasic 4.5. The Mentor controller was set to run the motor from -50 to -1000 in increments of -50 . An optical switch on the brake disc shaft triggered the software to log the analogue voltage. At each speed level, 100 data points were recorded of the analogue voltage and the computer jiffy clock was used to measure the total time taken for 100 revolutions of the shaft. This gave a linear characteristic between 0 and -950 on the Mentor display. The process was repeated in the forward (motor) direction with the result that the calibration was linear between -950 and $+950$ on the Mentor indicator.

A calibration value of $10.233 \text{ rad.s}^{-1}\text{V}^{-1}$ was used throughout the tests.

B.3 Torque calibration

The torque transducer was calibrated using a lever arm and deadweight. The brake disc was securely clamped and the driven side of the torque transducer was disconnected from the shaft. A horizontal bar was bolted to the input flange of the transducer and deadweights were hung from the outer end of the bar. The resulting applied moment was compared to the output voltage to obtain a calibration value.

A calibration value of 40.0 Nm.V^{-1} was used throughout the tests.

B.4 Pressure calibration

The Brüel & Kjær pressure transducer is driven by a driver board with a built-in zero and gain adjustment for the output analogue voltage. The transducer was calibrated using a standard Budenberg deadweight tester and the zero and gain controls were adjusted to give an output of 300 kPa.V^{-1} .

A calibration value of 300 kPa.V^{-1} was used throughout the tests.

B.5 Displacement calibration

The axial displacement of the brake disc is measured with 12 Brüel & Kjær type MM0004 non-contact capacitive displacement transducers. They operate by using a 200 V bias voltage and do not use a carrier frequency. Consequently they are limited at frequencies less than about 15 Hz but theoretically do not suffer from an upper frequency limit. The frequency range in this investigation ranged from 100 Hz to 20 kHz.

The output voltage from the transducer is inversely proportional to the square of the length of the air gap between the transducer and the brake disc. i.e. $V \propto d^{-2}$. With this non-linear relationship coupled with the requirement for all the transducers to produce a coherent output, a new calibration was performed each time the transducers were reset.

The calibration procedure was as follows:-

1. The transducers were mounted on the carrier plate with three levelling screws to give a 1 mm gap between each transducer and a flat table. The carrier plate was then mounted onto the support bracket and the carrier adjusted to maintain the 1 mm gap between the transducers and the disc. The levelling screws were removed.
2. The disc was rotated slowly and the axial run-out at the transducer radius was measured with a clock gauge.

3. The disc was run at high speed (20 Hz) and the transducer readings of the run-out were taken using unity gain.
4. The gain values for each transducer were calculated to match the run-out measured with the clock gauge.

B.6 Trigger calibration

The optical trigger was set high at +5 V and low at 0 V. A black stripe was placed on the chrome torque transducer flange. The change from chrome to black set the trigger to high and the change from black to chrome set the trigger to low.

Appendix C : Disc details

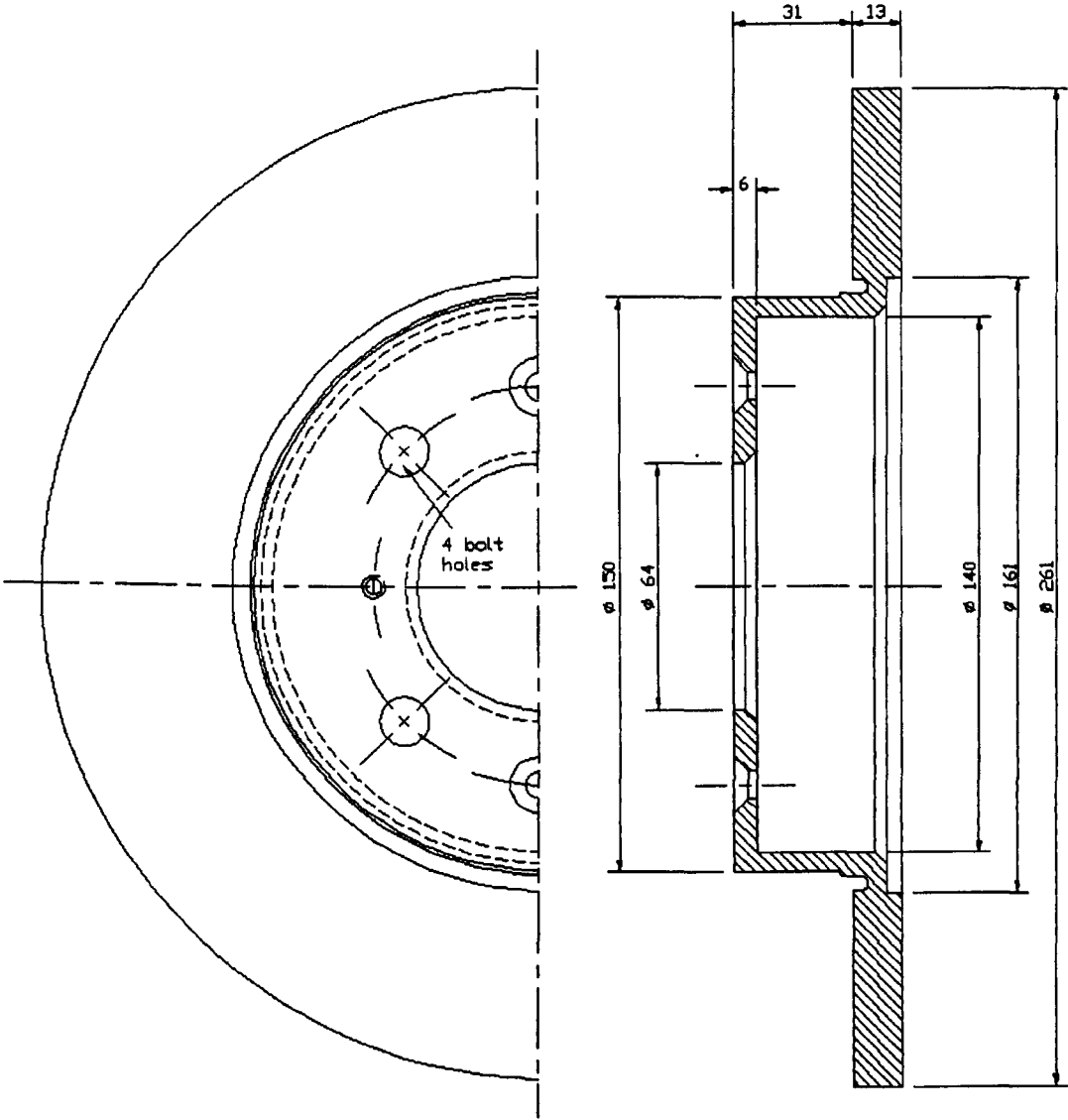


Figure C-1 : Detail of Rover disc

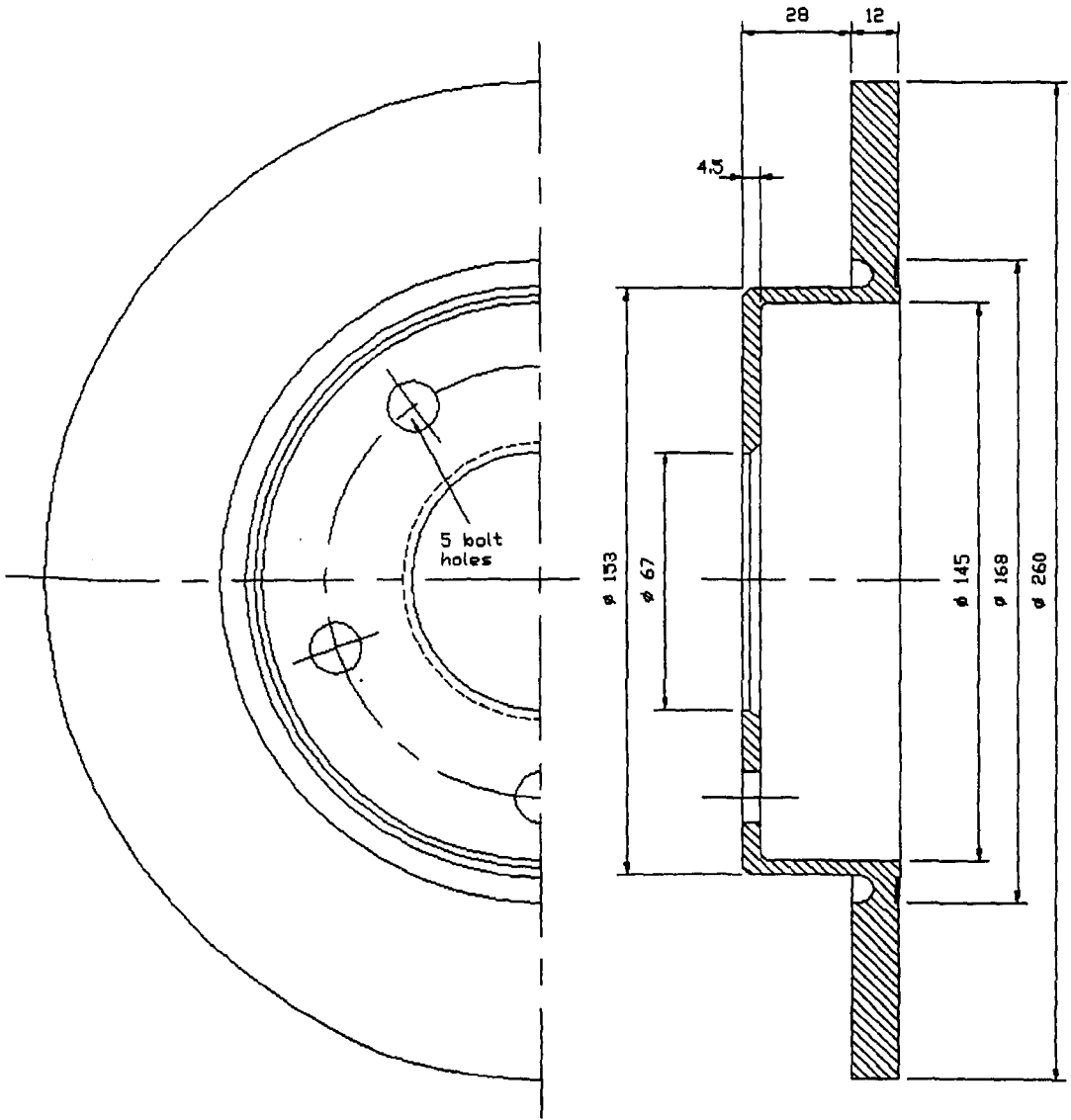


Figure C-2 : Detail of Mercedes solid disc

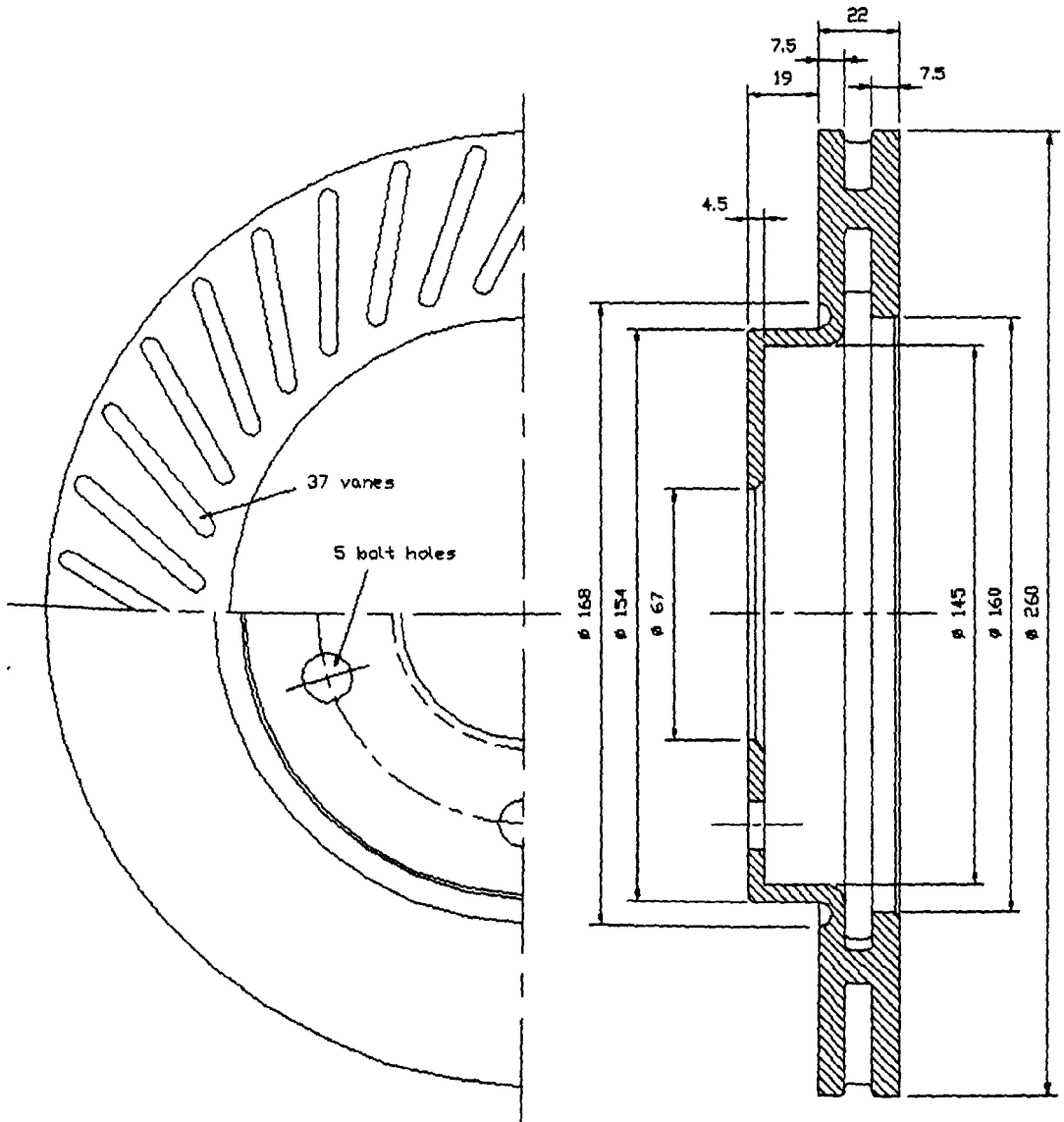


Figure C-3 : Detail of Mercedes vented disc

Brake disc	Run-out at displacement transducer radius (121 mm) μm	Thickness variation at outer radius (130 mm) μm
Rover solid disc	± 27	± 3
Mercedes solid disc	± 17	± 4
Mercedes vented disc	± 16	± 2

Table C-1 : Brake disc run-out and thickness variation

	Effective radius mm	Angular length degrees
Rover brake pad	110	55.4
Mercedes brake pad	111	45.2

Table C-2 : Brake pad effective radius and angular length